Soft Lithography for Applications in Microfluidic Thermometry, Isoelectric Focusing, and Micromixers

by

Razim Farid Samy

A thesis
presented to the University of Waterloo
in fulfillment of the
thesis requirement for the degree of
Master of Applied Science
in
Mechanical Engineering

Waterloo, Ontario, Canada, 2007

AUTHOR'S DECLARATION

I hereby declare that I am the sole author of this thesis. This is a true copy of the thesis, including any required final revisions, as accepted by my examiners.

I understand that my thesis may be made electronically available to the public.

Abstract

Microfluidics is gaining in importance due to its wide ranging benefits and applicability in chemical and biological analysis. Although traditional microfluidic devices are created with glass or silicon based fabrication technologies, polymer based devices are gaining in popularity. Soft lithography and replica molding are techniques for the rapid prototyping of such devices, utilizing Polydimethylsiloxane (PDMS) as the dominant material. Other benefits include its low costs and ease of fabrication. Even though soft lithography is a well researched and developed fabrication process, new applications have been discovered in which the technology can be applied. Often, changes in the fabrication process are necessary for their application in other areas of research. This thesis will address several applications in which the impact of soft lithography has rarely been explored. These areas of research include microfluidic thermometry, isoelectric focusing (IEF), and micromixers.

In microfluidic thermometry, a novel thin film PDMS/Rhodamine B has been developed allowing whole-chip temperature measurements. This is in contrast to traditional methods that are limited to in-channel measurements only. In addition, compatibility problems between Rhodamine B and PDMS microfluidic devices were resolved. The thin film fabrication process, experimental results, and issues with its use are discussed. Future work and attempts at improving the thin film performance are also provided.

IEF involves applications in which samples are separated according to its electrostatic charge. Two types of IEF applications are shown in which soft lithography has been shown to be beneficial to its development and performance. In isoelectric focusing with the use of thermally generated pH gradients, soft lithography allows for the rapid design, production and testing of different channel layouts. By utilizing the temperature sensitive thin film, heat transfer can be studied in these systems. Correspondingly, a study of factors (such as geometry and power input) and its effect on temperature distributions in PDMS devices is performed. In general, due to PDMS insulation and overall low heat transfer rates, the temperatures detected are more gradual than those previously reported in literature. IEF using carrier ampholytes are also discussed, with preliminary results in which devices fabricated using soft lithography are compared to commercially available IEF cartridges. Its fabrication issues are discussed in detail. Overall, performance of PDMS IEF devices is comparable to those obtained commercially.

In micromixers, soft lithography fabrication issues and overall integration with flow mechanisms is discussed. In general it is difficult to perform mixing in the microscale due to the predominantly laminar flow and flow rate restrictions. Channel geometry is insignificant, as can be seen through numerical simulations. However, its performance rivals that of large reactors.

Acknowledgements

First and foremost, I would like to sincerely thank my supervisor, Prof. Carolyn Ren, for her tremendous support and guidance, for "taking a chance" by hiring a fresh and unproven masters candidate, and through patience, training him to become a successful researcher.

I would also like to thank my co-supervisor Emily Moore, Santiago Faucher, and Cheryl Pearce for their help and guidance while at Xerox. The support of Xerox, through NSERC industrial postgraduate scholarship is gratefully acknowledged.

In addition, the efforts and vast knowledge of my colleagues at the Microfluidics lab has been valuable, whose resources allowed me to efficiently set up and run experiments. In particular, those that I closely worked with and wish to sincerely thank include Tom Glawdel, Jay Taylor, Zeyad Almutairi, Lin Gui, and Sean Wang, for their suggestions and help, without which I would not have been able to come so far. I will miss our enlightening research conversations and brainstorming sessions.

The endless support of my family and friends has also been crucial during these stressful years. I would like to especially thank my family: Farouk Samy, Barbara Samy, Rumjahnbee Samy, Sherif Samy, Farid Samy, Hameda Samy, Oscar, and Sparky. I also wish to thank Willie Tsui for her emotional support, organization and efficiency in arranging my day to day mundane activities so that I can concentrate on my research. Sammie Ngan, Irene Wijoyo, Christina Wei, Karina Ng, and May Yu are to be thanked for putting a social balance in my life (well, at least attempting to anyways). In addition, I wish to thank Simon Law for holding down the fort all this time; may XM and APS grow beyond our wildest dreams.

Dedication

In memory of Oscar;

And the realization that cancer not only affects everyone, but all walks of life.

Table of Contents

List of Figures

List of Tables

Chapter 1
Introduction

1.1 Background

Microfluidic devices are becoming increasingly popular in research and commercial areas. Microfluidics involves the study of fluidic flow in the micrometer scale, where the fluid channel widths are usually in the range of 20 to 100 μm. At the micrometer level, not only is it possible to manipulate samples of minute size and quantity, it is often more beneficial, providing increased control and efficiency compared to similar large scale processes [Serra et al. (2005)]. These devices provide benefits in the material synthesis and sample separation and focusing with direct applications in the biotechnology and chemical analysis areas, and especially in the development of Lab-on-a-Chip applications. The ultimate goal of Lab-on-a-Chip is to develop a palm-sized device in which chemical analysis can be performed in a cheap and effective way. Due to its small size, only small samples would be required for analysis. In addition, it would have the ability to produce immediate results, allowing for field portability. The chip may also contain miniaturized components such as pumps, mixing chambers, and detectors that are required in sample analysis.

Although the goal of Lab-on-a-Chip is still far from being realized, achievements have been made with respect to individual components, and increase in efficiency to certain processes that may become crucial to the operation of these devices. To aid in the overall research and development of these microfluidic devices, a soft lithography rapid prototyping method was developed, producing polymer-based microfluidic devices [Xia and Whitesides (1998)]. Their benefits over traditional glass and silicon based devices is that they can be produced at a fraction of the cost, utilize less hazardous materials and are quicker to fabricate. Based on this technology, further advances and development of soft lithography have also been made.

It is important to highlight that, the field of microfluidics is still at its infancy, with many unknown phenomenon that still requires research and development. In addition, many processes traditionally performed with large bench-top systems and their compatibility to the field of microfluidics and more specifically, to polymeric devices remains unknown.

1.2 Justification of Research

Soft lithography for the fabrication of polymeric microfluidic devices is a well known and extensively researched process. In general, the fabrication procedure for creating polymeric microfluidic devices have been thoroughly developed and optimized. However, many applications for which soft lithography can be applied to have yet to be realized. Thus, several applications have been chosen for the use of soft lithography. Applications discussed in this thesis relates to microfluidic temperature measurements, capillary isoelectric focusing (with and without carrier ampholytes), and micromixers. Temperature measurement has always been difficult to implement, or incompatible with polymeric materials. However, by adapting the soft lithography process, an easily implementable method was devised to overcome these incompatibilities. Isoelectric Focusing with thermally generated pH gradients represents a new method for sample isolation without the use of carrier ampholytes. With soft lithography, many different chip configurations can be tested in a short period of time, allowing rapid experimental verification of their operation. Capillary isoelectric focusing devices have always been difficult to fabricate. With the aid of soft lithography, the fabrication process was shortened with preliminary data showing comparable results with commercially available CIEF devices. Soft lithography also has benefits in the fabrication of micromixers.

1.3 Objectives of Thesis

The objective of the thesis is to utilize the soft lithography fabrication process for various applications which previously have been performed using other means. The main applications investigated include microfluidic thermometry, isoelectric focusing with thermally generated pH gradients, traditional capillary isoelectric focusing with carrier ampholytes, and micromixers. Due to the requirements and specifications of each application, the fabrication processes differ and are discussed. In addition, experimental validation of each is provided where possible. The performances and benefits of these fabricated devices are compared to current techniques and commercial devices.

In chapter 2, background information pertaining to each application is provided. Fundamental fluid flow mechanics and governing equations are discussed as it pertains to microfluidic devices. The soft lithography fabrication process is briefly reviewed, with an emphasis on the rationale for developing polymeric devices. Microscale fluid flow and thermometry techniques, as an integral part of the design and validation process, are discussed. In addition, electrophoresis separation techniques for biological sample analysis are provided.

In chapter 3, a detailed explanation of the soft lithography and replica molding are discussed. In addition, issues relating to the fabrication processes such as operation of the equipment, commonly encountered defects, and choice of substrate material are also mentioned.

In chapter 4, a new thermometry method and the design process involving the use of a temperature dependent fluorescence thin film PDMS is introduced. The rationale for its development, especially compatibility issues between commonly used fluorescent Rhodamine B dye with polymeric materials, is highlighted. As few researchers have attempted to spincoat PDMS, experiments correlating and optimizing the thin film thickness were performed and shown. In addition, observed problems from the fabrication process are mentioned and addressed. The thermometry performance of the thin film is presented and compared with in-channel Rhodamine B method.

In chapter 5, the thin film thermometry method developed in the previous chapter is applied to analyze heat transfer and distribution inside a isoelectric focusing device that utilizes thermally generated pH gradients for sample separation. Design factors affecting the heat distribution throughout the device are discussed and experimentally verified with various chip layouts. Issues relating to their operation such as thermal runaway, electrolysis, and bubble formation are addressed. The results are compared to simulations for different applied powers and an estimated pH range is provided.

In chapter 6, with the use of soft lithography a common method for capillary isoelectric focusing with the use of carrier ampholytes is modified to operate using a polymeric (PDMS) device. Performance comparisons with original silica capillary based design are shown. In addition, fabrication issues and experiments aimed at resolving these problems are addressed.

In chapter 7, a brief discussion on micromixers is provided. Common issues such as flow mechanism selection and implementation are discussed, with an emphasis on soft lithography fabrication. A 2D simulation of a typical micromixer is presented to highlight the difficulties their design. Methods for flow visualization are also discussed.

Chapter 2

Literature Review

2.1 Introduction

Traditionally, the role of a mechanical engineer is to understand the mechanics of a system. Typically, it involves building a system, understanding the stress and strain, modeling heat and mass transfer, and ensuring that as a whole, the different components of a system are compatible and working harmoniously with each other. Often, the topic of microfluidics is met with a hint of anxiety and fear for mechanical engineers, as it is a multi-disciplinary field involving mechanical engineering, electrical engineering, chemical engineering, and biology. However, upon closer inspection other than the difference in the dimensions, the role of a mechanical engineer in microfluidics remains essentially the same – fabricating the device, modeling and experimental verification of flow rates and heat transfer, and ensuring operational efficiency of the whole microfluidic system. In addition, successful design teams are usually a synthesis of members from each of their respective fields. To effectively communicate and convey ideas, it is especially important for mechanical engineers to possess a basic knowledge of the topics in microfluidics relating to each field. It is with this in mind that the following literature review has been compiled.

This chapter provides background information regarding basic concepts as it pertains to the design, fabrication, and operation of PDMS microfluidic devices. A review of governing equations and fluid flow types in the realm of microfluidics is discussed. Device fabrication, evaluation of material types and the justification for developing polymeric based devices is also provided. A basic review of fluid flow and thermometry methods for the characterization of device performance is given. In addition, due to the many different types of biological sample separation techniques available, a review on the major types is provided.

2.2 Transport Phenomenon in Microfluidics

The selection of a pumping method is an important aspect to microfluidic chip design. In certain tasks, some types of flow are beneficial compared to others and are more easily integrated into select device designs. Thus, a basic review of the different flow types is presented here to aid the reader in understanding the concepts covered in later chapters. However, it is in no way extensive; only background knowledge and text references are provided. For a fundamental review of fluid flow, heat transfer, and transport phenomenon concepts, the readers are referred to texts such as White (1999), Incropera and DeWitt (2002) and Bird et al. (1960). A more detailed overview relating specifically to the physics, chip fabrication, operation, and electrokinetic flows of microfluidics, texts such as Hunter (1981), Li (2004), Tabeling (2005), and Nguyen and Wereley (2006) are excellent review material.

2.2.1 Fluid Flow Governing Equations

Fluid flow in the microscale predominantly occurs in the laminar region, with the Reynolds number being generally a good indication of flow regime (Re = 2300 being the approximate threshold into turbulent flow). The Reynolds number is governed by the equation:

$$\mathrm{Re} = \frac{\rho V D}{\mu} \tag{2.1}$$

where Re is the Reynolds number, ρ is the density, V is the velocity of the fluid, D is the characteristic length of the channel and μ the dynamic viscosity of the fluid. Reynolds number in microfluidic applications are typically in the range of less than 0.1 to 10, which are several orders of magnitude smaller than that required for turbulent flow. Another important factor for consideration is the Peclet number, which is given in one of two forms:

$$Pe = \frac{Vw}{D_a} \tag{2.2a}$$

$$Pe = \frac{Vw}{\alpha_a} \tag{2.2b}$$

where *Pe* is the dimensionless Peclet number, *V* is the velocity of the fluid, *w* is the width of the channel, D_a and α_a are the mass diffusion coefficient and the thermal diffusivity of species “a”. Equation 2.2a is generally used to compare effects of convection to mass diffusion whereas equation 2.2b is generally used for comparison of convection to thermal diffusion effects. In macroscale, the flow velocity is large in magnitude, thus diffusion effects are limited. However, in microscale applications, diffusion gains significant importance as often their orders of magnitude are comparable to that of the numerator (due to slow fluid flow and small channel diameters). Thus, diffusion effects must be considered equivalently. In most micromixer designs where two streams of fluid flow in parallel, mixing is achieved mainly through diffusion; convective mixing through turbulent flow is difficult to perform under common circumstances.

Types of Pumping Methods

Microfluidic systems utilize several different flow generation techniques, such as pressure driven flow, capillary force, electro-osmotic flow (EOF), and electrophoresis. Pressure driven flow is a commonly used and extensively studied method, with predictable flow characteristics and flow profiles in the laminar flow regime. Pressure driven flow is easily established by external high precision syringe pumps. However, ensuring a leakage free connection to integrate between the realms of macroscale and microscale may prove challenging. Capillary force is another important method of fluid flow in which surface tension (where intermolecular liquid-solid force exceeds that of the liquid-liquid interactions) generates a force which propels the bulk fluid. This effect generally occurs with hydrophilic surface conditions. PDMS is hydrophobic by nature, requiring surface treatments such as plasma oxidation [Hellmich et al. (2005)] to become hydrophilic. This method is often difficult to implement when a continuous reliable fluid flow is necessary. EOF and electrophoresis are electrokinetic effects in which an external electric field is applied across a conductive fluid filled microchannel to induce bulk flow or migration of individually charged particles. Due to their relevance in this thesis, a detailed discussion is provided.

Electro-osmotic Flow

When a polar liquid is in contact with a charged surface, the counter ions (ions of opposite charge to the wall) are attracted to the wall surface, forming a dense immobile layer of ions commonly referred to as the Compact layer. The effect of the surface charge penetrates deeper into the fluid, forming a thicker mobile region of predominantly counter ions and some co-ions (ions of the same charge as the surface) forming an overall net charge. This second layer is referred to as the Diffuse layer. Combined, the two layers are called the Electric Double Layer (EDL). At a sufficiently far distance from the surface, there is no net charge, signifying the end of the EDL, as shown in Figure 2.1.

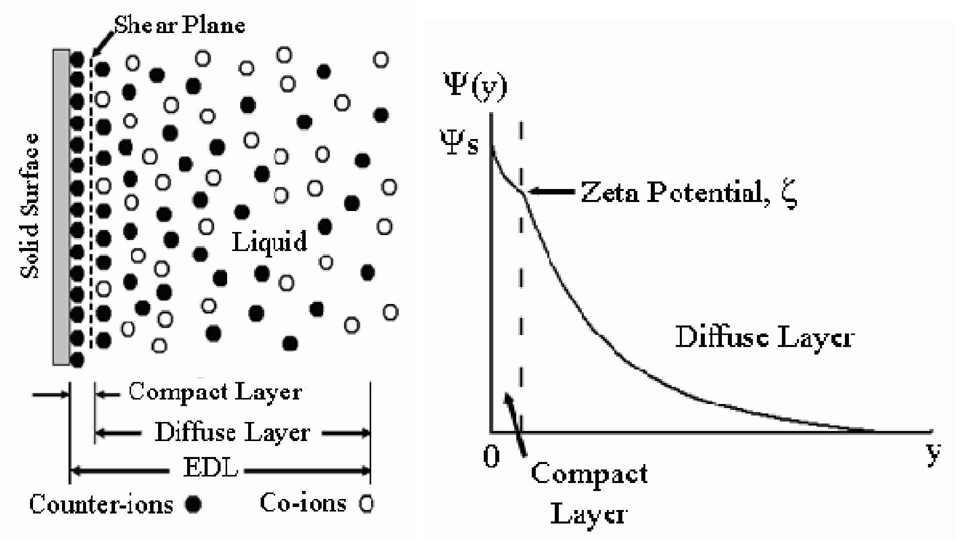

Figure 2.1: Illustration of the EDL [Taylor (2006)].

The potential generated at the shear plane is known as the zeta potential (ζ). Under an applied electric field, the ions at the diffuse layer moves, providing the force necessary to move the bulk fluid. The equations pertaining to the calculation of the EOF were derived by

Tabeling (2005). Most working liquids in microfluidic chips are newtonian and incompressible liquids, which satisfy the Navier-Stokes (NS) equation:

$$\rho\left[\frac{\partial \vec{V}}{\partial t}+(\vec{V}\cdot\vec{\nabla})\vec{V}\right]=-\vec{\nabla}P+\mu\vec{\nabla}^{2}\vec{V}+\rho_{e}\vec{E} \qquad (2.3)$$

where $\vec{V}$ is the fluid velocity vector, P is the pressure, μ is the viscosity, ρ_e the charge density, and $\vec{E}$ the applied electric field strength. The continuity equation is:

$$\vec{\nabla}\cdot\vec{V}=0 \qquad (2.4)$$

The last term of the NS equation refers to the electro-osmotic contribution to the fluid flow. The applied electrical field strength, $\vec{E}$, can be obtained by solving the applied potential field:

$$\vec{\nabla}\cdot(\sigma\vec{\nabla}\phi)=0 \qquad (2.5)$$

$$-\vec{\nabla}\phi=\vec{E} \qquad (2.6)$$

where σ is the electrical conductivity and ϕ is the applied electric potential across the channel. At steady state flow, the acceleration (first) term of equation 2.3 is neglected. Due to laminar flow, the convection (second) term is also neglected. Assuming no pressure gradients exists in the channel, equation 2.3 simplifies to:

$$0=+\mu\vec{\nabla}^{2}\vec{V}+\rho_{e}\vec{E} \qquad (2.7)$$

Using the Boltzmann distribution, the charge density of the electric potential through the equation:

$$\varepsilon\nabla^{2}\Psi=-\rho_{e} \qquad (2.8)$$

where ε is the fluid permissivity and Ψ is the electrostatic potential of the EDL at a specific distance from the wall. An estimate of the velocity of the EOF can be found by combining equation 2.7 and 2.8, and by assuming ideal conditions of flow in the x-direction between two parallel plates spaced apart by a distance of z, the equation is simplified to:

$$v(z) = \frac{\varepsilon E_x}{\mu}(\Psi - \zeta) \tag{2.9}$$

Applying boundary conditions, velocity at the wall surface is zero (or the no-slip boundary condition) since $\Psi = \zeta$. Conversely, at a location just outside the EDL in which $\Psi = 0$, the velocity reaches a maximum, which is represented by the equation:

$$v_{EOF}(z) = \frac{\varepsilon E_x \zeta}{\mu} \tag{2.10}$$

It is of interest to note that the same velocity applies everywhere outside the EDL, giving the signature "plug-like" velocity profile of EOF.

It is important to stress that the maximum velocity depends on the zeta potential, and that there is a rarely stated error related to the measurement. The zeta potential changes according to such variables as solution concentration and pH levels, all of which change during the process of the experiments. Unfortunately, there is no direct detection method for independently measuring zeta potentials.

Electrophoresis

Similar to EOF, when a charged particle is submersed in a polar medium, an EDL also forms around the particle. An external electric field is applied through the channel containing these particles, manipulating their speed such that the particles move through the medium. The derivation can be found from Nguyen and Wereley (2006). Performing a charge balance on the particle:

$$qE_x = 6\pi\mu v_x r_o \tag{2.11}$$

where q is the charge, and r_o is the radius of the particle. The equation can be simplified to:

$$v_E = \frac{2\varepsilon\zeta E_x}{3\mu} \tag{2.12}$$

for a EDL thickness that is comparatively larger than the size of a particle. For EDL thicknesses smaller than the particle, the equation becomes:

$$v_E = \frac{\varepsilon\zeta E_x}{\mu} \tag{2.13}$$

For flows combining EOF and electrophoresis (such as in Capillary Electrophoresis applications covered in a later section), the observed velocity is:

$$v_{TOTAL} = v_{EOF} + v_E \tag{2.14}$$

Electrophoresis plays an important role in Capillary Electrophoresis (CE) applications in which mixtures of proteins or DNA samples are separated due to their inherent surface charge differences. In addition, some variants of electrophoresis based separation techniques intentionally subdue the EOF in the channel by applying certain surface coatings, such that only the electrophoresis component of the velocity is detected.

2.2.2 Heat Transfer

Heat transfer is an important concept in the study of microfluidics, especially when applied electric fields are coupled to the system. At sufficiently high currents, insufficient heat transfer from a microfluidic system can cause severe Joule heating and evaporation effects, leading to bulk fluid loss and eventually arcing.

Similar to macroscale, heat transfer in the microscale is governed by conduction, convection, and radiation:

$$q_{cond} = -kA\frac{\partial T}{\partial x} \tag{2.15}$$

$$q_{conv} = hA(T_s - T_\infty) \tag{2.16}$$

$$q_{rad} = \varepsilon\sigma A({T_s}^4 - {T_{sur}}^4) \tag{2.17}$$

where q is the heat transfer, k the thermal conductivity, T_s the temperature, T_∞ the air temperature, T_{sur} the surrounding temperature, h the convection coefficient, ε the emissivity, and σ the Stefan-Boltzmann constant.

2.2.3 Integration Issues with Lab-on-a-Chip Devices

One of the greatest difficulties in microfluidics lies in the integration of power systems and actuation mechanisms necessary to operate these devices. The foreseen benefits of Lab-on-a-Chip devices lie in its small scale and portability, making them excellent candidates for on-field applications. However, in cases where pressure driven flow is used, external connections to syringe pumps are necessary. For flows requiring electrokinetic manipulation, an external high voltage power source is necessary. Capillary force is a good candidate as a pumping mechanism in field portable devices however flow control is limited, with few design and analysis processes available. Detection systems have been mostly based upon optical microscopy or laser aided systems. Current on-field microfluidic devices mostly depend on measuring changes in the resistance or chemical reactions that produce a visible change in colour in the reactants. These methods are easily implemented, but also limit the number of processes available for in-field detection. With such high expectations in performance given the size constraints, the study of transport phenomenon becomes increasingly important. Through understanding and application of the fundamental physics, Lab-on-a-Chip designs can be effectively modeled and verified experimentally, streamlined to reduce power consumption, and increase overall efficiency.

2.3 Fabrication and Implementation of Microfluidic Devices

There are many different fabrication techniques and materials for the production of microfluidic devices. In the past, these devices were generally composed of silicon or glass substrates, as the technology to manufacture and process these materials, mainly photolithography and etching, were mature and readily available in the electronics industry. An additional benefit is that their surface is negatively charged, taking advantage of their compatibility with electrokinetic transport phenomena.

However, these materials have several disadvantages with regards to their material properties and manufacturing. As a material, silicon is relatively expensive due to its fabrication and refinement process. It is also opaque in the visible and UV spectrum, thus posing difficulties for optical detection systems. Glass is difficult to etch, and correspondingly channels are non-rectangular in shape when wet etching is used. As a result, prototyping silicon and glass microfluidic devices are time consuming and labour intensive. In addition, the chemical etchants used are highly toxic. Therefore, a search for new materials such as polymers and new fabrication methods to accommodate these polymeric devices were sought.

2.3.1 Soft Lithography and Polymeric (PDMS) Devices

PDMS is a common polymeric material for the fabrication of microfluidic devices which is based upon soft lithography and replica molding fabrication techniques [Xia and Whitesides (1998) and McDonald et al. (2000)]. In brief, soft lithography is based upon utilizing photolithographic processes to produce a master containing a positive relief of the micro and nano sized channel features. The fabrication process is advantageous because it is less hazardous and requires comparatively less investment in time and money.

For the fabrication of the master, the surface of a pre-cleaned glass or silicon substrate is modified by creating and printing a design of the microfluidic chip onto it. The substrate is then used as a stamp or a mold to transfer its pattern onto a polymeric material. The advantage of such a system is the low cost and ease of producing the stamp or mold, and the ability to reuse the stamp to create many microfluidic chips of the same uniformity with few defects.

The main benefit of soft lithography is the ability for rapid prototyping. It is an advantageous process for the quick production and testing of micro-channel design prototypes in a laboratory setting; with the proper equipment, a microfluidic chip can be designed, fabricated, and tested in a single day. Usually, this process is not suitable for mass manufacturing for consumer or commercial use.

2.3.2 Advantages and Disadvantages of Polymer Materials

Polymeric devices offer many advantages including rapid prototyping of new designs, lower fabrication costs compared to glass and silicon, biocompatibility and stability over a wide temperature range. Micro-channels can be easily and safely made in polymers by molding or embossing methods compared to etching.

Unfortunately, there are several disadvantages with the material properties of polymers as well. In general, polymers require additional processing steps for surface property control and manipulation. For example, poly(dimethylsiloxane) (PDMS) is inherently hydrophobic to water and with a low zeta potential value which hampers the ability of electrokinetic effects to achieve fluid flow. Even though the zeta potential can be increased through the use of surface treatments such as plasma, the resulting zeta potential is unstable, with the charge reverting close to its native value within 24 hours. Another problem with polymeric materials such as PDMS is its absorption and adsorption of certain fluorescent dyes such as Rhodamine B and certain proteins. A close examination of Rhodamine B absorption into PDMS will be provided in detail in Chapter 4.

2.4 Characterization Techniques of Microfluidics Devices

2.4.1 Flow Techniques

An important aspect of designing microfluidic devices is the ability to accurately monitor and characterize device performance. Fluid flow detection has been a hot field of research and measurement methods have been well established. For EOF applications, the current monitoring technique [Huang et al. (1988)] provides a good estimate of flow rates. In pressure driven flow, syringe pumps provide flow rate readouts, reliable for single channels. For more complex designs, micro-PIV and other fluorescent flow visualization techniques can be utilized. A good review of flow monitoring techniques is provided by Mosier et al. (2002), and Sinton (2004). Flow measurements are essential in the study and validation of micromixers.

2.4.2 Thermometry Techniques

Unlike fluid flow measurements, discussions of heat transfer effects are often neglected. A common misconception is that, due to the small size and large surface to volume ratio of common microfluidic channel dimensions, heating due to electrokinetic effects and corresponding Joule heating, can be easily dissipated and thereby neglected. However, Venditti et al. (2006) discovered that for some electrolytes in PDMS/glass and PDMS/PDMS systems, a change in 60^{o}C can produce an increase in 50% of the zeta potential (although at a high concentration of 10mM KCl), and thereby underestimate the actual flow rates in EOF applications. In addition, PDMS is an insulative material having poor heat transfer characteristics, which may cause unintended high temperature regions killing biological cell specimens. Thus, providing temperature measurements especially in applications where the performance is highly sensitive to temperature (such as for Isoelectric Focusing with thermally generated pH gradients – to be discussed in Chapter 5), is integral to the design and verification processes. Owing to the lack of an all encompassing microfluidics thermometry review, an attempt is made to provide readers with several frequently used and most up to date methods.

A categorization of microfluidic thermometry methods can be separated into electric and spectroscopic types. Electric methods mainly involve the use of resistances (changes in fluid resistance with temperature) and externally mounted [Nishikawa and Kambara (1996)] or embedded micro-thermocouples [Allen et al. (2003)]. Typically these methods are sensitive to external effects and may react with channel chemistry. Spectroscopy techniques (studying the effects of radiation and matter), can be further separated into non-fluorescent and fluorescent techniques.

Thermochromic Liquid Crystals (TLC) has been successfully employed by Chaudhari et al. (1998) and Noh et al. (2005) for non-fluorescent microfluidic thermometry. Encapsulated liquid crystals are suspended in aqueous solution and injected into the microchannel. Once excited with white light through focused optical fibres connected to a halogen lamp, light is reflected whose wavelength is strongly dependent on temperature. Different formulations of the liquid crystals provide sensitivities in different ranges, but all exhibit colour changes in this sequence: colourless, red, orange, yellow, green, blue, violet, and colourless at high temperatures. Minimum resolution of ±0.5°C can be obtained. However, the particles may affect or constrict fluid flow, and evaporation changes the formulation and sensitivity of the method. Proton Nuclear Magnetic Resonance (NMR), employed by Lacey et al. (2000), was successfully applied to electrolyte temperature measurements in CE applications. This non-invasive method is based on the detection of the shift in proton resonance frequency detected from water, achieving sub-second temporal resolution, spatial resolution of 1mm, and an accuracy of 0.2°C which is dependent on the probe. The detection of water absorption of incident light has also been suggested as a non-invasive method by Otal et al. (2003) and Thompson et al. (2004). As temperature increases, the strength of hydrogen bonding decreases, thereby shifting and increasing their absorption bands. Only one of two water absorption bands (only the second overtone or 970nm) is detected. The setup consists of a light emitting diode (LED) with maximum emission at 950nm, and 2 photodiodes for detection. By empirically calibrating the detected signals, an equation of temperature versus absorption for 15°C to 90°C was found with 0.1°C error and 0.07°C precision accounting for signal to noise ratios. Another similar non-invasive method is Raman Spectroscopy and was applied to microfluidics thermometry by Davis et al. (1993) and Liu et al. (1994). When laser light excites water molecules (particularly the OH ion), the corresponding light is scattered and detected, with most of the light experiencing Rayleigh scattering where photons are at the same frequency (energy) as the laser source (representing an electron jump from ground state to energized level and back to ground state). A small amount will undergo Stokes scattering where the detected photons are shifted in frequency corresponding to a lessening of photon energy (representing an electron jump from ground state to energized state, but returning to another energized state). An even smaller amount will undergo anti-Stokes scattering where the detected photons have gained energy (corresponding to electrons jumping from energized states to higher states and back to ground state). The ratio of Stokes and anti-Stokes scattering is temperature dependent, however due to difficulties in its measurements, the method is rarely used. However, the effects between temperature and the electron cloud of OH can be measured *via* Raman Spectroscopy and used for thermometry purposes providing ±1^{o}C accuracy, ±0.1^{o}C precision, and 1-5μm spatial resolution. The process is limited to providing single point measurements.

General fluorescent based thermometry techniques for microfluidics involves fluorescent particles whose intensity varies depending on its temperature. Ross et al. (2001) described a simple process in which Rhodamine B, whose intensity is temperature dependent, is mixed into the bulk fluid and injected into microchannels, with possible applications for detection of Joule heating using electrokinetic effects. Observations were performed on an optical microscope, with a mercury arc lamp and filters designed for use with Rhodamine B fluorescence (energy excitation of 500nm to 550nm and emission >565nm). A CCD camera initially detects the room temperature intensity, and subsequently the operational intensity of a Rhodamine B filled microchannel during heating. Once normalized, results are compared to an empirical calibration curve relating normalized intensity to temperature, providing a temperature estimate of the fluid, achieving errors of maximum 3.5^{o}C, spatial and temporal resolutions of 1μm and 33ms, respectively. However, the method is prone to absorption problems in polymeric materials, and possible electrophoresis effects in EOF applications. A similar method was introduced by Sakakibara and Adrian (1999) (although not directly applied to microfluidics) in which two-colour laser induced fluorescence is used. Rhodamine B is mixed with Rhodamine 110 (whose intensity is relatively independent of temperature), and excited by 488nm laser. Two CCD cameras, one fitted with 570nm and the other fitted for emission of 495nm to 520nm, detected intensity of Rhodamine B and Rhodamine 110, respectively. By normalizing their intensities for a specific temporal and spatial coordinates, temperature can be measured independent of such factors as excitation light flux. Accuracy is estimated at ±1.4K. Another method utilizes a different type of fluorescent particles that is fabricated as a thin solid film [Davis and Das (2005)]. The film is formed by melting and cooling onto glass slides the synthetically created compound. The film is excited with 360nm monochromatic light from a 500W Xenon lamp source, with emissions detected at 520nm. The film exhibited reproducible fluorescence characteristics in a temperature range of 30^{o}C to 100^{o}C. However, the fabrication method of the film does not allow for the control of the film thickness, and has not been implemented in microfluidics. Fluorescence Lifetime Imaging (FLI), as demonstrated by Benninger et al. (2006), utilizes a fluorescent particle in which the decay in intensity of the fluorophore predictably varies with temperature, and is used for measurements. With this method, observed results are independent of dye concentration, excitation intensity, and provide precision of $\pm 1^{o}$C.

2.4.3 Electrophoresis Separation Techniques for Biological Sampling Applications

Electrophoresis based separation are powerful analytical techniques based upon the migration of particles with different net charges in a solution under an applied electric field. These techniques provide information on sample composition, purification for further analysis, and insight into the chemical structures of the samples themselves. One of the benefits of using microfluidics in performing biological analysis is that complex sample mixtures can be isolated to their fundamental components from small quantities in relatively short time scales.

For their design, it is important to understand the fundamental operations of several main electrophoresis based separation techniques. However, their development spans many different ingenious designs, with some developed for specific niche applications such that a review of all the separation techniques would be difficult. The reader is referred to other works such as a historical review by Righetti (2005), and other books providing fundamental concepts such as by Baker (1995), Kuhn and Hoffstetter-Kuhn (1993), a more practical oriented review of the techniques by Westermeier (2001), and a more in-depth discussion of Isoelectric Focusing (IEF) theory by Righetti (1983).

Electrophoresis separation techniques can be divided into three main groups: Zone Electrophoresis (ZE), Isotachophoresis (ITP), and IEF. In a typical ZE application, samples and electrolytes are injected into the mixing chamber. Under an applied electric field, the samples separate according to the magnitude of their net charge, and migrate towards the anode or cathode according to their polarity. Due to their difference in electrophoretic mobilities, the samples will reach the anode or cathode at different times. Inherently, this method involves EOF, such that the detected velocities are a combination of the electrophoretic and electroosmotic velocities. In the past, ZE had suffered from zone broadening, in which samples diffuse and spread apart slightly due to convective diffusion through Joule heating. Gel type electrophoresis techniques, in which separation is performed through a porous gel, allow for better heat dissipation (due to large surface to volume ratio), and provides additional separation abilities through sieving of molecular sizes larger than the gel pore sizes. However, disadvantages include adsorption and reactions with the gel, slow separation times and high labour intensity. Due to these problems, Capillary Electrophoresis (CE) techniques were developed in which small capillaries such as those used by Mikkers et al. (1979) were successful in reducing convection induced zone broadening. Silica capillaries [Jorgenson and Lukacs (1983)] were later used to allow for better integration of detection systems utilizing UV 280nm.

ITP involves the use of two different buffers, with the sample to be separated, sandwiched in between the two boundaries. The leading buffer has the highest mobility whereas the trailing buffer has the slowest mobility compared to the sample's components. Upon application of an electric field at constant current, the samples segregate within the boundaries as they migrate due to electrophoresis, with EOF suppressed. Due to the conduction of the ions, the samples and buffers travel at the velocity of the slowest mobility (trailing buffer). Within the sample boundary, particles with higher (or slower) mobilities than the average value will move towards the leading (or trailing) buffer, thereby segregating the sample. An advantage to this method is that, no diffusion problems occur, as any diffused samples are repelled back into place due to the differences in the mobility. However, the ITP process can only separate samples consisting of all anionic or all cationic particles; the separation does not work for a mixture of oppositely charged particles. ITP in general has evolved to utilizing capillaries and the process is known as Capillary Isotachophoresis (CITP) and is still actively in use. A good review of latest research can be found by Gebauer and Bocek (2002), with additional benefits as pre-separation techniques for CZE applications [Hirokawa et al. (2001) and Fung and Tung (2000)].

As Capillary Isoelectric Focusing (CIEF) is mainly covered in this thesis, a deeper understanding of its operation is included. In CIEF and related applications, pH gradient and electrophoresis effects combine to achieve sample separation in a capillary with EOF intentionally suppressed. Microscopically, different biological samples (such as protein types) will have different regions of positive and negative charge. Thus, the net charge as a whole may vary slightly for different protein samples. In addition, the overall charge of the substance also depend upon the pH (amount of anions and cations) surrounding the sample. Depending on the overall (combined inherent and surrounding) net charge, the sample will migrate towards the electrode of the opposite charge under an applied electric field. As it migrates, its velocity decreases until it reaches a point along the pH gradient in which the surrounding ions exactly balances the charge of the protein sample; the sample is neutral, and has approached its isoelectric point (pI). This separation technique can achieve separation bands with extremely narrow zones compared to that obtained from ZE methods. Samples are focused at fixed locations where the pH corresponds to the sample's pI, and are in a normalized distribution. Diffusion effects are minimal, as the diffusion occurring at the fringe of the focused zone is balanced by electrophoretic forces acting on the sample. A disadvantage of the method is that only charged particles such as proteins and ampholytes can be separated, and must have a pI value within the range of pH provided.

With CIEF, there are various ways of generating the pH gradient, among them the most well known method is the use of Carrier Ampholytes (CAs). Other CA-free focusing methods such as utilizing thermally generated pH gradients are also possible. A good review of such methods and general discussions of IEF process considerations can be found in Huang's (2003) PhD thesis. CAs are a family of synthetically made chemicals that are of low molecular weight, good conductivity, high buffering capacity for forming stable pH values, and are soluble in water. Typical CAs samples contain hundreds of ampholytes of slightly different pI values over a certain pH range. Many different values are necessary to generate a linear pH gradient. During CIEF, CAs are injected into the capillary. The cathode reservoir is filled with a basic solution while the anode reservoir contains acidic solution, with the pH values of both being higher and lower than the maximum and minimum pH range of the CAs, respectively. Initially, the CAs are randomly distributed throughout, with the solution having an average pH value. Upon application of a constant voltage electric field, CA with a lower pH than the average will migrate towards the anode while those of higher pH will migrate towards the cathode. For CAs at the extreme ends of the pH range, they will try to migrate into the reservoirs, but will be prevented by the pH of the reservoirs, thus fixing them into place. Subsequently, all the other pH ranges of the CAs align accordingly [Baker (1995)] forming a linear pH gradient.

Another method of pH gradient generation is through controlled Joule heating of the solution. When an electric field of constant power is applied to a non-uniform cross-sectional channel, the Joule heating created is also non-uniform throughout the channel, thus creating a temperature gradient throughout the channel length. The buffer, typically Tris-HCl, is chosen due to its pH dependence with temperature. The temperature distribution directly dictates the pH distribution along the capillary channel. The temperature distribution can be modified directly by changing the power input or by choosing the orientation (angle of divergence) of the channel prior to use. This method has been previously shown as a proof of concept [Huang and Pawliszyn (2002)]. In addition, the phenomenon has been modelled [Kates and Ren (2005)]. By performing experiments aimed at understanding the factors affecting temperature gradient, the corresponding pH values can be altered which ultimately affects the performance and efficiency of IEF designs. As a chapter of this thesis is devoted solely on experimental verification of thermally generated pH gradients, a more thorough discussion of this topic will be provided in Chapter 5.

Chapter 3

Soft Lithography and Replica Molding

3.1 Introduction

Soft lithography and replica molding is the process in which a polymeric microfluidic device is fabricated. This chapter will discuss the fabrication process in detail, discussing the required equipment and parameters which must be optimized to provide consistent and uniform PDMS surface properties. Since some of the chemicals used for the process can be dangerous, a brief summary on important safety issues and handling information will be reported. As well, for each fabrication step, this report will evaluate other alternative technologies available and how closely it can achieve the desired outcome. Common defect problems and design constraints for working with PDMS will also be discussed. By properly understanding all the factors affecting the fabrication process, a better insight can be gained and thereby improve the chances of producing high quality microfluidic chips.

3.2 Overview

The process of soft lithography and replica molding can be split into two portions: the creation of a master mold, and the creation of the subsequent individual polymeric microfluidic device. An overview of the fabrication process is shown in Figure 3.1.

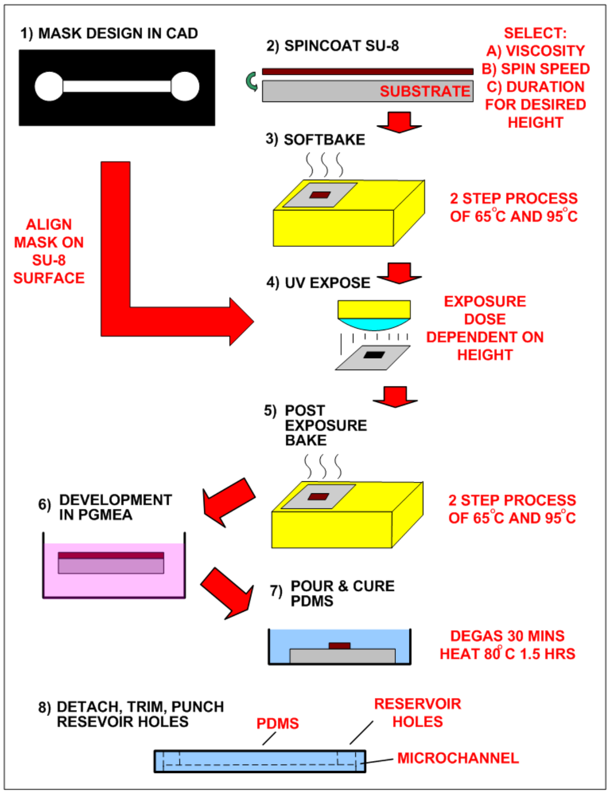

Figure 3.1: Overview of soft lithography and replica molding fabrication process [after Xia and Whitesides (1998)].

The creation of the master involves the following procedure. First, a substrate is dehydrated at 200°C for 20 minutes, and cooled to room temperature for 15 minutes. An SU-8 photoresist with the correct viscosity corresponding to the desired thickness is chosen and deposited onto the wafer through a spincoater. The wafer is then soft baked initially at 65°C, then at 95°C, and then cooled down through several intermediate steps. After cooling in room temperature for 15 minutes, it is exposed to UV radiation underneath a laser-printed mask transparency. Afterwards, the wafers are post exposure baked at 65°C, then at 95°C, and then cooled down to room temperature. Next, the substrate with the photoresist is developed in PGMEA, rinsed, and dried.

The replica molding for creating the PDMS polymer microfluidic chips from the masters is as follows. PDMS pre-polymer in a 10 to 1 ratio of base to curing agent is mixed and poured onto the masters. The mixture is degassed in a vacuum oven at room temperature for 30 minutes. The mixture is then heated at 80°C for 1 hour at atmospheric pressure.

At every step, there are many variables that can greatly affect the final quality of the microfluidic device and the overall fabrication process. This chapter will discuss in detail, each of the steps involved in fabricating a PDMS fluidic chip.

3.3 Mask Fabrication

Soft lithography begins with a design that is printed onto a mask. A mask contains transparent and opaque regions corresponding to the patterns which are transferred onto the photoresist for the master fabrication. The photoresist used is SU-8, a negative photoresist that, when exposed by UV light, undergoes crosslinking thereby hardening the material and reducing the etching rate compared to non-crosslinked material. Therefore, the transparent regions on the mask must correspond to the raised channel regions on the master.

3.3.1 Designing the Layout

By using Computer Aided Design (CAD) programs, it is possible to create the blueprints for any microfluidic device layout with very minimal costs. Once the design is complete, it is printed onto a mask, either directly using a laser printer with a transparency medium, or using an electron or laser beam source directed onto a chrome mask.

There are two main types of masks commonly used for soft lithography applications. Chrome masks are used when high resolutions and small feature sizes in the range of 10 μm to 500 nm are required for the microfluidic channel layouts. Laser printed transparency masks are used when the channel widths are larger than 10 μm. It is interesting to note that the channel size in the fabrication of the master is dependent on the resolution of the printed mask; the widths and lengths of channel structures depend on the printed mask alone, however, the depths obtainable in the channel structures are dependent on the spincoated thickness of the photoresist, which will be discussed further in this chapter.

3.3.2 Chrome Mask

The utilization of a chrome mask can bring benefits in specific applications, such as the manufacturing of small rectangular posts for enhancing turbulent mixing in high Reynolds number flow [Nguyen and Wu (2005)], as points of adhesion for seeding and growing cells [Tan et al. (2004)], or as structural support of microchannels consisting of small heights but large widths which are prone to collapse. Due to its high costs and difficult fabrication process, all applications discussed in this report do not involve the use of chrome masks.

3.3.3 Laser Printed Transparency Mask

A more common method for producing masks in soft lithography applications is the use of commercial or “off the shelf” laser printers. Mask designs are printed using monochrome laser printer onto a normal transparency film. For laser printers, the constraining variable is the dots per inch (dpi) achievable by the printer. Commercial laser plotters can achieve a resolution of 20,000 dpi providing minimum feature sizes of approximately 12.5 µm. Due to the high initial and maintenance costs of such a printer, usually the design is outsourced.

Lower resolution printers may be utilized depending on the application but should be used with caution. For example, transparency masks can be printed with a laser printer with 2400 dpi resolution, which can be utilized to fabricate structures larger than a width of approximately 500 µm. However, as the required feature sizes (such as channel width) decreases, the powder particles of the laser printer becomes relatively large compared to the channel width. In the extreme case, where the structures are at a scale that is just resolvable by the printer, certain sections of the channel will be blocked.

3.4 Substrate Types and Preparation

After the mask is obtained, the actual fabrication process begins with the selection of the substrate. The photoresist is then applied to the chosen substrate to form the master mold. The most common substrates used are glass and silicon. Glass substrates used in the fabrication of microfluidic devices are of the 1” by 3” microscope slides or 3” x 4” rectangular slides. These slides are inexpensive to use, with the average price of $0.50 for a microscope slide and $7.00 for a large slide. However, these have to be cleaned either using RCA or piranha-etch cleaning processes. In addition, due to its amorphous molecular structure, typically glass has a high degree of surface roughness, providing poor adhesion. Subsequently, these substrates require a more complicated fabrication process to compensate for their poor physical features, and also detrimentally affecting the reusability of the finished master. Only simple (one level) fabrication involving relatively large dimension structures (greater than 500 μm in both length and width) should be made on glass substrates. Large surface area structures provide more points of contact between the photoresist and the substrate, providing better adhesion properties and subsequently improving reusability.

On the other hand, silicon substrates are regularly used in the electronics fabrication industry, in which tight constraints such as surface uniformity and flatness is tightly controlled. Thus, the surface roughness is small and the substrate is uniform. This helps promote adhesion between the wafers and that of the SU-8 photoresist. In addition, no cleaning is necessary, as silicon wafers are fabricated directly for clean-room facility use. However, the disadvantage includes its relatively high costs of approximately $25.00 per wafer. In addition, due to the larger surface areas, more photoresist is required for spincoating. To increase the cost effectiveness, several designs are usually combined into each silicon wafer.

It is possible, but rare for PDMS to be used for substrates. Due to the softness of the PDMS material, the substrate may deform, such that it is harder to control the accuracy of the relief structures. Any errors would be correspondingly transferred onto the final PDMS product.

Even though the soft lithography fabrication process does not require a clean-room environment, it is important that the air is dust-free. In addition, all substrates should be cleaned prior to use. Any dust particles contaminating the substrate during photoresist deposition or during subsequent soft baking will distort the surface. For example, if the substrate contained dust particles during SU-8 deposition and spincoating, the contaminants acts as barriers to the flow of the photoresist, creating streaking patterns throughout. In addition, if dust particles fall onto the substrate during soft baking, these will result in halo patterns and pits surrounding the particles, as shown in Figure 3.2.

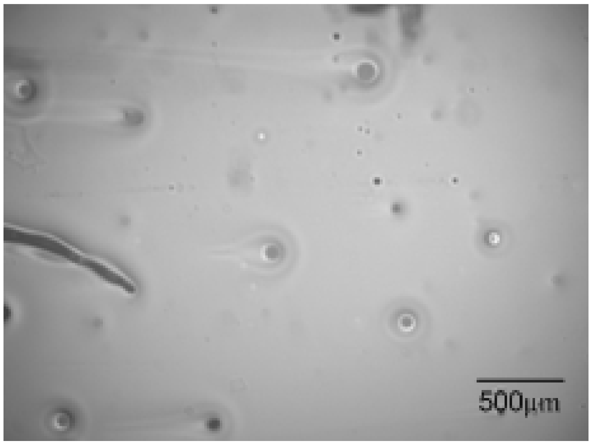

Figure 3.2: Halos and pits surround locations of bubbles formed during spincoating.

Thus, air filters and frequent equipment cleaning should be implemented to reduce dust, and substrates should be pre-cleaned using piranha-etch or RCA cleaning before photoresist deposition.

Prior to the depositing of photoresist, the substrate should be heated to 200°C for 20 minutes to dehydrate the substrate surface. SU-8 is not compatible to water, such that any water vapour residue residing on the substrate will cause poor adhesion. Afterwards, the substrate should be cooled in room temperature for at least 15 minutes before photoresist deposition. Due to the difference in thermal expansion of SU-8 compared to glass or silicon, it is important to reduce the possibility for thermal stresses by spincoating only after sufficiently cooling substrates to room temperature.

3.5 Photoresist Spincoating

The photoresist used for spincoating is SU-8. It is a toxic substance, and should be handled with care. In the spincoating process, the spincoater is important for achieving the desired thickness and quality of the coating. Thus, this section discusses SU-8 properties and the intricacies of spincoating.

3.5.1 SU-8 Photoresist Properties

In general, photoresist can be split into two groups: positive and negative photoresist. For positive photoresists, areas exposed to UV light will undergo a reaction in which the material will soften, and be susceptible to a chemical developer. Correspondingly, the mask design will have transparent and opaque areas corresponding to unwanted and wanted areas on the photoresist, respectively. For negative photoresist such as SU-8, the reverse is true. Once exposed to UV light, the exposed areas undergo crosslinking, thereby hardening the exposed material. In this case, the unhardened resist is developed and washed away.

SU-8 is a polymer material which undergoes crosslinking when subjected to UV light. The crosslinking process is extremely complex. In brief, when the SU-8 is exposed, the compounds inside the photoresist undergo a reaction, dissociating and forming an acid as one of its products. The acid initiates the crosslinking process by reacting and allowing for the combination of multiple chains. This process is thermally driven during the post exposure bake step, and ultimately forms a stable network of monomers with an average of 8 monomers connected together throughout the material (Figure 3.3) [Teh et al. (2005)].

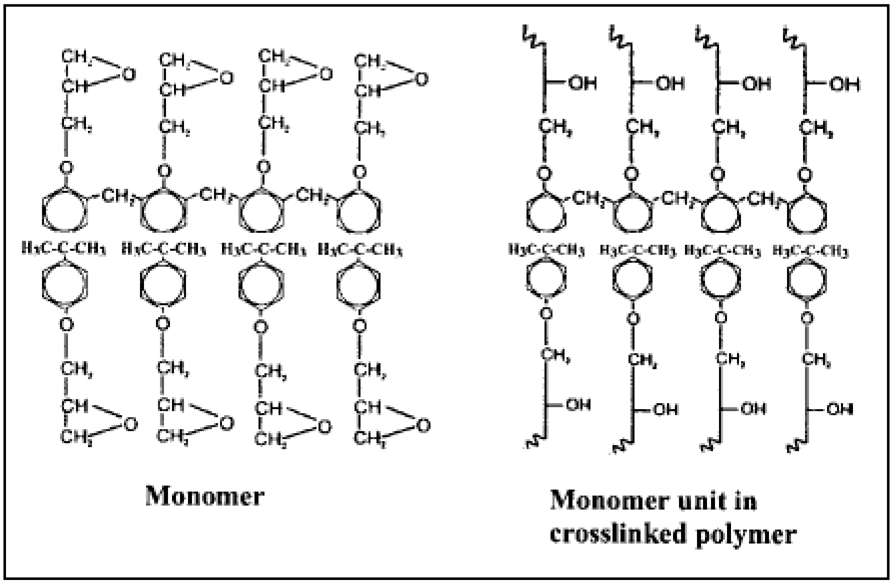

Figure 3.3: Diagram of Uncrosslinked and Crosslinked SU-8 Polymer [Teh et al. (2005)].

The advantages of SU-8 include the ability for achieving high aspect ratios compared to other photoresists with maximum structure heights of 2 mm, straight side wall profiles after chemical development, and uniform thickness during substrate deposition. The disadvantages include reported shrinkage of 7.5% upon curing at a postbake temperature of 95°C, and its inability to reflow after crosslinking. Heating SU-8 also causes the material to crosslink, thereby hardening the polymer material and increasing its resistance to developing solution.

With the introduction of SU-8 2000 series (MicroChem Corp., Massachusetts) the original SU-8 is becoming obsolete. The older version utilized a gamma-butyrolactone (GBL) solvent. Even though it provided high solvency and low cost, it provided poor adhesion on glass and silicon. During initial experiments in which the old series is used, cracking of the resist features can be observed if the substrate is cooled too fast. Thus, tight thermal control and slow cooling of the SU-8 structures is required. Cracks and voids formed in this way occur at the substrate-photoresist interface and propagate through to the resist surface. The newer version utilizes cyclopentanone as the solvent. It has similar properties as GBL, but provides improved adhesion, uniform spread of photoresist on low energy substrates, and faster drying times, potentially increasing the turnover rate of the fabrication process. In addition, a reduction in thermal stresses is observed, thus lowering the required amount of time for substrate cooling.

It is interesting to note that, there appears to be some incompatibility if both series are utilized to create mutli-level structures or as a method for increasing structure height. During one set of experiments, SU-8 5 and 2075 were used to create an adhesion layer of 5um, and an intended channel structure height of 120um. However, the resulting channel height was only 60um. More of the SU-8 2075 was spun off the substrate during spincoating, due to the different surface properties between depositing onto the adhesion layer or directly on glass. In addition, some spincoating exhibited receding of the bulk channel layer after spincoating and subsequent baking, possibly due to a more hydrophobic surface condition existing between the two SU-8 types.

3.5.2 SU-8 Handling

Due to the solvents involved in the SU-8, the photoresist is a relatively toxic material and special handling equipment is required. It is a combustible material, and must be stored in a cool and dark environment, since crosslinking can occur in sunlight or heat. When working with the material, proper ventilation or fume hood is required. It can cause irritation to the skin, eyes, and respiratory tract; therefore proper handling must be followed. When handling SU-8, rubber gloves and safety goggles are required. NIOSH or self-contained breathing apparatus may be required for prolong exposure. The toxic portion of SU-8 is the solvent. Ingesting high concentrations of GBL has caused reversible coma. GBL is also easily absorbed into the skin, such that the toxicity for oral ingestion and skin contact is essentially equal.

3.5.3 Spincoater Specifications

For all fabrication purposes involving photoresist deposition and PDMS spincasting (discussed in Chapter 4), a Cee Model 100CB (Brewer Science Inc., Rolla) spincoater and hotplate system is utilized. An important component of the spincoater is the chuck, a circular flat disc attached to the top of the motor in the centre of the spin bowl. The role of the chuck is to apply suction onto the buttom of the substrate, ensuring the substrate remains on the chuck during high speed rotations. A threaded screw with a hole machined in the middle allows the connection of the chuck to the motor, while allowing the application of a vacuum through the hole to an external vacuum pump.

The design of the spin chuck depends on the substrate shape. For silicon wafers that are typically circular in shape, small circular concentric recessed grooves machined along the chuck surface distributes the vacuum evenly throughout the substrate allowing good suction during high velocity spinning. Due to its design, the wafer size must be larger than the spin chuck for proper suction.

When spincoating on glass microscope slides, previously a chuck machined with a recessed rectangular area for placing the slide and a threaded screw with vacuum hole was used. However, it is ineffective, as with repeated spincoating, the SU-8 overflows to the glass edges and penetrates into the vacuum hole. This contaminates the vacuum line, and provides an extra barrier between the glass substrate and spin chuck. Subsequently, the barrier causes improper sealing and insufficient vacuum, hindering the spincoating process. Another spin chuck in which a flat spin chuck with a threaded screw with a vacuum hole but without vacuum grooves is currently used. A circular groove surrounding the threaded screw is machined and inserted with an o-ring washer, which is slightly raised higher than the chuck. When the glass microscope slides are loaded onto the o-ring on top of the spin chuck, a vacuum is created inside the area of the o-ring which provides better sealing, but eliminates the possibility of the photoresist flowing underneath and into the vacuum line.

3.5.4 Spincoater Parameters

The thickness of the deposited photoresist is governed by three main parameters: viscosity (or grade of SU-8), spin duration, and spin speed. A large resistance to flow provides thicker photoresist. The viscosity is directly dependent on the amount of solvent content inside the film. A lower SU-8 grade number corresponds to a higher solvent content, which allows for thinner resists to be created for a specific velocity. Higher spin speeds and longer spin durations also creates thinner photoresist films.

Once a desired thickness is chosen, a grade of SU-8 must be chosen according to the desired thickness. In general, the lower grade levels are preferred as the low viscosity photoresists are easier to dispense by pouring directly from the container. In addition, spin speeds between 1000 rpm and 3000 rpm are ideal, as slower than 1000 rpm will create uniformity problems (Figure 3.4 and Figure 3.5).

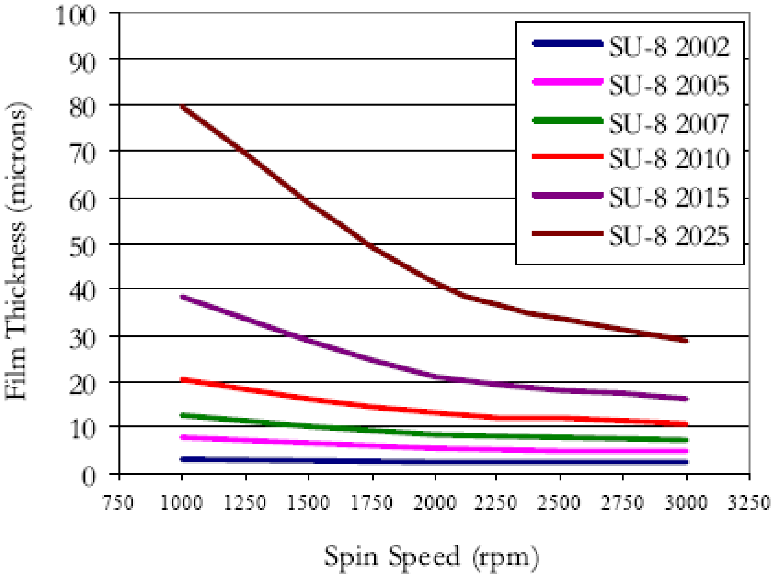

Figure 3.4: Graph of Film Thickness versus Spin Speed for SU-8 2000. [MicroChem Corp.]

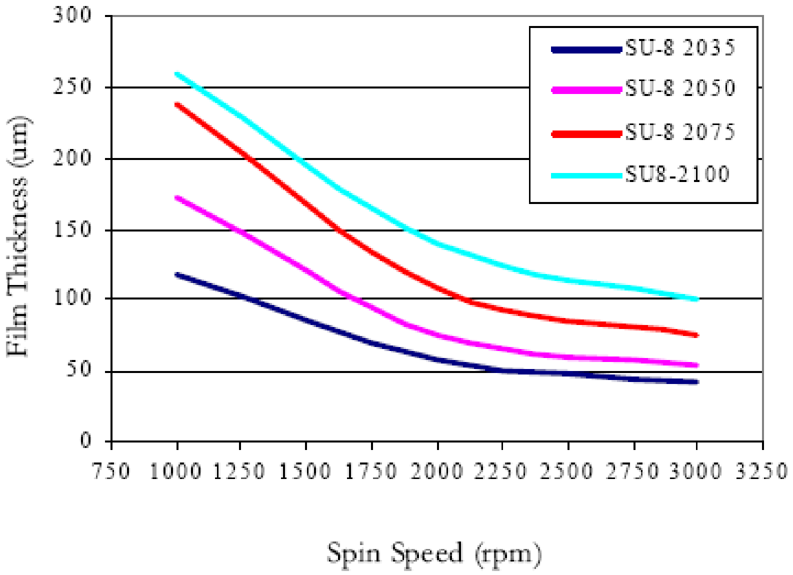

Figure 3.5: Graph of Film Thickness versus Spin Speed for Higher Grades of SU-8 2000. [MicroChem Corp.]

3.5.5 Photoresist Dispensing and Spincoating

After preparation of the substrate during dehydration bake, the slide is then loaded into the spincoater. Previous literature states that syringes can be used to dispense photoresist. However, syringes should not be used as when drawing out the solution, even the lowest viscosity resist may introduce microscopic bubbles which when dispensed onto the substrate, will create defects. Instead, the resist is first slowly poured (to prevent entrapment of bubbles) into a small UV-blocking bottle (Fisher-Scientific), and allowed to sit for 24 hours to naturally degas any trapped air bubbles from the pouring process. Photoresist should never be degassed under vacuum as it evaporates the solvent and thereby changes the viscosity of the resist, making the spincoating process unreliable. The UV-blocking bottle is used for two reasons. First, pouring from the small bottle provides better handling and control compared to pouring from a large bottle. Second, the possibility for contamination of the large photoresist bottle is reduced.

In general, the bottle mouth of the SU-8 is lowered as close to the centre of the wafer or substrate as possible. For glass microscope slides the resist is dispensed along the length of the slide in one pass. Multiple back-and-forth passes creates multiple overlapping surfaces, which traps bubbles in the resist. Due to the circular shape of silicon wafers, when bottle dispensing is used the SU-8 is poured at the centre of the wafer and allowed to pool and spread until the resist covers approximately two-thirds of the diameter of the wafer. Afterwards, the bottle neck is wiped clean after each pour with Kimwipes and acetone. Without cleaning, the excess resist remaining on the bottle neck dries and cracks, eventually dropping into and contaminating the photoresist in the bottle. Utilizing the contaminated resist will produce many pitting defects in the coating.

During photoresist spincoating, the velocity, acceleration, and hold time are the main parameters that affect the spincoating. Higher velocities and accelerations, with longer hold times expel more of the resist from the substrate surface making the film thinner. However, the proper acceleration is dependent on the viscosity of the resist. The spincoater parameters vary slightly depending on the wafer selection and the corresponding dispensing type.

When spin coating on glass microscope slides or SU-8 2005 (or lower grade) on silicon wafers, the spincoating process begins with an acceleration of 100 rpm/s for 5 seconds until 500 rpm is reached, and held for 5 seconds. This allows time for the resist to spread uniformly throughout the glass. Then, an acceleration of 300 rpm/s is used until the desired velocity is obtained. The spinner is held at that speed for 30 seconds to drive off the rest of the excess resist, thus obtaining the desired thickness.

When the bottle dispensing method is used for high viscosity resist on silicon wafers, a large recessed ring appears. The outer ring region consists of the intended height, whereas the inner recessed ring region is approximately 5um to 20um lower. The size of the inner ring region coincided with the area of the pooled SU-8 that was poured onto the wafer before the spinning process. Thus, dynamic spincoating (in which the dispensing occurs during the spinning of the substrate) is used to eliminate the ring defect. The process begins with an acceleration of 100rpm/s for 5 seconds, and held at 500 rpm for 25 seconds. During this time, the dispenser continuously deposits resist at the centre of the wafer, which pools and spreads to approximately two-thirds of the diameter of the wafer within the 25 seconds. At this point, an acceleration of 300rpm/s is applied until the desired velocity is obtained, and held for 30 seconds.

3.5.6 Alternatives for Increasing and Decreasing SU-8 Heights

As the SU-8 2000 series comes in bottles of 500 ml and costs on average $450 per bottle, it is not cost effective to purchase every single grade available. Often to achieve a thicker resist, it is possible to perform a multicoating process. For example, to obtain 80 µm with SU-8 2025, perform the first 41 µm thick coating. After the soft bake process, repeat the procedure again, adding another 41 µm thick coating. However, the soft bake time for the second process will have to be extended to 7 minutes (a general increase of approximately 50%) to compensate for the extra layer of coating.

In addition to building up structures, cyclopentanone can be added to SU-8 to reduce the viscosity and correspondingly, reduce the channel heights. The general formula for the mixture is [The SU-8 Photo-resist for MEMS]:

$$\frac{C_{stock}}{C_{t\arg et}} \times 100 - 100 = V_{cyclopen\tan one} \tag{3.1}$$

where C_{stock} represents the percent solids concentration in the SU-8 stock from which the dilution is made, $C_{t\arg et}$ represents the solids concentration of the target SU-8 grade, and $V_{cyclopen\tan one}$ represents the volume of cyclopentanone required.

3.6 Soft Bake

3.6.1 Conventional Ovens versus Hotplates

A convection oven provides a flow of air or selected gas as the medium in which heat is transferred from the resistance coils in the oven walls to the wafer itself, thereby heating and driving the solvent away from the coating. However, a major problem with these ovens is the formation of stratification regions, or zones of different temperatures inside the oven. This is due to uneven heating and heat losses by the inside air with the surfaces of the oven. Non-uniform heating can severely affect film quality. As well, if a batch of substrates is placed in the oven for heating, substrates closest to the edge may absorb more heat than that of the substrates near the centre due to a lack of heat exchange. Therefore, the substrates in a batch under the exact same heating conditions may produce different results. In addition, the films are cured from the top surface to the bottom surface, due to the heated surrounding air. Thus, a skin layer forms at the film surface before the inside of the film is properly cured. This poses a problem for thick coatings, as solvent is trapped underneath the skin. Upon complete curing of the film, the solvent vaporizes leaving bubbles in the film which leads to adhesion problems or failure.

A hot plate provides consistent temperature and heating throughout the plate. Since the substrate is very thin, and the temperature of the plate itself is relatively constant and easy to control compared to the temperature of the air in conventional ovens, a more controlled and consistent heating effect can be produced, which greatly increases quality of coating and general repeatability.

Since the substrates are placed on the plate surface, conduction is the primary mode of heat transfer. The heat is transferred more quickly and efficiently compared to heat transfer through convection. This allows the substrate to heat up faster compared with ovens. As the substrates are heated from the bottom up, solvents are evaporated from the films before the formation of a skin. Due to the superior heating abilities and short processing times, all heating of the master substrate is performed using hotplates.

3.6.2 Heating Times

Often a two step process is used for soft baking; the substrate is first pre-heated at 65°C, and then soft baked at 95°C. The pre-heat step allows more of the solvent to evaporate from the coating, resulting in better coating uniformity and better resist to substrate adhesion. The heating times at each step depends upon the thickness of the coating itself. It is important to ensure that the environment is dust-free, as the coating is still in a liquid form during curing and will deform to encircle any dust particles.

Afterwards, the substrate is returned to 65°C for 45 seconds, and left in room temperature for at least 15 minutes to sufficiently cool the substrate.

3.7 UV Exposure

After soft baking, the next step in producing the master mold is to place the mask and substrate into a mask aligner and expose the resist to UV light.

3.7.1 UV Source Specifications

An Oriel Mask Alignment Tool and Flood Exposure Source (Newport, California) is utilized for resist exposure. The mask alignment tool includes a precision slide, a mask alignment fixture, a substrate wafer holder, and a photomask holder. These pieces help align the mask with the resist during exposure. The exposure source utilizes mercury lamps to produce the UV light and an i-line filter. It is capable of producing a flux density of 43 mW/cm^2 in the 350 to 450 nm wavelength range. The equipment rests on a vibrationless table to ensure higher accuracy and vibration isolation.

The alignment tool is a fixture that allows for vacuum contact between the mask and the resist surface. After placing the tool underneath the UV light source, opening and closing the light source shutter effectively exposes the substrate to UV light. The exposure time depends upon the flux (which is constant for the power source) and total amount of energy required for the substrate. For example, if 210 mJ/cm2 of exposure dosage is required at 365 nm wavelength, the exposure time would be approximately 5 seconds. However, an integrated control system continuously detects the output energy and automatically operates the shutter to provide accurate exposure doses.

3.7.2 SU-8 Exposure Dose

SU-8 is designed to be utilized in the near UV spectrum, between the 350nm and 400nm wavelengths. A wavelength of 365nm works well and is normally used for exposing SU-8. Photons having the required wavelengths are absorbed and cause a reaction in the material, producing acid which is used to initiate crosslinking during PEB. Above 400nm, the material becomes transparent; the photons are not absorbed and no reactions occur. However, the resist becomes very absorbent to photons with wavelengths below 350nm, such that only a thin top layer absorbs all the photons, leaving the bulk material unexposed (Figure 3.6).

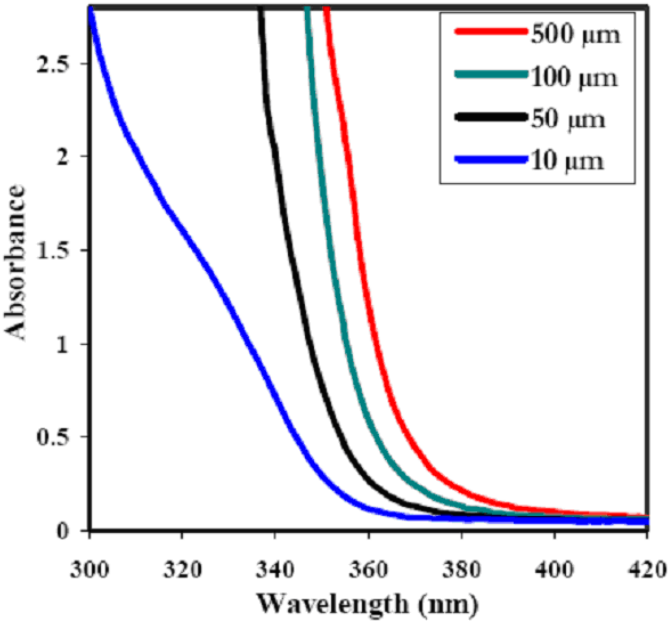

Figure 3.6: Absorbance versus UV Wavelengths for Different Resist Thickness. [MicroChem Corp.]

Usually a filter is used to prevent over absorption of photons with wavelengths below 350nm. The exposure dose is an important parameter and should be controlled to provide proper exposure and crosslinking. In addition, UV light diminishes as it passes through the i-line filter and mask, such that the exposure dose must compensate for this loss. Also, the amount of UV required depends on the substrate material, as reflective substrates such as silicon will reflect more of the UV back into the photoresist compared to glass. The general trend for larger coating thicknesses is to increase the exposure energy accordingly. Thus, a calibration curve should be performed to analyze the ideal UV energy required by the machine to expose the resist, accounting for all the losses. A general film thickness versus exposure dose for reflective and non-reflective surfaces is presented (Figure 3.7).

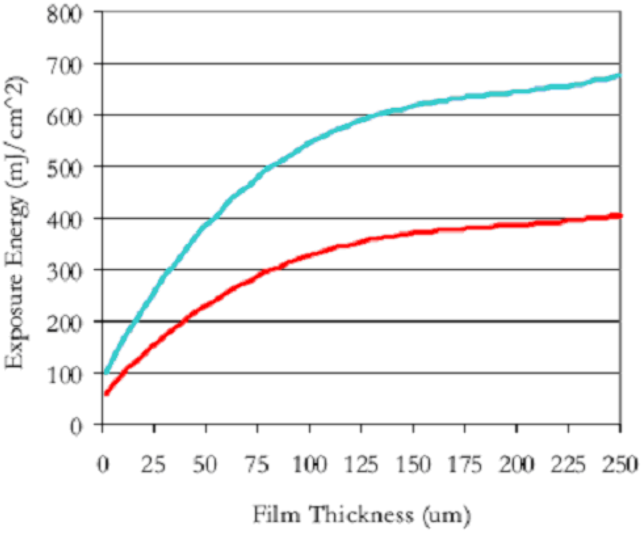

Figure 3.7: Exposure Energy Required versus Film Thickness for SU-8 2000 for reflective and non-reflective surfaces. [MicroChem Corp.]

In addition, the exposure process must be performed with the mask in vacuum contact with the substrate to prevent defects such as T-topping and negative side wall profiles.

3.7.3 T-topping and Negative Side Wall Profiles

Defects can occur if the vacuum contact between mask and substrate is insufficient. T-topping is a common fabrication failure which form due to several different factors. In general, T-topping defects are characterized by the formation of a lip near the surface of a relief structure, which in extreme cases, may form a bridge between two relief structures in close proximity with each other. It also causes irregular or exaggerated side wall profiles.

T-topping defects occur for negative resist if the exposure source contains low wavelengths below 350nm, which causes over absorption of UV at the resist surface. This generates vast amounts of acids near the surface. During subsequent PEB the heat, combined with the large acid concentration gradients, causes acid diffusion. Crosslinking not only occurs in the intended region, but in the surroundings as well. When the structures are developed, exaggerated and irregular wall shapes appear near the surface, however the base of the structure corresponds to a well exposed and developed structure (Figure 3.8).

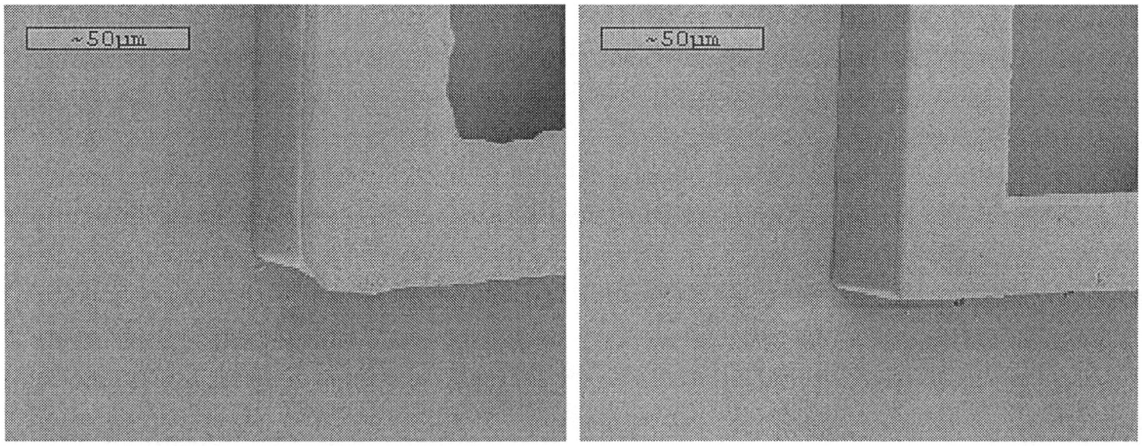

Figure 3.8: SU-8 Photoresist Structure after Development in PGMEA Without Low Wavelength Filter (left), and With a Low Wavelength Filter (right). [The SU-8 Photoresist for MEMS]

Another possible reason for T-topping defects to appear is due to the mask alignment during photolithography. If air gaps exist during the exposure process, Fresnel diffraction patterns create irregular side wall profiles in the resist [Chuang et al. (2002)]. Through experiments, it was observed that T-topping effects were caused by light which, upon hitting the air-transparency interface, bends due to refraction. Any air barriers introduced between the mask and the substrate surface will also increase the refraction of the incident UV light. These air barriers effectively create standing wave patterns to propagate along the surface of the photoresist, thereby inadvertently exposing areas alongside the intended pattern. Thus, it is important to use vacuum contact printing, to eliminate air gaps. In addition, it is important to ensure that the printed side of the transparency mask is directly on the photoresist, to eliminate any diffraction patterns due to the UV light passing through the transparency material.

3.8 Post Exposure Bake

After exposing the resist, acid is generated. PEB allows the acid to initiate and sustain the crosslinking process. Often, cracking and adhesion failure appear after PEB. There are two possible reasons for the defects. First, failures can occur due to insufficient exposure dose, such that the relief structures have not sufficiently crosslinked. Second, thermal stresses during heating and cooling also causes defects in the coating as previously explained. The resist has a high thermal expansion coefficient of 50ppm/K, whereas a glass substrate normally has 10ppm/K. Thus, when the material experiences a temperature change, stress is created in the interface between the SU-8 and the glass interface.

Another method to reduce the stress in the interface is to utilize a two step PEB process on a hotplate or in a convection oven. The first and second PEB step is performed at 65°C and 95°C respectively. The PEB heating time also depends on the thickness of the coating, with thicker coatings requiring longer second step PEB times (Table 3.1).

Table 3.1: Thickness and Post Exposure Bake Durations for Various SU-8 2000. [MicroChem Corp.]

Product Name	**Thickness (μm)**	**1st PEB (mins)**	**2nd PEB (mins)**
SU-8 2010	10	1	2
	13	1	2
	20	1	2
SU-8 2025	25	1	3
	41	1	3
	75	1	7
SU-8 2050	50	1	5
	75	1	7

	165	1	12
SU-8 2075	75	1	7
	110	1	10
	225	1	15

Afterwards, a reduction to 65°C for 45 seconds should be utilized to provide gradual cooling to room temperature. The substrate should rest in room temperature for at least 15 minutes before further processing.

3.9 Developing the Photoresist

After the PEB process, the SU-8 resist is ready to be developed for the removal of uncrosslinked regions. Usually the developer used is propylene glycol methyl ether acetate (PGMEA) or known commercially as SU-8 Developer (MicroChem Corp., Massachusetts). The development process and toxicity of PGMEA will be discussed.

3.9.1 PGMEA Developer

After sufficient cooling to room temperature, the substrate is placed inside a container filled with PGMEA. A steady stream of nitrogen is injected into the PGMEA to induce convection which aids in the removal of the uncrosslinked SU-8. The time required for the immersion depends upon the agitation provided. Especially for high aspect ratio (thicker resists), very strong agitation is required for successful development. An approximation of the development time and thickness at room temperature for several common SU-8 grades is provided (Table 3.2). In general, the thicker the resist, the longer the development time required.

Table 3.2: Thickness and Development Time for Various SU-8 2000 Resist. [MicroChem Corp.]

Product Name	Thickness (μm)	Development (mins)
SU-8 2010	10	2
	13	3
	20	3
SU-8 2025	25	4
	41	5
	75	7
SU-8 2050	50	6
	75	7
	165	12
SU-8 2075	75	7
	110	10
	225	12

After development, the substrate is rinsed with isopropyl alcohol which reacts with uncrosslinked photoresist to form milky white precipitates, effectively acting as a detector for insufficient development. If precipitates form, the development process should be repeated for another minute. The substrate is rinsed once more with PGMEA and dried with a slow stream of nitrogen air.

3.9.2 PGMEA Handling

PGMEA is relatively toxic to handle. Potential health effects for inhalation at high concentrations include irritation of the respiratory tract, and causes nausea, vomiting, numbness, and other symptoms affecting the central nervous system. It is also readily absorbed through the skin, and harmful if swallowed. Breathing products during ingestion or vomiting may cause lung damage or death. PGMEA is easily combustible, and must be stored in cool and dry places. It produces a vapour that spreads along the ground and may collect in low, confined areas. For handling purposes, goggles and laminate gloves should be worn, and for long exposure times, a NIOSH-certified P or R series particulate filter and organic vapour cartridge respiratory devices should be used.

3.9.3 Post Development Process

After the development and rinsing process, the master mold substrate is complete. At this point, the relief structures are checked under a microscope for cracking defects, side wall features, uniformity, and other important characteristics specific for the final microfluidic device.

3.10 Reusability of Glass and Silicon Masters

It is very important to select the most suitable substrate for fabrication, which depends on such factors as costs, dimensional constraints, and size of the structures. Thus, substrate selection for durability of these masters is discussed. Due to the high degree of surface roughness, structures fabricated on glass tend to fail due to poor adhesion, and as a result, must be replaced frequently. A closer analysis of the structures under microscope shows that for a straight channel, regions of bright intensity occur at the edges of the features (Figure 3.9).

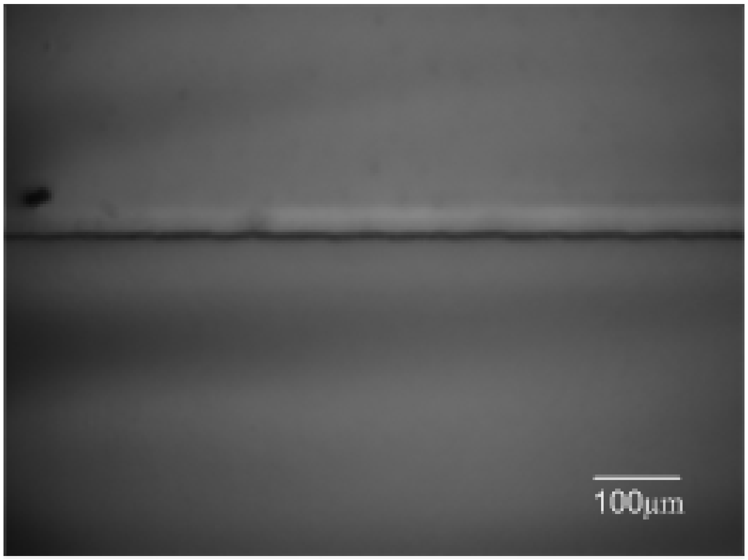

Figure 3.9: Top view of SU-8 structure. A bright band at the interface represents an air gap region due to poor adhesion.

These bright regions represent poor adhesion areas; locations where due to the large surface roughness and microscopic voids, the PGMEA seeps underneath the SU-8 structures, and after drying, leaving air gaps. With high aspect ratio fabrication, lower viscosity SU-8 photoresists are utilized to create tall structures. In this case, due to the difficulty in which the resist flows, even more voids form compared to low aspect ratio fabrication. Coupled with the fact that, taller structures require longer development times which often corrode the adhesion sites at the base of the structure, overall glass substrates complicate the fabrication process requiring tight controls of the development time. When the adhesion layer is implemented, the poor adhesion problem is eliminated. However, glass should not be used when fabricating long, thin, and high aspect ratio structures.

For structures fabricated in silicon, problems with poor adhesion are not observed, as the surface roughness of silicon is lower. Standard fabrication processes results in straight and well defined channel layouts without the bright intensity markings characteristic of voids. However, fabricated structures are prone to breaking due to a stronger adhesion between cured PDMS to silicon. Thus, when silicon wafers are used, an adhesion layer should be added before fabricating the channel structures. In addition, after fabrication, the masters should be coated with TCMS which aids in the peeling of the PDMS mold from silicon wafers.

Although trends in the reliability of glass and silicon substrates can be readily observed, it is difficult to quantify the amount of use a master can provide before failing. It depends greatly on such things as fabrication process, feature size and shape, and method of peeling the PDMS mold, just to mention a few. For the fabrication process, long amounts of development time and large induced thermal stresses will detrimentally reduce the master's reusability. In general, large feature sizes and shapes, and low aspect ratio designs help sustain the adhesion between the substrate and the SU-8. On the contrary long, tall, and narrow channel structures promote poor adhesion. In addition, peeling the PDMS mold while hot helps increase the life of the master. This may be explained by the fact that the PDMS has a higher thermal expansion coefficient than the SU-8 or the glass substrate. Thus, upon cooling of the cured PDMS mold, it creates a compressive stress upon the SU-8, reducing the long term survivability of the master.

As a rough estimate, the amount of reusability depending on the substrate and fabrication process is shown in Table 3.3.

Table 3.3: Estimated reusability of different substrates and fabrication process.

Substrate/Fabrication Process	Reusability (number of times)
Glass Substrate Only	1 to 3
Glass Substrate with Adhesion Layer	3 to 5
Silicon Substrate with TCMS	3 to 5
Silicon Substrate with Adhesion Layer and TCMS	7 and up

Often a 5um adhesion layer fabricated from SU-8 2005 is added to promote adhesion. It is a crosslinked (exposed and PEB) coating applied before depositing the main microfluidic channel structure. As the coating and subsequent structures form one continuous SU-8 layer in the final master product, it acts to prevent developer solution seepage. In addition, instead of just the structures, the whole SU-8 coating layer acts as the adhesion between the photoresist and the glass, effectively increasing the surface area and allowing for more resistance to thermal stress.

It is of interest to note that the application of HMDS to the glass substrate surface before spincoating SU-8 has little benefit. HMDS is used as another type of adhesion layer to promote bonding between photoresists and substrates. However, upon application of the HMDS and spincoating of the SU-8, the deposited film recedes away from the surface. Therefore, HMDS is not used in any of the fabrication process for adhesion promotion.

3.11 Mix and Curing the PDMS Material

As PDMS is the main material used for the fluidic chips, understanding its chemical properties and its handling information is important for any fabrication process.

3.11.1 Mixing and Fabrication Process

PDMS is a polymer (or specifically, an elastomer) that can be purchased from Dow Corning, under the commercial name of Sylgard 184. It comes in a package of two containers: a base, and a curing agent. The base and curing agent is usually mixed in a ratio of 10:1, however, different properties such as increased hardness can be observed if the amount of curing agent is increased. After mixing, the PDMS is in a pre-polymer liquid state. The master mold is placed inside an aluminum weighing pan (VWR, Mississauga) with the relief structures facing up. Next, the PDMS is then directly poured onto the master mold for curing. The container is placed inside the vacuum oven for degassing at -25mm Hg for 30 minutes. Often, bubbles are still noticeable inside the PDMS material. As a remedy, the vacuum is removed such that the bubbles can shrink to a negligible size. After curing at 80^{o}C for 1.5

hours, the PDMS is peeled off while it is still warm, thereby reducing compressive thermal stress on the structures of the master. For the peeling process, the border regions surrounding the master are lifted. The PDMS is peeled in the direction that is parallel to the length of the features.

3.11.2 General Uses and Properties of PDMS

The material is mostly used for insulation of electronic circuits and components, as barriers against environmental contaminants, and due to its elastic nature, as stress-relieving and vibration absorbers. It is a transparent material, thereby allowing the integration of optical equipment for flow detection. PDMS has a low interfacial free energy of 21.6 mN/m, and is chemically stable. Other materials that come into contact with the PDMS surface during patterning or molding do not irreversibly bond or react with the PDMS. Another advantage for biology is that the membrane is gas permeable, thus allowing living cells inside microfluidic channels to breathe. However, there are also many problems. PDMS shrinks 1% when cured, and swell when in contact with nonpolar organic solvents such as toluene or hexane. Also, the elasticity and thermal expansion of the material makes accuracy difficult to obtain.

Another major issue is the aspect ratio of the structures on the PDMS, and it directly affects the channel density (amount of structures in a design) and depth allowed for a fluidic chip. The aspect ratio is defined as h/d, where h is the depth of the structure, and d represents the width of the microchannel. Due to the softness of the material, sagging can occur which effectively constricts the microchannel (Figure 3.10).

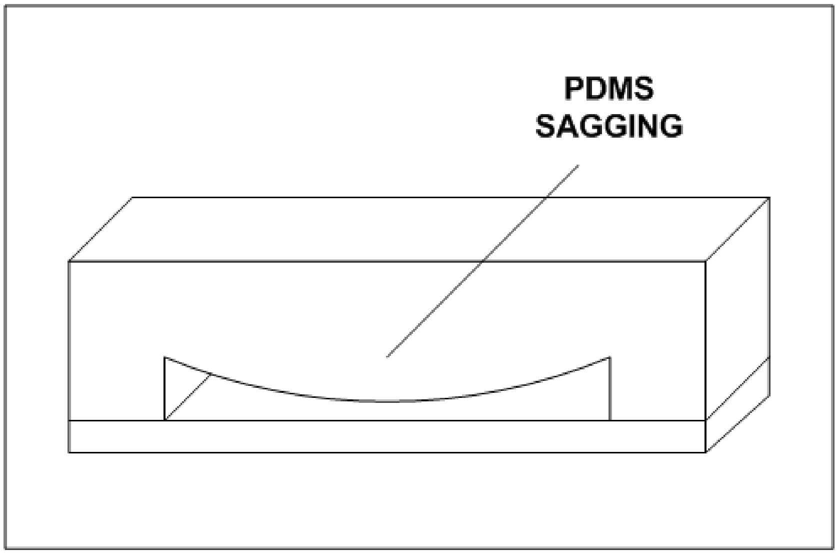

Figure 3.10: Typical cross-section of PDMS/glass where sagging has occurred. Due to PDMS flexibility, sagging can occur, restricting and blocking segments of the channel.

As a remedy, square support posts can be added throughout the channel to support the middle sections. As the fluid flow is predominantly laminar, the addition of posts has negligible impact on the fluid flow, so long as the total cross sectional area of the microchannel remains the same. Another possible method is to increase the curing agent content, as it effectively creates a stiffer PDMS material.

3.11.3 PDMS Handling Information

In general PDMS is a relatively safe material for handling purposes. For normal handling of the base and curing agent, no gloves or respirators are required. Of course, eye protection should always be worn, and washing hands after handling is an adequate safety measure.

3.12 Surface Modification via Plasma Treatment

After peeling the PDMS, the molds are cut and trimmed to size. The surface containing the microchannels is treated with plasma.

3.12.1 Plasma Cleaner

The plasma cleaner is used for treating the PDMS surface to achieve three main objectives: surface cleaning, increasing surface charge, and promoting irreversible bonding of the surface. For plasma treatments, the main component is the ionized oxygen atoms, as they are the primary ingredient that allows for cleaning and modifications of the material. However, for PDMS use, no specially concentrated oxygen is required; atmospheric air contains enough oxygen for the ionization process and surface treatments.

Surface Cleaning

One of the benefits of the plasma cleaner is its ability to remove organic contaminants from samples. When ionized oxygen bombards any surface, oxygen atoms combine with the hydrocarbon chains in organic contaminants forming CO_2 and CH_4, which are exhausted out of the plasma cleaner system. However, the disadvantage is that it is limited to only organic molecules which can readily react with oxygen.

Increasing Surface Charge

For microfluidic applications, it is essential to obtain a substrate that has a consistent, net surface charge which can promote electrokinetic effects such as EOF. Native (non-treated) PDMS has a small negative surface charge and is hydrophobic to water. By performing surface modification with an oxygen plasma, the surface charge increases in magnitude. As a comparison, Vickers et al. (2006) reported an increase in EOF mobility from 4.1×10^{-4} cm^2/Vs to 6.8×10^{-4} cm^2 V/s, effectively doubling the surface charge.

The increase in surface charge is due to bombardment of oxygen ions, where an oxygen atom substitutes into and effectively “kicks-out” a carbon atom from an individual “mer” unit (O-Si-CH3 or “methyl groups”) of the polymer PDMS. These methyl groups effectively change into (Si-OH or “silanol groups”) during the reaction. In addition to increasing the zeta potential charge, when these structures come into contact with a polar medium such as water, they readily dissociate to SiO- and H+ ions which attracts to water, thus changing the surface from an initial hydrophobic structure to a hydrophilic structure. [McDonald et al. (2000) and Efimenko et al. (2002)]

A problem with oxygen treated PDMS surfaces is their reactivity in air. The surface loses their hydrophilic characteristics if exposed to air for longer than 30 minutes, unless submersed in a polar medium such as water. It is theorized that PDMS reverts back to a hydrophobic surface structure because of a 5 nm thin silica layer that forms on the surface during the plasma treatment process. This material is very brittle and will likely form cracks over time allowing the upwards migration of uncured low molecular weight PDMS to the surface, thus causing the hydrophobic recovery.

As an alternative, ultraviolet light have been investigated [Efimenko et al. (2002), Wang et al. (2003), and Hellmich et al. (2005)]. This method is found to have worse material characteristics (such as large cracked silica formations along channel walls), a slightly less electroosmotic mobility value, and longer processing time requirement. For example, UV surface treatments require long exposure times of approximately 60 minutes compared to 60 seconds for oxygen plasma to create hydrophilic properties on PDMS surfaces.

Irreversible Bonding

A third benefit of plasma treatment is the ability to change PDMS surface properties to allow for irreversible bonding. Bonding is important because the micro-channels are often enclosed inside PDMS. However, the replica molding process can at most only fabricate three sides of a channel. Thus, another piece of material (not necessarily PDMS) is often bonded to enclose the channel. PDMS can readily bond and provide a reversible, watertight seal with another piece of PDMS, glass or silicon substrate without the use of plasma treatment. However, these channels can only withstand small pressures of 5 psi. Through bonding *via* plasma treatment, pressures of 30 to 50 psi can be sustained.

In the plasma treatment process, the creation of silanol groups also provides the necessary chemical composition for strong bonding. For example, when two surface-treated PDMS substrates are brought together, strong Si-O-Si bonds are created with the release of H_2O as a by-product. It can also readily bond with other materials containing silicon and any one of OH, COOH, or ketone groups [McDonald et al. (2000)].

3.12.2 Manufacturing Process

After the PDMS has been peeled, it is placed inside the plasma cleaner chamber and a vacuum is produced. The plasma is turned on for approximately 30 to 60 seconds. Exceeding 60 seconds causes extensive cracking on the surfaces due to a high formation of silica. After the treatment process, the PDMS substrates should be combined together (within the first minute) to reduce the exposure to oxygen air, which may react with the PDMS surface and reduce the quality of sealing. Also, it is important not to press the two surfaces together too hard, or features in the microfluidic chip might restrict or block the channels. It is also important to submerse the channels in a polar liquid such as water to ensure the surface does not allow hydrophobic reversion.

3.13 Summary

In the fabrication of a microfluidic device, many factors must be considered.

- The smallest microchannel size dictates the selection of the substrate. In general, glass can be employed for large cross sectional channels and features whereas silicon wafers should be employed for small features.

- Dimensions such as length and width of the microchannels are mainly constrained by the minimum resolution obtainable by commercial printers. In addition, once the masks are obtained, the lengths and widths of the microchannel layouts cannot be changed.

- Conversely, the microchannel depth can be changed for different masters depending on the fabrication process based upon the following spincoating parameters:

    - Photoresist viscosity (or grade)

    - Spin speed

    - Spin duration

- UV exposure dose, soft bake, PEB, and development times are dependent on the thickness of the photoresist layer.

- Slow cooling rates and sufficient wait times in between heating processes should be employed to reduce thermal stresses and prolong reusability of the masters.

Chapter 4

Thin Film PDMS/Rhodamine B for Microfluidic Temperature Measurements

4.1 Introduction

Based on the concepts and fabrication process provided in the previous chapters, microfluidic devices were fabricated for testing purposes. Due to the small sizes of microchannels, it was often difficult to perform on-chip temperature measurements such as with a thermocouple. One common method was to inject Rhodamine B, a fluorescent dye whose fluorescent intensity was dependent on the temperature, into a microchannel. By monitoring the change in the fluorescent intensity in the microchannel, the temperature of the microchannel was retrieved. This dye has been widely used in microchannels fabricated in glass and PDMS. However, there were problems with its use. Photobleaching and electrophoresis of the particles were two common problems. In addition, although there appeared to be no absorption issues with glass, the dye experienced absorption and adsorption on PDMS microchannels. To understand how the problem arose, utilization process of the dye will be discussed in this section. The extent of the problems and its effects on the PDMS microchannels are investigated. To resolve these issues, a thin film PDMS/Rhodamine B device was fabricated using soft lithography equipment and techniques, and the fabrication process will be discussed in this chapter.

4.2 Problems with Rhodamine B for Temperature Measurements

The standard method of whole field temperature measurements involved the mixing of Rhodamine B, a temperature dependent fluorescent dye, with the bulk operating fluid and introduced into the device. Several problems existed with utilizing this method.

4.2.1 Fluorescence and Photobleaching

Fluorescent dye particles such as Rhodamine B consist of a fluorophore segment as part of its molecular structure, allowing the particle to be fluorescent. These particles exhibit a characteristic in which photons of a specific energy is absorbed and subsequently reemitted at another wavelength. To take advantage of this phenomenon in the experiments, light from a halogen or mercury lamp source with a broad white light spectrum was first passed through a filter (allowing only wavelengths between 500nm to 550nm for Rhodamine B), and the emission (>560nm for Rhodamine B) was detected by the CCD camera.

Photobleaching is a process in which these excited fluorescent particles undergo a chemical reaction in the fluorophore preventing further fluorescent emissions. Overall, this effectively reduces the fluorescent intensity of Rhodamine B particles over a short period of time, changing its performance and reducing its reliability as a temperature measurement indicator. The photobleaching rate depends on the photon flux and the temperature, with higher temperatures and higher photon flux corresponding to a quickening of the photobleaching process. It is an unavoidable process but may be reduced by increasing the fluorescent particle concentration, and thereby reducing the amount of exposure dose and intensity required for its detection. However, an optimum amount of dye concentration will be reached, after which further increase in concentration will reduce the fluorescence effect.

4.2.2 Electrophoresis

Electrophoresis refers to the process in which charged particles migrate under an applied electric field, potentially increasing or decreasing the local concentration. Rhodamine B remains neutral only when the surrounding solution has a pH value between 6.0 and 10.8 [Schrum et al. (2000)]. In addition, for applications involving electroosmotic pumping, pockets of high Rhodamine B concentrations may be produced. This results in the formation of intensity gradients throughout the microfluidic device and adds an additional degree of uncertainty to any temperature measurements.

4.2.3 Absorption and Adsorption

Recently, compatibility issues between polymer based microfluidic chips and neutral hydrophobic dyes such as Rhodamine B [Pittman et al. (2003), and Roman et al. (2005, 2006)] and caged dye [Ross and Locascio (2003)] were reported. It was shown that PDMS readily and irreversibly absorbed Rhodamine B dyes, with the overall effect of altering the zeta potential and consequentially the electroosmotic flow in microchannels.

Rhodamine B absorption and adsorption was demonstrated through experiments in which a 150μm wide by 100μm high PDMS microchannel was flushed with 0.1 mM Rhodamine B (mixed in de-ionized water). After 30 minutes, a fluorescent image was obtained in Figure 4.1.

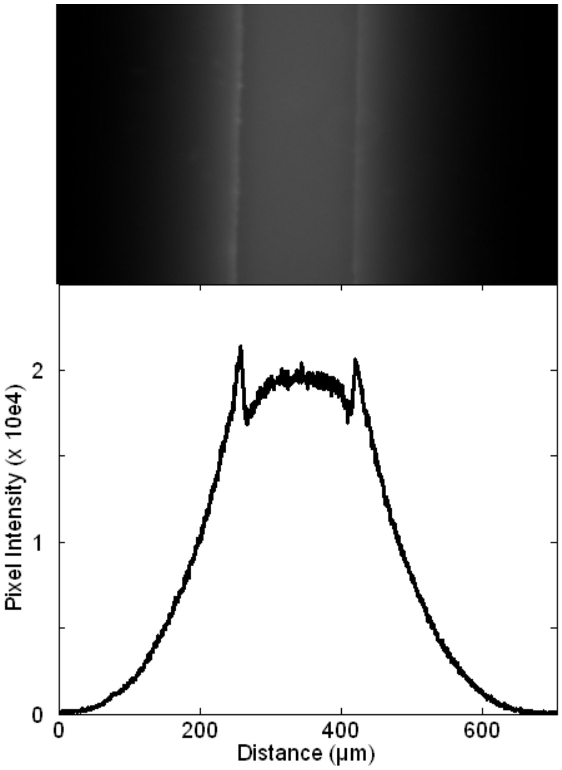

Figure 4.1: Image of a 100µM Rhodamine B filled PDMS microchannel after 30 minutes and the corresponding fluorescent intensity profile. Absorption and adsorption is evident due to the detectable fluorescent intensity extending beyond the channel walls, and the peak intensities occurring at the solid-liquid interface.

Large amounts of Rhodamine B initially existing only in the microchannel, had migrated into the surrounding PDMS material. In addition, large adsorption was seen, represented by the double peaks, each located at the solid-liquid interface of the microchannel. The peaks were a result of a stacking effect due to a high concentration of the Rhodamine B particles at the channel walls. Combined, the absorption and adsorption artificially exaggerated the Rhodamine B intensity, and understated the temperature (since the intensity increased for decreasing temperature).

It is interesting to note that, although the dye diffused from the channel into the PDMS, the Rhodamine B concentration in the fluid did not decrease due to a continuous replenishment from the reservoirs. On the contrary, the fluorescent intensity increased with respect to time due to the continuous replenishment and subsequent diffusion. The intensity growth phenomenon was illustrated in Figure 4.2, in which a straight 150μm wide by 100μm high PDMS microchannel was flushed with 0.1 mM Rhodamine B. Fluorescent intensity measurements were taken along the axial length of the channel initially, and after 20 minutes and 60 minutes respectively (Figure 4.2).

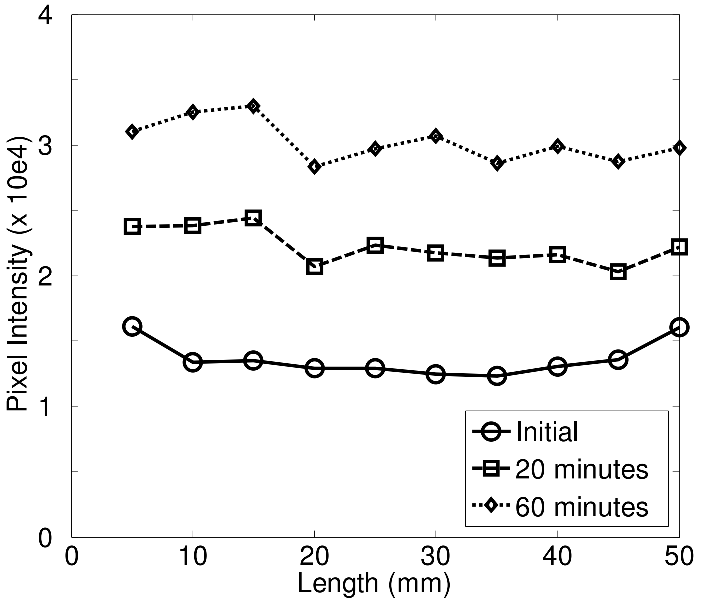

Figure 4.2: Fluorescent intensities of 100μM Rhodamine B filled PDMS microchannel with dimensions of 150 μm wide x 100 μm height x 50 mm long. Intensities are recorded along the axial length initially, at 20 minutes and at 60 minutes after dye introduction.

To address these issues, a new method of temperature detection was devised, in which a thin film PDMS was soaked in a bath of 5mM Rhodamine B solution, and subsequently used to measure temperature. The thickness of the film was important as it affected the temperature detection sensitivity. Thus, a correlation between PDMS film thickness and spincoating parameters was performed and several additional modifications were investigated to obtain thinner film thicknesses. The results are shown in the next section.

4.3 Development of the Temperature Measurement Device

4.3.1 Overview of PDMS Spincoating Process

Experiments were performed in which PDMS was spun onto glass microscope slide substrates to obtain an experimental relationship between spin speed and thickness. For all the experiments, a base to curing agent ratio of 10:1 was utilized unless otherwise stated. For all PDMS spinning, the general spincoater program shown in Table 4.1 was used.

Table 4.1: Spincoating speed and duration settings.

Step	Spin Speed (rpm)	Acceleration (r/s)	Duration (s)
1	0 to 500	100	5
2	500 to X	300	Y
3	X	0	Z

In Table 4.1, X represents the final desired spin speed, and Y represents the time required to accelerate from 500rpm to the desired spin speed with an acceleration of 300r/s, and Z represents the spin duration at the final constant spin speed. After spincoating the PDMS onto the glass wafers, the wafers were cured by placing onto a hotplate at 95^{o}C for 5 minutes.

4.3.2 Native PDMS Results

Initially, PDMS without any additives (referred to as native PDMS) were utilized for the spincoating experiments. No degassing was necessary, as the viscosity appeared to be low enough such that all bubbles were eliminated during the process, resulting in a uniform coating. Approximately 1ml of native PDMS was deposited and spun onto glass microscope slides with dimensions of 3” by 1” without any prior cleaning of the slides. The PDMS samples were spun at different durations and different final spin speeds to obtain a calibration curve; however the same acceleration was applied to all specimens. The resulting thicknesses were measured and plotted (Figure 4.3).

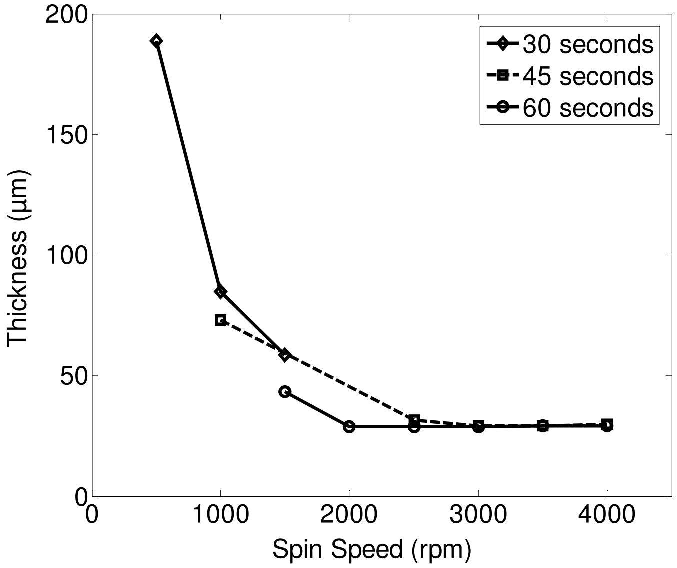

Figure 4.3: Thickness versus spin speed for different durations. Film thickness decreases with longer durations and higher spins speeds, but a plateau at approximately 30μm is reached.

Generally, longer spin duration and higher spin speeds produced thinner PDMS films. Extending the spin duration allowed the film more time to remove the PDMS material, and the higher spin speeds provided more force to remove the material. Based on the graph, the thickness versus spin speed followed an inverse curve, thus a small change in spin speed at low speeds dramatically affected the thickness. However, due to machine constraints there was a maximum speed limit of 6000rpm which could not be exceeded. In addition, a plateau was reached at approximately 30 μm in which the thickness could not be reduced further. Thus, another method was sought to further reduce the thickness of the PDMS film.

4.3.3 Low Toluene Concentration Additive Results

Small amounts of Toluene were added as a thinning agent with the goal of spincoating thinner PDMS. Thus, varying amounts of Toluene was added to PDMS and the corresponding thin film thickness was measured and shown in Figure 4.4 and 4.5.

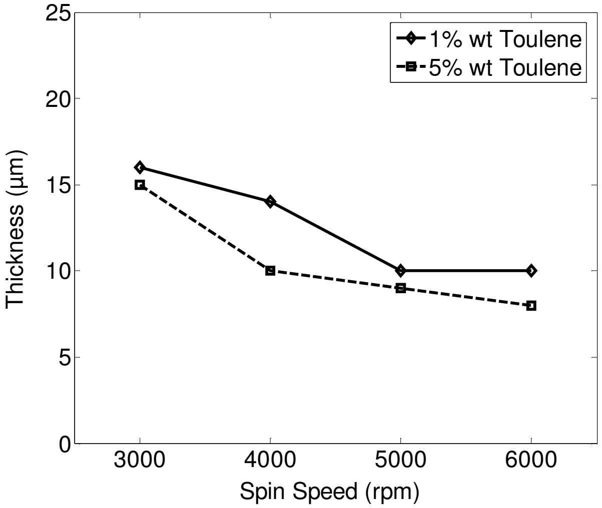

Figure 4.4: Thickness versus Spin Speeds for PDMS (10:1) Thinned with 1% and 5% (wt) Toluene at 45 Second Spin Duration.

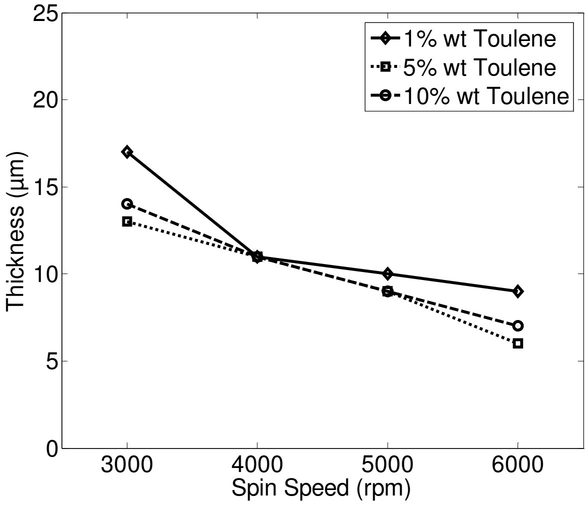

Figure 4.5: Thickness versus Spin Speeds for PDMS (10:1) Thinned with 1%, 5%, and 10% (wt) Toluene at 60 Second Spin Duration.

Based upon previous results, spin speeds lower than 3000rpm were not utilized as these settings had negligible effect on reducing film thickness. In general, after mixing the PDMS with Toluene, the resultant viscosity of the mixture was lower than that of native PDMS. Thus, more of the material was removed for the same spin conditions and the resulting film thickness was lower. This was seen in Figure 4.3 and 4.5, when a setting of 4000rpm and 60 seconds was utilized, the thickness for native and 1% (wt) Toluene thinned PDMS was 30um and 10um, respectively. In addition, the higher the Toluene concentration, the thinner the resultant film became. However, a plateau was reached at high amounts of Toluene content as the reduction in thickness was almost negligible between films with 5% and 10% Toluene additives.

4.3.4 High Toluene Concentration Additive Results

Experiments using Toluene in high concentrations involved Toluene to PDMS mass ratios (mass of Toluene divided by mass of PDMS) in excess of 1:1. The motivation for using high concentrations of Toluene was that during spinning, most of the mixture was quickly spun away or evaporated leaving behind a small thin film of PDMS which spread evenly along the substrate. For the calibration experiments, mixtures of Toluene in PDMS with mass ratios of 1:1, 5:1, and 10:1 were initially chosen, utilizing previously mentioned mixture deposition methods and acceleration parameters. The experiments were repeated with different spin speeds as shown in Figure 4.6.

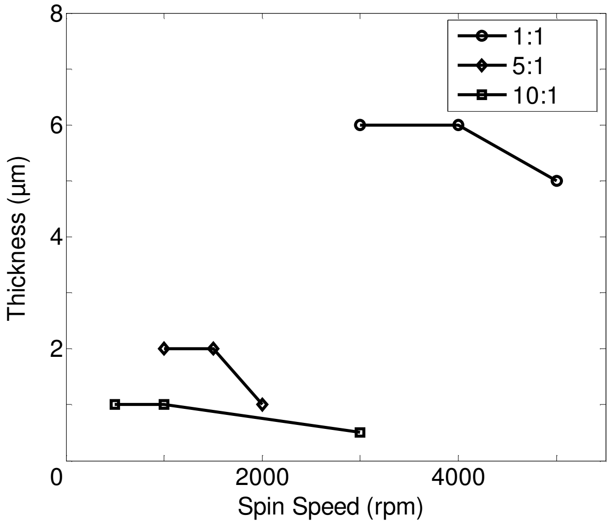

Figure 4.6: Thickness versus Spin Speeds for Toluene to PDMS Ratios of 1:1, 5:1, and 10:1 at Varying Spin Speeds with a 60 Second Spin Duration.

As expected, higher Toluene concentrations reduced the thickness of the PDMS film. However, the incremental benefits were small at high Toluene contents with only a 1um reduction in film thickness between 5:1 and 10:1 Toluene to PDMS ratio. Experiments were also performed for different mass ratios at 6000 rpm as shown in Figure 4.7.

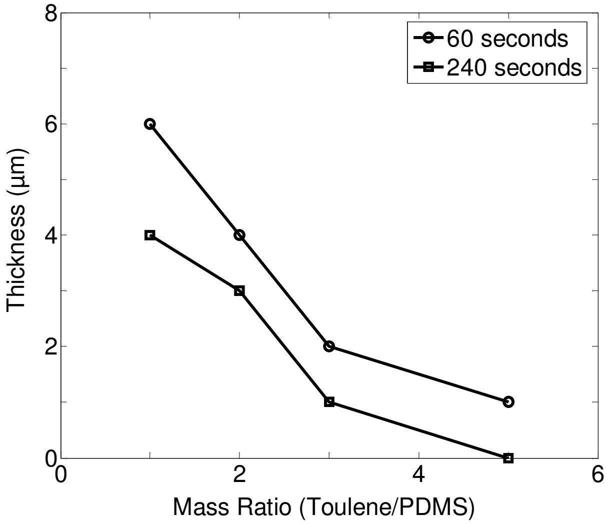

Figure 4.7: Thickness versus Different Mass Ratios for Toluene/PDMS Mixtures Spun at 6000rpm for 60 and 240 Second Spin Duration.

As expected, with higher concentrations of Toluene and higher spin speeds, the resultant film thickness decreased. It is interesting to note that, utilizing longer spin durations in excess of 4 minutes only reduced the film thickness by approximately 1um for a specific mass ratio.

4.4 Improving Film Quality

With the utilization of high concentrations of Toluene, three major problems were observed in the quality of the spincoating. First, with mass ratios in excess of 3, coverage problems occurred, in which the film would not cover the whole slide. Secondly, micropores and pits with diameters in the order of 0.5mm were observable under the microscope and uniformly distributed throughout the film, as shown in Figure 4.8. Thirdly, streaking patterns (lines that appear to emanate from the centre of the spin axis) were also observable by the naked eye.

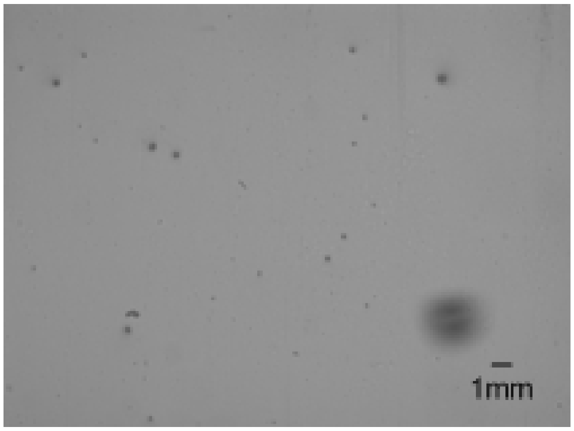

Figure 4.8: Microscopic Pitting on 4um PDMS Coated Glass Slide.

A common procedure to resolve thin film coverage problems was to utilize low acceleration and thereby provide more time for the mixture to cover the slide evenly before higher centrifugal forces remove most of the material. In addition, surface chemistry was also known to be a factor, as providing a wafer with good surface wettability allowed for better contact of the mixture with that of the substrate surface. For the problems with pitting and streaking, these defects were commonly attributed to contamination of the mixture, substrate, handling materials, or processing equipment. The problems could also have been associated to lack of degassing of the mixture. The above mentioned problems and attempts at finding a solution will be discussed.

4.5 Slide Coverage Problem

To resolve the slide coverage problem, substrate dehydration, substrate surface modification and acceleration were utilized.

4.5.1 Effects of Substrate Dehydration

It was thought that, the coverage problems may have been attributed to the presence of water molecules residing in the substrate preventing proper bonding between the PDMS with the glass. Prior to spincoating, the glass slides were dehydrated at 200^{o}C for 20 minutes to release moisture trapped on the wafer surface. However, no improvements on film coverage were observed, thus proving dehydration had negligible effect on slide coverage.

4.5.2 Effects of Substrate Surface Modification

A common surface modification technique was to utilize oxygen plasma to change the surface chemical properties of the wafer. This method increased the hydrophilic surface properties of glass, providing for a conformal contact of the liquid to the wafer surface. Better contact allowed for the Toluene/PDMS mixture to remain on the surface of the wafer for longer periods of time, and thus increase the slide coverage.

Prior to spincoating, the wafer was placed in an oxygen plasma unit for 5 minutes. After spincoating, analysis of the film showed that the process did not improve the film coverage. In addition, it also had no effects on the film thickness. However, the plasma treatment caused enlarged pitting on the film surface. One possible reason was that, the oxygen plasma may have created large micro voids on the glass surface. Upon spincoating, the material seeped into these micro-voids creating enlarged pitting effects. Thus, oxygen plasma should not be used to enhance the spincoating process.

Hexamethyldisilazane (HMDS) was another method used to modify the surface of wafers before spincoating. It was hypothesized that HMDS would provide surface modification without damaging the wafer surface as with the oxygen plasma method. To apply the HMDS, the following steps were used. First, the wafers were dehydrated at 200^{o}C for 30 minutes, and then cooled to room temperature. HMDS in a liquid form was applied and allowed to saturate the glass surface for 60 seconds. The substrate was then spun at 3000rpm for 60 seconds to evaporate the chemical. These wafers were then used for spincoating PDMS.

However, it appeared that the surface modified in such a way created a worse effect as the contact angle of the Toluene/PDMS were much smaller than without any surface modification. After spincoating, film coverage was worse than when no surface modification was employed.

4.5.3 Effects of Higher Acceleration

A common method utilized in spincoating processes was to utilize intermediate spin steps, as it allowed time for the film to spread evenly before higher velocities forced the liquid material off the wafer. In addition, low accelerations and longer ramp up times were utilized for the spincoating process. However, these methods produced unexpected results, with consistently poorer slide coverage.

A further analysis of these films gave clues to understanding the phenomenon being observed. After spincoating at low accelerations, these poor coverage films would exhibit the same two-arm spiral shapes leading from the centre to the edge of the wafer, as shown in Figure 4.9.

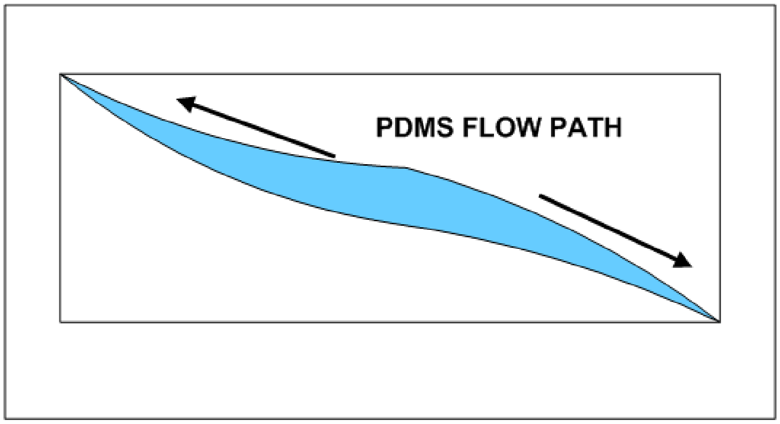

Figure 4.9: Typical poor coverage problem when spincoating PDMS on glass. During spinning, spiral arms appear, providing a path of least resistance for the liquid PDMS to travel, thereby avoiding other regions of the slide.

It appeared that, due to the high content of Toluene and the correspondingly low viscosity, that upon acceleration of the wafer, the liquid had spread as tendrils and upon reaching an edge, a path of low resistance was formed, such that most of the liquid flowed through them. Since the liquid resided mostly along this path throughout the whole spincoating process, as the Toluene evaporated, the residual PDMS particles were left behind and formed the thin film along the path.

Thus, a method to counter this phenomenon was to increase the acceleration. The spincoating process was modified as follows. Approximately 1.5ml of the Toluene/PDMS mixture was deposited onto the glass wafer, ensuring that the whole surface was fully covered. Then, the film was spun with an acceleration of 3000rpm/s (chosen due to machine constraints) for 2 seconds. The film was then spun with a constant speed of 6000rpm for 60 seconds. The resultant film covered the entire wafer even at mass ratios of 5.

4.6 Surface Defect Problem

In general, pitting and streaking may be caused by particles embedded inside the film. Thus, slide cleaning and degassing were performed.

4.6.1 Effects of Slide Cleaning

With the spincoating process of SU-8 in soft lithography, slide cleanliness played an important role in the uniformity of the final film. The presence of microscopic dust and dirt particles on the wafers created mini barriers during spincoating. These barriers locally prevented the outwards flow of the resist, creating streaking patterns on the wafer surface.

Glass slides cleaned using the RCA method (a commonly utilized method for cleaning silicon wafers in the electronics industry) was utilized for spincoating. Cleaned glass slides had negligible effect on the overall quantity of defects. Silicon wafers that were cleaned and packaged in a clean and controlled environment were also utilized as substrates for spincoating the Toluene/PDMS mixture. There were also no observable improvements to the film quality. With these experiments, substrate contamination was eliminated as the cause of poor film quality. Thus, other contamination sources which could not be controlled such as environmental conditions (dust in the air) or equipment contamination (dirty spincoater) may have contributed to the defects.

4.6.2 Effects of Degassing

During mixing of the Toluene/PDMS mixture, gas may have been introduced which would also act as barriers to film dispersion. Gas bubbles formed halos and pitting deformations as they evaporated. To degas the mixture, the Toluene-PDMS mixture was placed under vacuum inside a vacuum chamber for 30 minutes. Afterwards, the mixture was spincoated onto glass wafers. In general, no improvements to the quality of the film were noticed.

Even though, none of the techniques implemented were able to significantly improve the coating qualities of the PDMS, nevertheless a first generation temperature measurement device was created based on the use of native PDMS.

4.7 First Generation Thin Film/Rhodamine B Fabrication and Utilization

The calibration curve and process optimization relating the spincoating parameter to the thin film thickness allowed for the development of a microfluidic thermometry method. Initial designs utilized native PDMS to create a 30μm thin film soaked in Rhodamine B. The general purpose was to demonstrate the temperature measurement device as a proof of concept. In addition, the fabrication process utilized soft lithography equipment and techniques, illustrating its applicability and ease of manufacture. It should be noted that, the thin film PDMS/Rhodamine B would be used as a design tool only, allowing researchers to experimentally verify the temperature of the channel and surrounding material during the design stage. However, when the microfluidic chip design is finalized and mass produced, the thin film would not be included in the final product.

4.7.1 Fabrication Process

Two methods for fabricating the thin film using conventional soft-lithography technology were considered. The first method involved mixing Rhodamine B directly with PDMS pre-polymer and spinning it onto a substrate to form a thin PDMS/Rhodamine B layer. This option provided exact control of the concentration of Rhodamine B within the PDMS film; however, Rhodamine B stained most surfaces and it would contaminate the spin coater and future spin coating processes. Also, during the curing of the PDMS/Rhodamine B film, high temperatures increased the rate of photobleaching and as a result lower the overall fluorescent intensity. Therefore, to avoid the above mentioned problems and to simplify the fabrication process, an immersion method was used in this study with the following procedures.

PDMS (Dow Corning, Midland) was mixed in a base-to-curing agent ratio of 10:1 and 1 mL was then spun onto a microscope glass slide (VWR Intl., Mississauga) at 3000 rpm for 60 seconds in a spincoater (Brewer Science Inc., Rolla) to create a 30μm layer. The thin-film was then cured on a hotplate at 95^{o}C for 5 minutes. Afterwards, the substrate was submersed into a 5mM solution (DI water) of laser grade Rhodamine B (Fisher Sci., Ottawa) for 5 days and stored in the dark to ensure complete saturation of Rhodamine B. The substrate was then dried and used as a temperature sensitive thin film.

Initially, the PDMS/Rhodamine B film was directly bonded to the PDMS microchannel mold, however, the Rhodamine B particles would quickly diffuse back into the liquid and then into the walls of the PDMS mold. To prevent the backwards diffusion of Rhodamine B, a 150 μm-thick cover glass slide (Brain Research Lab., Waban) was plasma treated (Harrick Plasma, Ithaca) with a power of 29.6 W for 45 seconds and bonded between the PDMS channel mold and the thin film as shown in Figure 4.10. The cover glass successfully segregated the Rhodamine B from the microchannels and the thin film was applied to measure temperature distributions of IEF applications using thermally generated pH gradients, which will be discussed in Chapter 5.

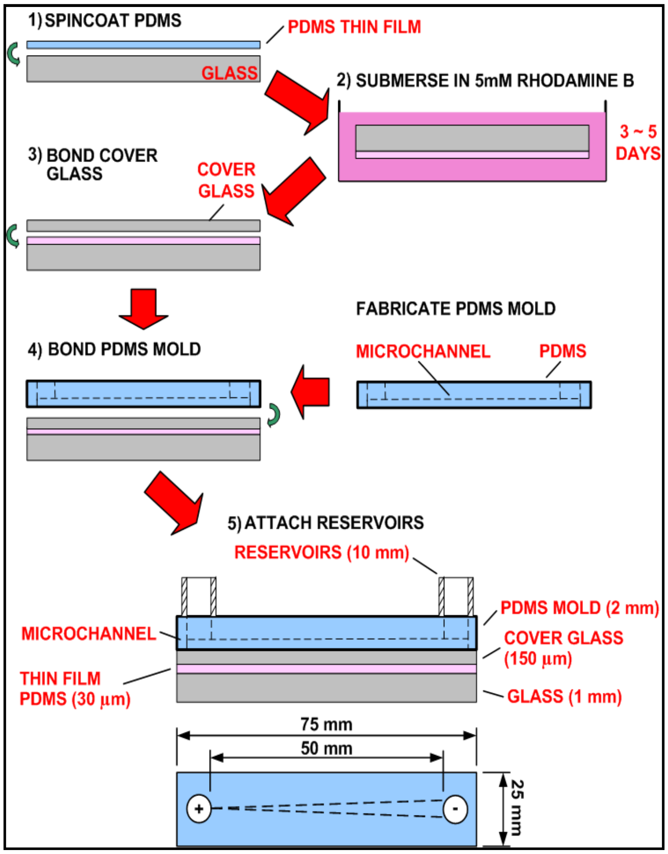

Figure 4.10: Fabrication Process of Thin Film PDMS/Rhodamine B for On-Chip Temperature Measurements [Samy et al (accepted 2007)]

4.7.2 Imaging Process

The thin PDMS/Rhodamine B film (excitation, 500-550nm, emission >565nm) was excited by a 100W halogen lamp light source through a neutral density filter with a 25% transmission to reduce the amount of photobleaching. A 5x objective in an inverted microscope (GX-71, Olympus) along with a 1392 x 1040 pixel CoolSNAP ES Monochrome

CCD camera with progressive scan (Photometrics, Tuscon) was used to record the images with an exposure time of 8 seconds. Each image was analyzed by selecting and averaging the intensity values in a 20x20 pixel, representing an area of 25x25 µm. First, a room temperature intensity image was taken. After chip operation and subsequent heating, another image of the same area was taken and the intensity was normalized with the previous intensity value. The temperature was found by substituting the normalized intensity into a calibration curve. All experiments were performed in the dark and the lamp shutter was closed when images were not being taken to prevent unnecessary photobleaching.

4.7.3 Film Calibration

Intensity measurements can change due to factors such as Rhodamine B concentration, and equipment specific factors such as light intensity, uniformity, and exposure dose. By normalizing operating temperature intensity to room temperature intensity from two images taken at the same location, these factors can be isolated, producing a performance calibration curve that is independent of these factors. The calibration procedure used was adapted from experiments employed by Ross et al. (2001) and Erickson et al. (2003) for conventional liquid based Rhodamine B measurements. In brief, a room temperature intensity image of the thin PDMS/Rhodamine B film was first taken. The film was then heated to a temperature of approximately 90°C and cooled to room temperature. During cooling, a thermocouple (Omega, Laval) molded to the PDMS surface measured the corresponding temperature and one intensity image was taken at the same point. The film was allowed to cool to room temperature, and a new baseline image was taken before reheating the film so that photobleaching effects were not compounded. The recorded intensities were normalized with the room temperature intensity and plotted accordingly to obtain a calibration curve. Since a calibration curve of thin PDMS/Rhodamine B film had never been reported, the calibration experiment was repeated for concentrations of 1mM and 5mM Rhodamine B solution dissolved into 30um-thick and 60um-thick thin films. These experiments showed that Rhodamine B concentration and PDMS film thickness had negligible effect on the performance. The calibration curve was compared to results published by Ross et al. (2001) as shown in Figure 4.11. The general trends of both calibrations were similar with larger discrepancies appearing at higher temperatures. The cause of this discrepancy was not known; however a change in the fluorescence properties of the Rhodamine B after bonding to the PDMS was suspected. Applying a third-order polynomial fit to the data, the resulting equation of temperature as a function of fluorescent intensity was:

$$T = -96.904\, I^3 + 228.02\, I^2 - 250.25\, I + 141.53 \tag{4.1}$$

where I represents the normalized fluorescent intensity and T represents the temperature in Celsius degrees.

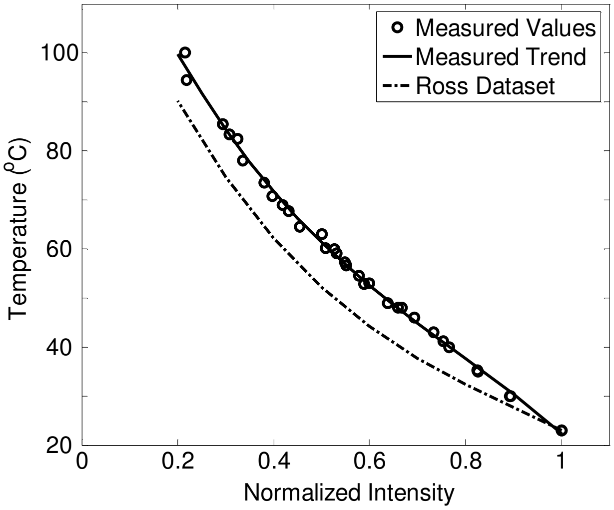

Figure 4.11: Calibration Data of Thin Film PDMS/Rhodamine B Compared to Dataset [Ross et al. (2001)]

In this process, there are two major uncertainties to consider: error of the probe and that of the optical microscope. The probe used was a J-thermocouple with an error of 2.2°C. Although no tolerance was expressly stated of the fluorescence imaging process and optical microscope, out of a set of 21 images of the background intensity (in the absence of fluorescent dye), the average background intensity was 6.2 with a standard deviation of 0.28.

4.8 Second Generation Thin Film/Rhodamine B Design

During use, the thin film exhibited certain qualities that could have been improved upon. Although a finished second generation temperature measurement chip was not successfully completed, a discussion of the problems and experimental results in its development is provided.

4.8.1 Problems with First Generation Design

With the first generation of thin film PDMS/Rhodamine B design, the thickness of the thin film and glass barrier was large compared to the depth of a typical microchannel (which was in the order of 200µm or less). Considering the thermal resistance of PDMS, the equivalent thermal resistance of the combined thin film and glass barrier was large (equivalent to approximately 400 µm in thickness of glass). To reduce the thickness of the PDMS layer, Toluene additives were considered in the design of the second generation temperature measurement devices. In addition, SU-8 was experimented upon to create a thinner barrier to replace the glass. To more accurately predict the temperature existing inside microchannels, it was important to reduce and if possible, eliminate any heat transfer retention that the thin film could cause in the microfluidic chip.

4.8.2 PDMS thin film and SU-8 Rhodamine B Barrier

It was decided that a Toluene:PDMS concentration with a mass ratio of 1:1 would offer the optimal conditions considering the tradeoffs between film quality and uniformity. With such a concentration and spin speed of 6000rpm for 60 seconds, a 5 µm thick PDMS thin film was produced with good film uniformity throughout while providing the least amounts of surface pitting and streaking.

To replace the glass barrier, another method providing a smaller thickness was explored. SU-8 was chosen as a prime candidate as the goal of the thin film was to create a temperature measurement technique which would be easy to fabricate and implement. In addition to the ease with which the thin film was fabricated by adapting general soft lithography techniques, the SU-8 was investigated for its properties in blocking Rhodamine B. Important benefits of SU-8 included its transparency at observable wavelengths and especially at excitation and emission wavelengths necessary to visualize the Rhodamine B, and its accessibility as it was readily available as part of the soft lithography fabrication process.

4.8.3 Proposed Second Generation Chip Fabrication Process

An alternative fabrication process was devised to produce a 5um thick PDMS soaked rhodamine B film with a 1um thick SU-8 barrier for the purpose of Rhodamine B segregation. An illustration of the fabrication process is shown in Figure 4.12.

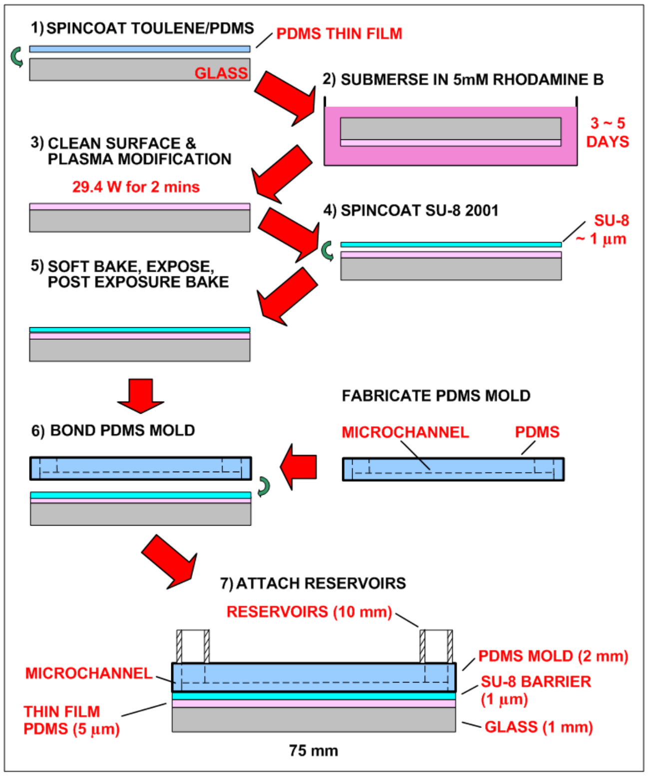

Figure 4.12: Proposed Fabrication Process of 5µm Thin Film PDMS/Rhodamine B with 1µm SU-8 Barrier.

In brief, PDMS (with base to curing agent in 10:1 mass ratio) was mixed with Toluene in a 1:1 mass ratio. Approximately 1.5ml of the solution was deposited onto a 1”x3” glass microscope slide (ensuring that the whole surface was covered by the solution). A spincoater setting of 6000rpm for 60 seconds, with an acceleration of 6000r/s was utilized. The coated glass slides were heated for 5 minutes on a 95^{o}C hotplate and cooled to room temperature for 15 minutes. Afterwards, the slides were placed inside a bucket containing 5mM rhodamine B and submersed for 5 days to ensure saturation. After submersion, the slides were dried and the film surface was cleaned using adhesive tape to remove surface contaminants and loose PDMS particles that inadvertently appeared during the fabricaton process.

4.8.4 SU-8 Barrier Development

For the selection of the SU-8 barrier, thicknesses of 1µm, 2µm, and 5µm were tested. Thin PDMS/Rhodamine B films of 5um thickness were created beforehand for SU-8 barrier deposition and testing. Various SU-8 thicknesses were created by mixing cyclopentanone with SU-8 2005 to create SU-8 2001 and SU-8 2002 according to equation 3.1. For mixing SU-8 2001 and 2002, Table 4.2 was utilized.

Table 4.2: Solids Content and Required Cyclopentanone Volume for Dilution.

SU-8 Grade	Solids Content	Cyclopentanone Volume (per 100ml of stock)
2005	45%	N/A
2002	29%	55.17 ml
2001	22%	104.55 ml

After soaking, the thin film PDMS were taken out of the Rhodamine B solution and dried. Thickness of 1µm, 2µm, and 5µm were spun onto the thin film PDMS with the previously mentioned SU-8 grades and correspondingly processed.

Initially, the SU-8 films were only soft baked to reduce any unnecessary photobleaching. However, when water droplets were applied onto the SU-8 barrier surface to simulate the conditions inside the fluidic channels, after 24 hours white spots appeared on the SU-8 barrier. The appearance of white spots may possibly be due to water absorption or penetration through the barrier. Thus, UV exposure and PEB was necessary, effectively cross-linking the SU-8 and thereby providing long term prevention of Rhodamine B diffusion. After the SU-8 barrier was fabricated, water droplets were added to the surface to test for any possible Rhodamine B diffusion into the water. After 24 hours, the water droplets were placed onto a clean microscope slide and analyzed for the presence of Rhodamine B by passing light with excitation energy for the visualization of the dye, and measuring the emitted intensity through an inverted microscope. The tests were repeated three times with samples taken from water droplets residing at three different locations on each microscope slide. These experiments were performed on all three SU-8 barriers of different heights. The intensities of each test were listed and compared to the background intensity (measured intensity of the microscope slide without any water). The pixel intensity values have a maximum of 256. The results are listed in Table 4.3:

Table 4.3: Pixel intensity of water droplets sampled from the SU-8 barrier surface.

Film Thickness	Test 1	Test 2	Test 3	Background
1um	6.6	6.6	6.6	6.5
2um	6.3	6.5	6.2	6.5
5um	6.2	6.5	6.5	6.6

All three film thicknesses were able to prevent Rhodamine B absorption. Since the thinnest barrier was desired to reduce heat transfer effects and increase sensitivity of the thin film, the 1μm layer of SU-8 was utilized. A further analysis of SU-8 2001 thickness versus spin speed was performed for several different thicknesses measured using a profilometer as shown in Figure 4.13.

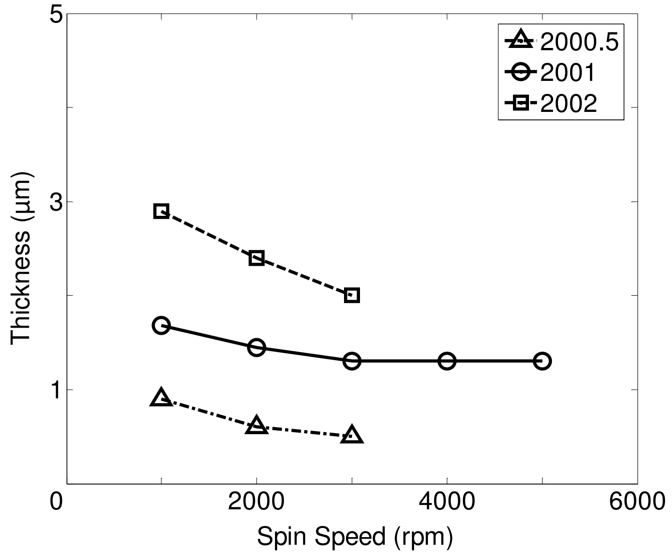

Figure 4.13: Thickness versus spin speed for manually mixed SU-8 2001. As comparison, the reported thicknesses of SU-8 2002 and 2000.5 are included as comparison (MicroChem Corp., Massachusetts).

The experiment shows that with the mixed solution, the thickness was approximately 1.3µm. For simplicity, 1µm was used for all modeling and calculations.

4.8.5 SU-8 Recession and Plasma Treatment

During initial tests, it was noticed that SU-8 adhered poorly to the PDMS thin film, such that after spincoating, the coating appeared to be hydrophobic, receding and beading up along the surface. The implementation of surface oxygen plasma appeared to resolve the recession issue. However, through further experiments, prolonged use of plasma treatment drastically decreaseed the Rhodamine B intensity (discussed in the next section). Thus, to understand the effect of PDMS thin films on the spincoating quality of SU-8, several coating experiments were performed.

Different slides spincoated with PDMS were treated for 15, 30, 45, 75, 105, and 180 seconds with plasma at a power of 29.4 W prior to deposition and spincoating of a 1µm barrier utilizing SU-8 2001. Soft bake, UV exposure, and PEB were also utilized in forming the layer. At 15 seconds plasma treatment duration, recession of the SU-8 was evident, with “halos” of greater than 200µm in diameter forming around pits throughout the film as shown in Figure 4.14.

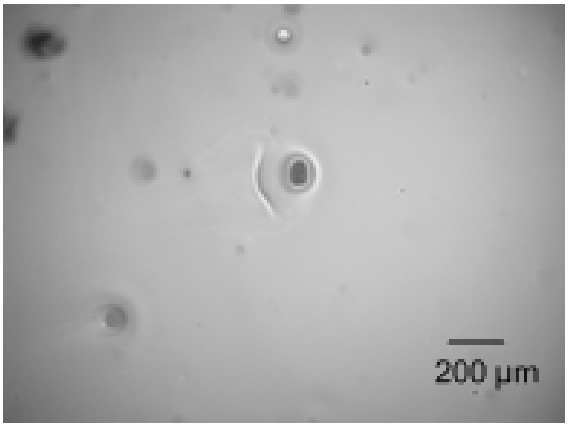

Figure 4.14: Typical Surface Features of µm PDMS Coating with Subsequent Plasma Treatment for 15 Seconds and SU-8 2001 Coating of 1um on Glass Showing Some Recession of SU-8.

After 45 seconds of plasma treatment, the recession halos appeared to be smaller, with average sizes in the order of 200µm or less. The contours of the halos appeared to be less exaggerated as well, as shown in Figure 4.15.

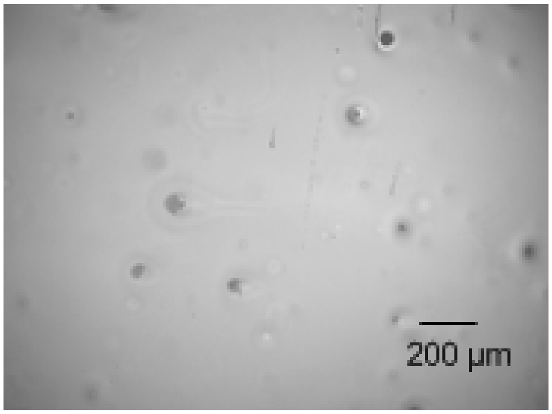

Figure 4.15: Typical Surface Features of 5um PDMS Coating with Subsequent Plasma Treatment for 45 Seconds and SU-8 2001 Coating of 1um on Glass. Recession Halos Are Similar in Size but Less Exaggerated.

Further analysis of the 75 seconds, 105 seconds, and 180 seconds resulted in no reduction in halo size or improvements in the SU-8 coating uniformity. This was in contrast to samples of SU-8 spuncoated on PDMS that had been soaked in Rhodamine B, as shown in Figure 4.16.

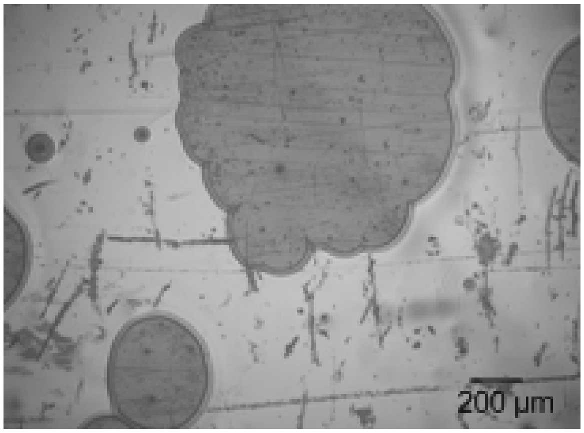

Figure 4.16: Typical surface features of insufficiently plasma treated PDMS/Rhodamine B with SU-8 2001 surface coating.

There appeared to be large regions of recession spread throughout the surface of the film and halo regions. The fabrication process was similar to that of the PDMS chips; the only difference was that the sample was submersed into Rhodamine B for 5 days, with insufficient plasma treatment. Recession areas were in excess of 1mm in diameter. From analyzing the surface coating, it was assumed that the Rhodamine B was very hydrophobic to SU-8, causing the resist to recede drastically. Only by utilizing a 2 minute plasma treatment at a power of 29.6W was a sufficiently hydrophilic surface induced for uniform SU-8 bonding.

4.8.6 Sources of Fluorescent Intensity Reduction

With thinner films, Rhodamine B content inside the PDMS film was less, thus affecting the total detected fluorescent intensity when visualized through a microscope. In addition, heating and subsequent exposure to light may cause photobleaching to the thin film. Thus, it was important to understand all the parameters reducing the amount of fluorescent light in the fabrication process.

For the proposed fabrication process, a fluorescent intensity image was taken at each step in which the intensity may decrease. Fluorescent intensity images (with a maximum pixel intensity value of 256) in a 20x20 pixel (25µm x 25µm area) were taken at each step of the fabrication process as shown in Table 4.4. A 5x lens and a 3 second exposure time was used.

Table 4.4: Fluorescent intensity values after each fabrication process.

Fabrication Step	Fluorescent Intensity (max. 256 pixel)
Unmodified thin film PDMS/Rhodamine B	205.5
After surface cleaning with tape	98.1
After 2 minute plasma treatment	75.8
After spincoating and soft bake	53.3
After exposure to UV at 400mJ/cm^2	54.3
After post exposure bake	53.1

Approximately 50% of the Rhodamine B was removed due to the surface cleaning with adhesive tape. This was due to the removal of the Rhoadmine B particles which adsorbed onto the surface of the PDMS. However, the surface cleaning process should have negligible effect on the concentration of the Rhodamine B inside the film. It should be noted that the cleaning step was necessary, as during the soaking process, the surface became grainy as it captured particles, resulting in a poor non-uniform SU-8 coating. Significant reductions in intensity also occurred during plasma treatment and spincoating of SU-8, causing a reduction of 25% in each process, respectively. The fluorescent intensity was relatively unchanged after PEB, suggesting that both soft bake and PEB heating processes created negligible photobleaching. Rather, the pouring of SU-8 onto the surface of the thin film may have dissolved and removed some of the Rhodamine B from the film. This process would be unavoidable, such that the creation of the SU-8 coating layer cannot be optimized. Adjusting the plasma treatment time would not be possible, as the proposed 2 minutes was required to sufficiently treat the surface to ensure uniform coating.

4.8.7 Problems with Low Fluorescent Intensity

When the 5μm temperature sensitive film with SU-8 barrier was bonded reversibly or irreversibly to a PDMS microchannel design of an 80μm depth and subsequently filled with PVP for EOF suppression purposes, the fluorescent intensity decreased within the microchannel location, as shown in Figure 4.17. An image of the film after removing the reversibly bonded microchannel is shown in Figure 4.18.

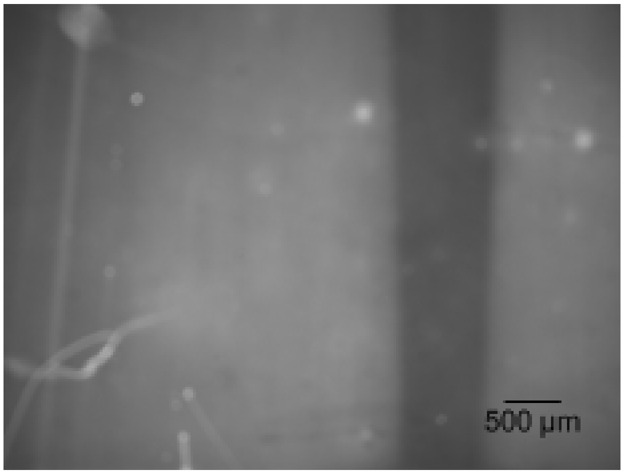

Figure 4.17: Intensity image of a 5µm thin film with reversibly bonded 80µm depth tapered channel, and subsequent injection of PVP.

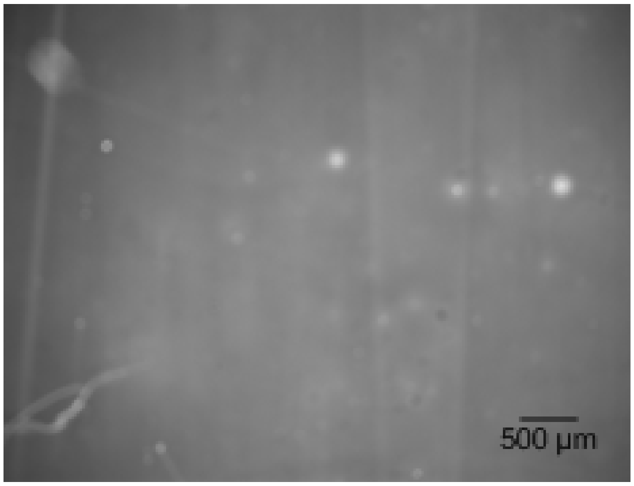

Figure 4.18: Intensity image of the 5µm thin film with microchannel removed. Light areas represent residue from the PVP coating process, which has negligible effect on the channel intensity.

Out of a maximum value of 256, the pixel intensity prior and after liquid injection into the microchannel was 107 and 97, respectively. The decrease in intensity was possibly due to a low Rhodamine B intensity value in the thin film, as a result of the fabrication process. Fluorescent light was partially blocked by the fluid, making intensity measurements unreliable. As increasing the fluorescent intensity was not possible in the current fabrication process, other methods were explored to increase the intensity.

4.8.8 Other Methods to Increase Intensity

Rhodamine B – Toluene – PDMS Mixtures

Increasing the Rhodamine B concentration in the film would increase the overall intensity. Instead of submersing PDMS thin films, Rhodamine B with 40mM concentration was added to a mixture of Toluene and PDMS in a 1:1 mass ratio and directly spincoated onto glass slides, in the hopes of ensuring high dye concentrations existed in the film. However, Rhodamine B did not appear to be soluble in Toluene, producing films in which Rhodamine B particles clustered together and were kept segregated from the PDMS material as shown in Figure 4.19.

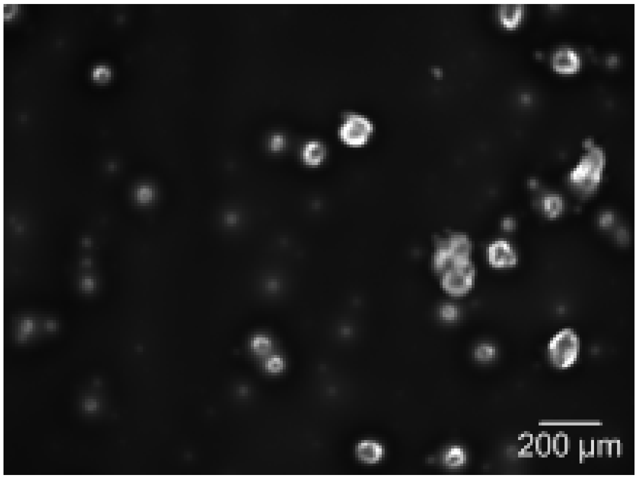

Figure 4.19: Intensity image of 40mM mixed in mass ratio of 1:1 Toluene to PDMS, spincoated onto glass slides. Rhodamine B particles are concentrated into spheres embedded in PDMS. A four second exposure rate is used.

An intensity analysis of the images showed that the surrounding PDMS contained only trace amounts of Rhodamine B, with an intensity value of 16, compared to background intensity values of 6, with a maximum possible value of 256.

Rhodamine B – SU-8 Mixtures

Rhodamine B at different concentrations was mixed into SU-8 2005 and directly spincoated onto glass slides. The process created a thin film of 5µm thickness embedded with the fluorescent particles. Intensity images with a 4 second exposure rate were taken of the cured films and their results are summarized in Table 4.5.

Table 4.5: 5µm SU-8 film embedded with Rhodamine B and the corresponding pixel intensity at different temperature and concentrations.

Concentration (mM)	Temperature (Celsius)	Pixel Intensity (max. 256)
5	23 ± 1.1	30.24
20	23 ± 1.1	102.7
20	60 ± 1.1	115.5
20	63 ± 1.1	118.4
100	23 ± 1.1	150.4
100	52 ± 1.1	156.2

At 5mM, the fluorescent intensity was too low for general use. Higher concentrations provided brighter fluorescent intensities. Contrary to normal Rhodamine B behaviour in which higher temperatures produced lower film intensities, as the temperature of the SU-8 film increased, the fluorescent intensity increased slightly. The phenomenon may be due to chemical reactions between SU-8 and the dye. Unfortunately, the incremental change in intensity was relatively small for large temperature changes; this phenomenon could not be adapted for use in whole field temperature measurements.

4.9 Summary and Recommendations

The ultimate goal is the development of a PDMS/Rhodamine B thin film capable of providing whole field temperature measurements for polymeric microfluidic devices. These chips are fabricated based upon generally accepted soft lithography techniques and commonly accessible equipment.

- The minimum thickness that can be spincoated using native PDMS is 30µm. Further thinning of PDMS is possible, but require relatively large quantities of Toluene.
- An advantage of thinner PDMS films and thinner devices is less thermal resistance, allowing better temperature approximation of microchannels. However, a disadvantage of thinner PDMS films is the lower fluorescent intensity, making measurements and the interpretation of the results difficult.
- First generation design involves a glass base, with a 30µm PDMS film soaked with 5mM Rhodamine B, a 150µm glass to prevent Rhodamine B back diffusion, and a PDMS microfluidic device.
- The development of second generation thin films for temperature measurement has been so far unsuccessful. One possible reason is due to the poor compatibility between PDMS, SU-8 and Rhodamine B. Other materials with larger Rhodamine B solubility should be investigated as a replacement for PDMS material. In addition, instead of utilizing a barrier fabricated from liquid such as SU-8, a solid barrier similar to glass but with a smaller thickness should be chosen. This eliminates the observed problem in which Rhodamine B particles diffuses into the SU-8 layer during spincoating.

Chapter 5
Isoelectric Focusing with Thermally Generated pH Gradients

5.1 Introduction

Isoelectric focusing with thermally generated pH gradients is a high resolution fractionation technique based upon charge differences between amphoteric compounds. The technique depends upon the intentional formation of non-uniform Joule heating along the axial direction of a microfluidic device. Certain buffers such as Tris-HCl have a pH dependence on temperature. Thus, if a microchannel or capillary is heated unevenly (such as in the axial direction), a temperature gradient forms allowing a corresponding pH gradient to establish without the use of Carrier Ampholytes (CAs). The thermally generated pH gradient technique has many benefits compared to traditional CA based CIEF. A discussion of CA based CIEF technique is provided in Chapter 6.

Main issues with CA include its relatively high costs, may chemically interact with protein samples, and are difficult to isolate from protein samples after separation, limiting its use in lab-on-a-chip devices where the ability for multiple analysis and processing steps are desired. In addition, there is great difficulty in creating batches of CA with the same pH gradients, creating uncertainty when CA from different companies are utilized.

This chapter discusses the design, experimental validation, and estimated performance of different channel layouts for IEF with thermally generated pH gradients. As heat transfer is integral to their performance, these designs are characterized by the thermometry method developed in the previous chapter. In addition, one of the designs is chosen for further heat transfer simulation and comparisons with actual detected temperatures. Although fluid flow measurements are integral to microfluidic device development, it is not necessary for the case of IEF devices. For this application, channel surfaces are intentionally coated to suppress EOF.

5.2 pH Dependence of Temperature for Tris-HCl

Tris-HCl is a common buffer used in the study of IEF, with a pH value that is sensitive to temperature, as shown in Figure 5.1.

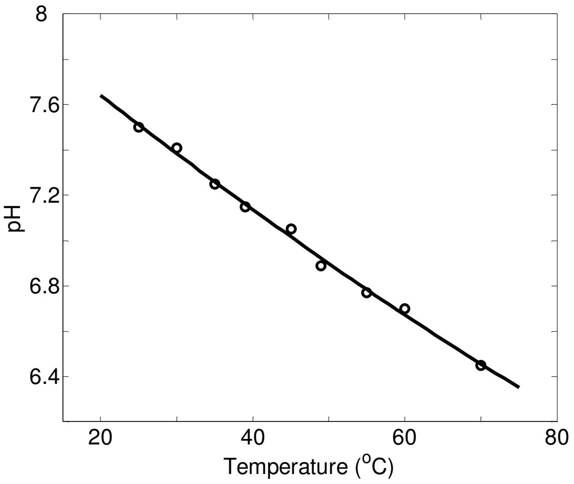

Figure 5.1: pH versus Temperature for Tris-HCl (pH of 7.5 at room temperature).

The equation of the trend line was experimentally found to be:

$$pH = -0.0235T + 8.0852 \tag{5.1}$$

where T is the temperature in Celsius degrees.

5.3 Theoretical Derivation of Temperature Distribution

Theoretical derivation and numerical modeling were performed based upon Samy et al. (2007). In brief, joule heating was formed when a voltage difference was applied to the liquid in the microchannel through electrodes plugged into the two reservoirs, based upon the equation:

$$\dot{Q} = \sigma(T)\vec{E} \cdot \vec{E} \tag{5.2}$$

where $\dot{Q}$ is the volumetric heat generation in Wm^{-3}, $\sigma(T)$ is the temperature dependent electrical conductivity of the buffer in Sm^{-1}, and $\vec{E}$ represents the applied electric field in Vm^{-1}. Electric field varied along the channel when the buffer was heated due to temperature, and the change in the cross sectional area along the axial direction of the microchannel. Thus, the electric field was expressed as:

$$\vec{E} = \frac{I}{\sigma(T) \cdot A(x)} \tag{5.3}$$

where I represents the current in A, *A(x)* represents the local cross sectional area of the microchannel in m^2. Substituting into the previous equation, the heat generation was expressed as:

$$\dot{Q} = \frac{I^2}{\sigma(T) \cdot A(x)^2} \tag{5.4}$$

The temperature field at steady state was described by the equation:

$$\rho C_p[\vec{u} \cdot \vec{\nabla} T] = \vec{\nabla} \cdot (k\vec{\nabla} T) + \sigma(T)\vec{E} \cdot \vec{E} \tag{5.5}$$

where ρ is the density in kgm^{-3}, C_p is the specific heat (J kg^{-1} K^{-1}), $\vec{u}$ is the velocity vector (m s^{-1}), and k is the thermal conductivity of the material (W m^{-1} K^{-1}). However, the microchannels were treated with Poly vinyl pyrrolidone (PVP) prior to use, preventing EOF, and thereby eliminating the convection term. The electric conductivity of Tris-HCl versus temperature was measured and expressed in the form:

$$\sigma(T) = (1 + \alpha(T - T_o))\sigma_o \tag{5.6}$$

where α is the thermal coefficient (0.035 $^{\circ}C^{-1}$), and σ_o is the conductivity (1691 μS cm^{-1}) unless otherwise stated, and the reference temperature T_o is 22.5°C.

The electric field required as part of Joule heating was described by the following equations:

$$\nabla(\sigma \cdot \nabla \varphi) = 0 \tag{5.7}$$

$$\vec{E} = -\nabla \varphi \tag{5.8}$$

where φ is the electric potential (V). Most material properties remain relatively constant over the typical temperature range of 25°C to 80°C for this application. Thermal properties of Tris-HCl were approximated as pure water.

The set of equations provided above was solved for a 3-D model using commercial finite element software (MULTIPHYSICS v3.3, COMSOL, Los Angeles, CA). The computational domain consisted of a hybrid PDMS/glass microfluidic chip including a tapered channel and fluid reservoirs with platinum electrodes. To reduce the number of mesh elements, the thin PDMS/Rhodamine B film was replaced by a thermally equivalent thickness of glass (240 μm) through the equation: $k_{PDMS} / L_{PDMS} = k_{Glass} / L_{glass}$. Due to symmetry, one half of the geometry was chosen for the computational domain, as shown in Figure 5.2.

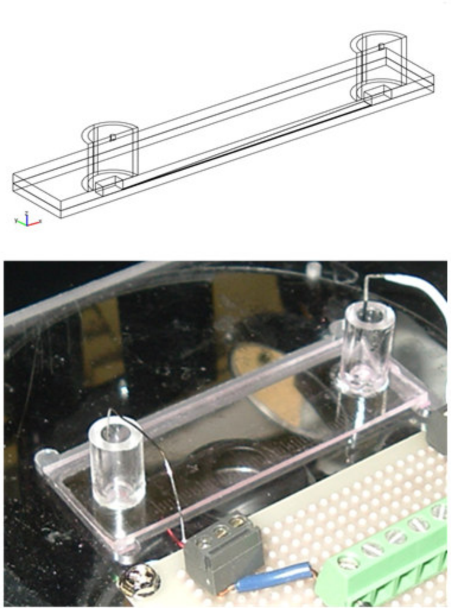

Figure 5.2: Computational domain of the simulated microfluidic device (top) and the physical device setup (bottom) [Samy et al (accepted 2007)]

An insulation boundary condition was placed along the edges. A constant power was applied in the channels by utilizing the equation:

$$P=VI \tag{5.10}$$

applied at one electrode, and a ground condition applied at the other electrode. Due to the suspension of the chip inside a custom made acrylic holder, the main heat transfer mechanism was the limited natural convection at the top and bottom. Due to the thickness of the surrounding PDMS, conduction to the sides of the chip was negligible. The natural convection heat transfer coefficient was computed from Nusselt and Rayleigh numbers for the scenario of a heated top plate, heated bottom plate and heated side walls for the reservoirs.

5.4 Justification of Tapered Channel Design

For the design of isoelectric focusing devices utilizing thermally generated pH gradients, an understanding and control of heat transfer and temperature distributions throughout the chip was paramount. From analyzing the set of equations, potential factors affecting the temperature distribution included the power input into the chip, and the cross sectional area (or the angle of divergence) of the microchannel. The conductivity may also change the temperature distribution, however it was not considered as it was a temperature dependent variable that was difficult to manipulate for design purposes.

Previously, there has never been a reliable method for measuring temperature inside microfluidic devices made of PDMS. Thus, the new method for whole field temperature measurement discussed in the previous chapter was employed to visualize the temperature distributions for several designs. Understanding temperature distributions allowed for the estimation of the pH levels inside the devices.

Kates and Ren (2006) performed simulations to determine the temperature distributions in a glass microfluidic device in which the cross sections were rectangular. The chip layout was a tapered design, but with the inlet and outlet widths at 50µm and 4mm respectively. With such a narrow inlet, higher temperatures were observed at the inlet, such that a steep drop in temperature occured for different applied voltages and angle of divergence as shown in Figure 5.3 and 5.4.

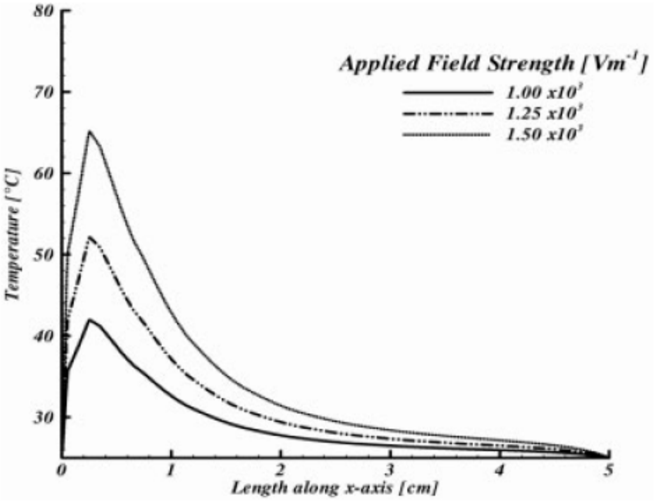

Figure 5.3: Axial temperature distribution along channel length at various applied electric field strengths [Kates and Ren (2006)].

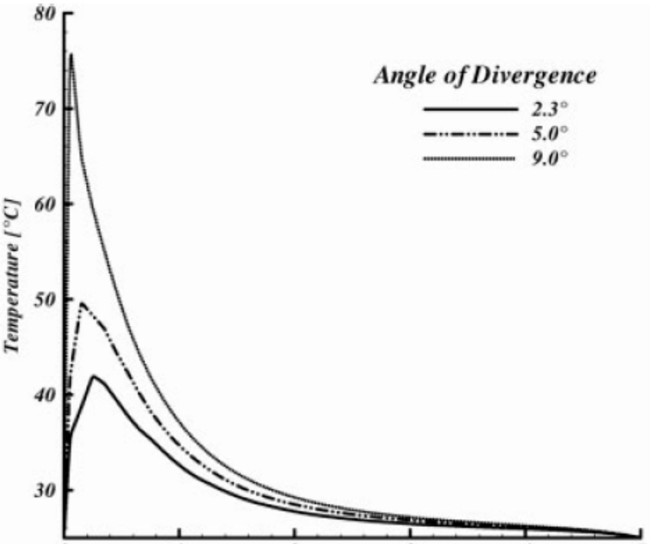

Figure 5.4: Axial temperature distribution along channel length at different angle of divergences [Kates and Ren (2006)].

Steep non-linear drops in temperature along the axial direction were not desired, as the corresponding pH gradient would not be linear, making the determination of the protein separation location difficult. A wider inlet would allow for a more gradual reduction of the temperature along the axial length of the chip. Thus, a wider inlet similar to that described by Huang and Pawliszyn (2002) was chosen for fabrication. Their device was fabricated by using polyester film of 120µm that was cut with a tapered design of 400µm and 4mm at the inlet and outlet, and bonded in between two UV transparent glass microscope slides. When this design was duplicated in PDMS and tested, large amounts of electrolysis and bubble formation was observed inside the channel. By reducing the height to 75µm, electrolysis became manageable.

5.5 PDMS Fabrication, Design and Experimental Setup

Microchannels of varying tapered designs were fabricated in PDMS by utilizing soft lithography and replica molding processes. The three different design categories that were tested upon were straight tapered, parabolic tapered and zigzag designs, as shown in Figure 5.5. It is of interest to note that soft lithography was advantageous because an important factor in determining the heat transfer was the cross sectional area. Soft lithography was one of the few methods available that can allow for the rapid design and fabrication of a wide variety of different arrangements.

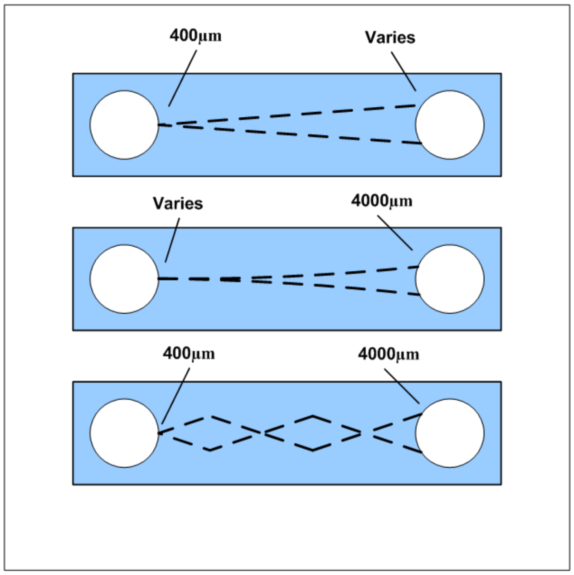

Figure 5.5: Microchannel layouts of the three different categories of tapered channels. Certain dimensions were varied to study its temperature distribution effects.

Certain dimensions in each category were adjusted to observe its effects on temperature distribution. For the straight tapered design, the results of three different outlet dimensions of 2000µm, 4000µm, and 5000µm were compared. For the parabolic design, the narrow inlet of 50µm and 400µm were used. For the zigzag pattern, no changes in the inlet or outlet dimensions were performed. All channels are 50mm long, and are 75µm in height. Make-shift glass reservoir extensions were cut from glass tubes with dimensions of 1.5cm high, 1/4” inner diameter and 3/8” outer diameter, and attached to the inlet holes by applying and curing PDMS.

The masters of the above mentioned designs were fabricated on silicon substrates to ensure good uniformity, durability, and to prolong reusability. PDMS microchannel molds were then created from the masters with a PDMS mixing ratio of 5:1 base to curing agent. This was chosen due to its hardness compared to the standard 10:1 ratio, which was causing the PDMS to sag. The molds were cut to size and fluidic inlet holes were punched at both ends of the tapered channel. The PDMS was irreversibly bonded *via* plasma cleaner (at 29.6W for

45 seconds) to the temperature sensitive film/glass substrate discussed in the previous chapter.

To prevent EOF during testing, a 0.5% polyvinyl pyrrolidone (PVP) was flushed through the channels for 5 minutes before use. Next, the channel was flushed with a 25mM Tris-HCl buffer (with a pH of 7.5 and conductivity of 1691µS/cm). For temperature measurements, intensity images were taken at room temperature and during device operation with a GX71 inverted microscope with a 5x lens, neutral density filter with a 25% transmission, excitation (500 nm to 550 nm) and emission (> 565nm) filters. A 1392 x 1040 pixel CoolSNAP ES Monochrome CCD camera with progressive scan (Photometrics, Tuscon) was used to record the images with 8 second exposure times. Each image was analyzed by averaging a 20 x 20 pixel window, near the centre of the image if possible. All experiments were performed in the dark with the lamp shutter closed unless images were being taken, to prevent unnecessary photobleaching. A schematic of the experimental setup is shown in Figure 5.6.

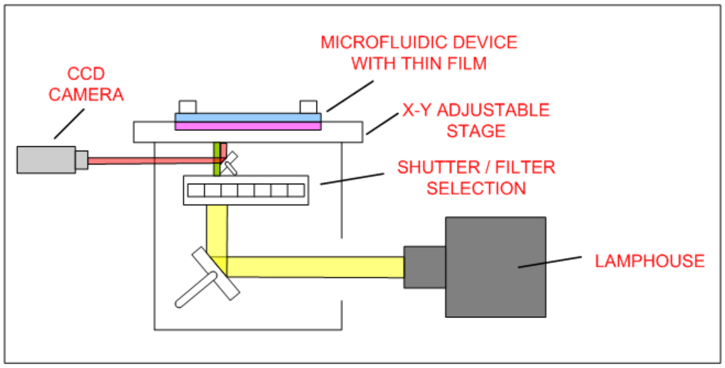

Figure 5.6: Schematic diagram of experimental setup. Light from halogen lamp source passes through a Rhodamine B excitation filter, and the corresponding light emissions are detected by the CCD camera [after Samy et al (accepted 2007)]

5.6 Problems with Constant Current and Constant Voltage

Initially, constant current or constant voltage was applied to create Joule heating in the devices. However, steady state temperature could not be reached. When a constant voltage was applied, thermal runaway was observed, which can be understood as follows. Due to the Joule heating occurring inside the Tris-HCl buffer, the temperature of the solution rose. This caused the conductivity of the solution to increase and correspondingly drew increasing amounts of current. Higher currents created ever increasing amounts of Joule heating as the power input (which is a product of voltage and current) increased. This caused an endless loop of increasing power consumption and higher temperatures, which ultimately created electrolysis inside the channel, causing bubble formation and fluid evaporation.

The reverse trend was true when constant current is applied. The voltage decreased and induced a lowering of the power consumption of the chip and thus a reduction of the Joule heating. A typical trend was observed when a constant current of 250uA was applied to a tapered channel of 60um height as shown in Figure 5.7.

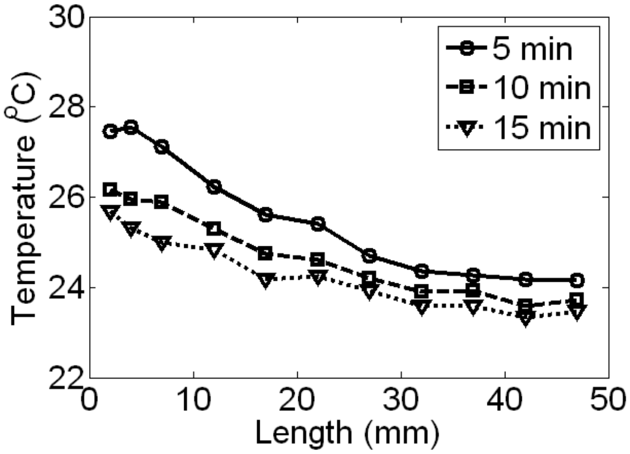

Figure 5.7: On-chip temperature measurements of tapered channel over time under an applied 250µA constant current at different time intervals. The temperature profile decreases with respect to time without reaching steady-state.

Over time, the recorded temperature steadily decreased, such that reliable steady state temperature gradients could not be produced. However general trends and conclusions were observable from these experiments. With higher currents, higher temperatures were obtainable, even though steady state temperatures were unattainable, as shown in Figure 5.8.

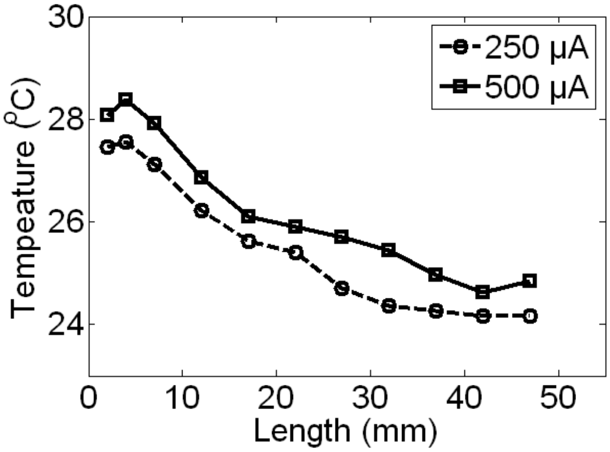

Figure 5.8: On-chip temperature measurements of tapered channel at 5 minutes for 250μA and 500μA of applied current. Even though steady state was never reached, general trends can be observed in which higher currents produce higher temperatures.

With constant current, the peak temperatures at 5 minutes of 250 μA and 500 μA of applied constant current were 27.5°C and 28.5°C, respectively. In addition, decreasing the channel height for the same applied current increased the peak temperature. The resistance was increased for smaller cross sections, effectively increasing the voltage draw. The overall Joule heating was increased, providing the tapered channel with a wider axial temperature distribution as shown in Figure 5.9.

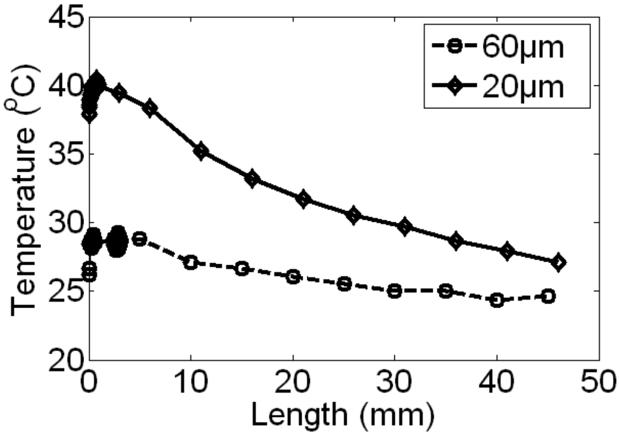

Figure 5.9: On-chip Temperature Measurements of Tapered Channel at 5 minutes for 500μA Applied Current at Different Channel Heights.

After 5 minutes, a peak temperature of 40°C was recorded at the narrow end of the tapered channel in the 20μm high tapered channel, compared to a peak of 29°C recorded for a 60μm height. It is interesting to note that the temperatures measured at both ends was consistently higher than room temperature, suggesting that even though the reservoirs were large in volume, it was inaccurate to assume that both ends of the tapered channel was constantly at room temperature throughout the experiments.

5.7 Electrolysis and Overheating

Significant electrolysis was observed during chip operation. Gas bubbles formed at both electrodes due to polarization which effectively reduced the surface area that was in contact with the liquid, and thereby affecting the current draw. In addition, bubbles can also be introduced into the channels if the solution was not degassed prior to injection, and can diffuse into the channel from the reservoirs. These small bubbles created pockets of gasses trapped inside the channel, which locally reduced the cross sectional area, increased the resistance and induced higher temperatures at these sites. With continued Joule-heating and electrolysis, these regions contract until a critical size was reached, in which the temperature became sufficiently high as to vaporize the buffer. Flashes of light were seen inside the channel in these cases, possibly due to arcing.

To prevent electrolysis, several improvements were implemented. First, large glass reservoirs were introduced to provide large buffering capacity. In addition, the electrodes were kept away from the inlets to reduce the possibility of bubbles flowing into the channel. The Tris-HCl buffer was also degassed before use. Reducing the height of the channel helped reduce the bubble diffusion, and had the effect of increasing the resistance, providing higher temperatures at lower powers. However, due to the large channel widths used combined with the flexibility of PDMS, the channels easily collapsed, sealing segments of the channel. PDMS in ratios of 5:1 were used to decrease the flexibility and prevent sagging.

5.8 Experimental Results Using Constant Power

The thin film PDMS/Rhodamine B was analyzed for its applicability in temperature measurements and the results were compared to simulated results based upon previously derived equations.

5.8.1 Photobleaching Effects

For Rhodamine B dye used as part of the thin film thermometry method, the effects of photobleaching was not entirely eliminated. However, as an estimate of potential error, the effects of photobleaching are reported here. Experiments with a tapered channel bonded to the thin film/glass setup were performed for three room temperature intensities. First, the initial intensity at room temperature was recorded along the length of the tapered channel. Next, a constant power of 276mW was applied for 10 minutes after which the thin film was subjected to halogen light excitation for 8 seconds. Subsequently, the microfluidic chip was cooled to room temperature and a second set of intensity measurements were taken. This process was repeated for the room temperature intensity after a constant power of 506mW was applied, as shown in Figure 5.10.

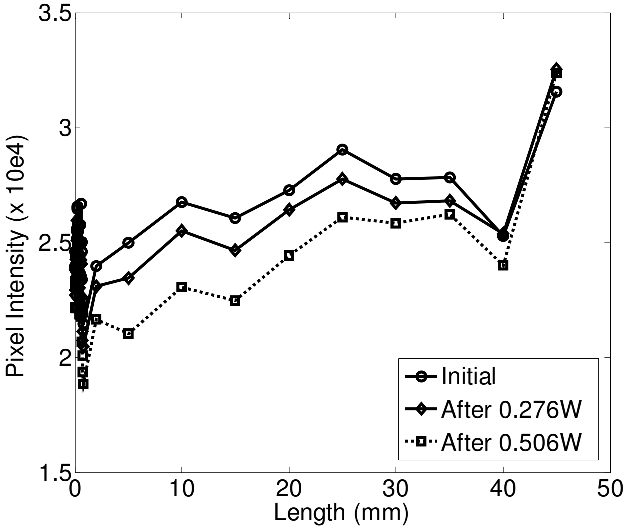

Figure 5.10: Changes in room temperature intensity readings due to photobleaching. A higher power corresponds to higher peak temperatures and a larger difference in intensity.

The narrow inlet was represented at a length of 0mm, whereas the wide outlet was located at 50mm. Larger differences in pixel intensity was seen closer to the narrow region (with approximately 8% maximum reduction), which consistently experienced higher temperatures than other parts of the channel. At the wide end, only 0.1% pixel intensity reduction was observed. In addition, higher applied powers provided more Joule heating, further decreasing the pixel intensity throughout the chip. Since diffusion had been prevented with the use of the glass barrier, any discrepancies in the intensity were solely due to photobleaching. Thus, for applications requiring repeated exposures, photobleaching should be accounted for by taking a baseline room temperature intensity after each Joule heating and exposure; repeated exposure doses compounded the photobleaching effect which further enlarged the errors after each subsequent exposure and measurement.

5.8.2 Effects of Increasing Applied Power

A control system was written for the Labsmith high voltage power supply in which a feedback loop provided the means for outputting a constant power. This eliminated the thermal runaway problem, as a feedback loop continuously measured the current and adjusted the voltage such that the total power was constant. Experiments were conducted for several different applied powers to a tapered channel with 400μm inlet, 4000μm outlet, and a consistent height of 75μm, as shown in Figure 5.11. As a comparison, simulation results are also presented.

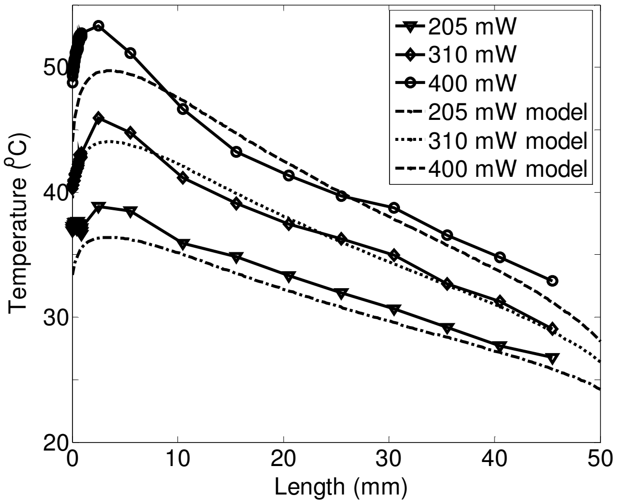

Figure 5.11: Experimental and simulated results for different applied powers. Higher than expected peak temperatures are detected at the inlet [Samy et al (accepted 2007)]

As expected, higher applied powers provided higher peak temperatures. The experimental results provided a similar trend to that of the simulated results. However, the peak temperatures at the inlet appeared to be higher than that predicted, with peak temperatures of

39°C, 46°C, and 53°C compared to simulated results of 37°C, 43°C, and 49°C for an applied power of 205mW, 310mW, and 400mW respectively. At most, there appeared to be a 4°C difference between the results. This trend may be due to a higher than expected Joule heating effect occurring at the reservoir. It is interesting to note that, with such a large reservoir, the temperature at the inlet often exceeded room temperature, and may increase past 50°C depending on the applied power. The reservoir provided some cooling to the channel, but was insufficient in cooling the narrow region to room temperature.

In addition, it should be mentioned that for lower power input of 205mW, the linear region existed at 10mm and extended to the end of the channel, representing good characteristics for measurement of protein separation. However, the peak temperature was relatively low; the range of separation would be very narrow due to the induced pH values. At higher temperatures, higher peaks provided a larger range of pH values for separation, but the temperature distribution became less linear, complicating the measurement process. The experimental values for 400mW were also plotted with simulated temperature distributions at different film thicknesses and at the fluid temperature as shown in Figure 5.12.

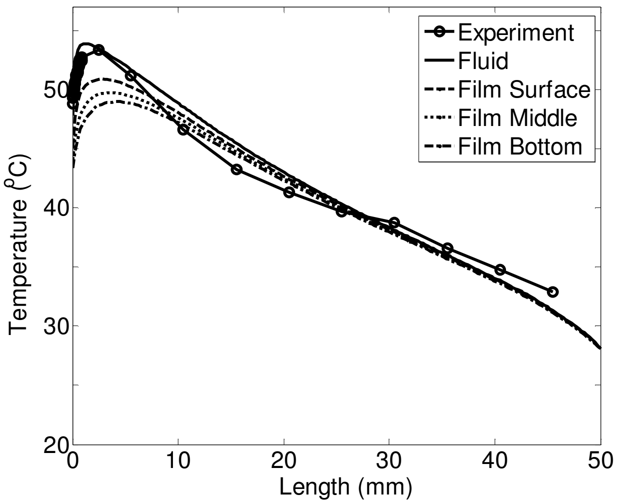

Figure 5.12: Experimental and simulated results for 400mW applied power. Simulations show heat transfer effects on temperature at the fluid, top, middle and bottom of the film, respectively [Samy et al (accepted 2007)]

The film middle represented the simulated temperature measured from the film. The results showed that the film surface and bottom had a maximum of 2°C difference located at the peak temperature. In addition, the simulated measured temperature and the fluid temperature had a maximum difference of 3.5°C. A temperature mapping overlaid with a tapered channel layout was shown at approximately 5mm from the inlet. Heating effects extended past the side wall. Such an image allowing temperature visualization of the material surrounding microchannels would not be possible with the previous Rhodamine B in liquid method (Figure 5.13).

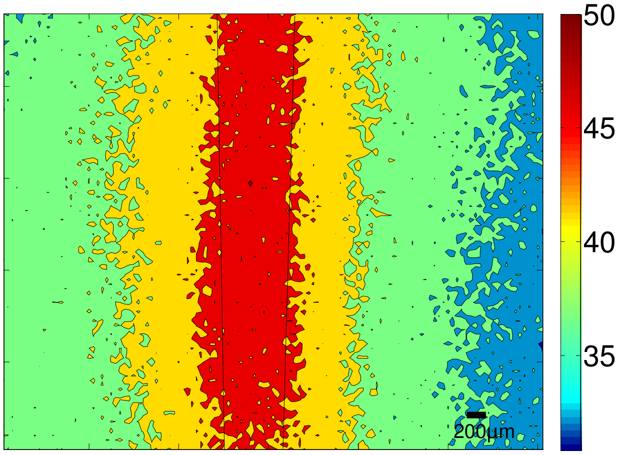

Figure 5.13: Temperature contour map overlaid with channel layout at 5mm from inlet [Samy et al (accepted 2007)]

Alternative Means of Experimental Verification

As an alternative method of validating the temperature measurement process using thin film PDMS/Rhodamine B, the traditional method of pre-mixing Rhodamine B into the bulk fluid and subsequent injection into the microchannel was performed. A complex process was devised to minimize overall Rhodamine B absorption and adsorption, with results shown in Figure 5.14.

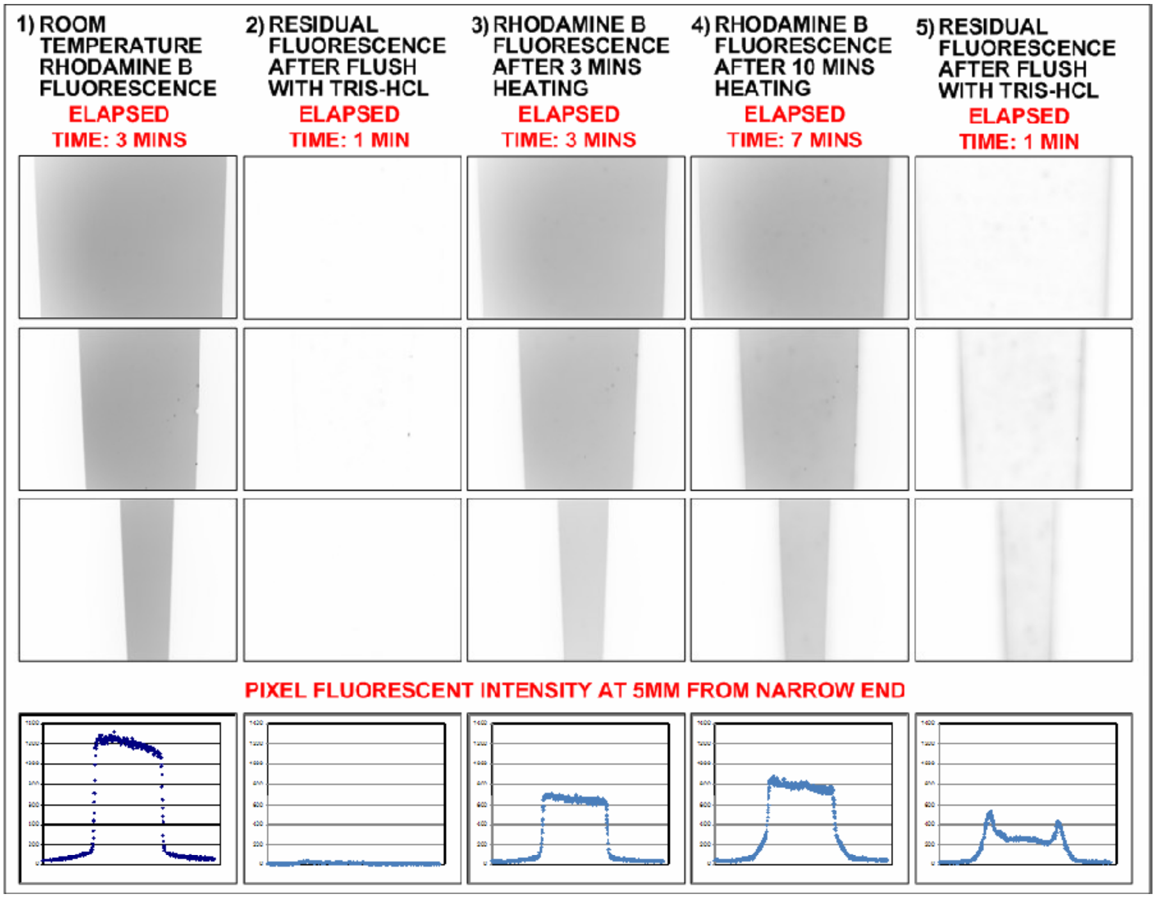

Figure 5.14: Inverted fluorescent intensity pictures and images at three positions along the tapered channel (5mm, 20mm, 35mm, taken from the narrow end) in which Rhodamine B dye (100µM) is initially mixed into Tris-HCl (25mM) and injected as a liquid into the microchannel. In addition, fluorescent intensity graph at 5mm for different steps is also provided for comparison purposes [Samy et al (accepted 2007)]

At step 1, the channel was flushed with PVP (for 5 mins) to eliminate electroosmotic flow. Afterwards the Rhodamine B solution was injected into the tapered channel and images were taken at three locations along the tapered channel (5mm, 20mm and 35mm from the narrow end). The elapsed time between the injection and imaging was 3 minutes. At step 2, the solution was flushed out and replaced with pure Tris-HCl (25mM). Images were taken again to detect any residual fluorescence, in which negligible amounts were observed. At step 3, the Tris-HCl was heated at a constant power of 400mW for 10 minutes to ensure that the heat penetrated into the surrounding side walls. Tris-HCl was then flushed and replaced with the fluorescent solution (Tris-HCl solution with Rhodamine B dye mixed), heated further for 3 minutes (at 400mW) and imaged. At step 4, another set of images was taken after 7 more minutes of heating (for a total of 10 minutes heating of the fluorescent solution). At step 5, the channels were imaged after replacing the fluorescent solution with a pure Tris-HCl solution at room temperature to observe the residual Rhodamine B due to absorption. A fluorescent intensity graph is presented at each step for the segment located 5mm from the narrow inlet.

Based upon the results of the previous thin film experiments, at the stated locations of 5mm, 20mm, and 35mm, the corresponding temperatures were 52^oC, 41^oC, and 38^oC, respectively. The traditional Rhodamine B injection method showed that after 3 minutes of heating, the resulting temperatures were 46^oC, 33^oC, and 30^oC, respectively, based on the calibration curve equation stated by Ross et al. (2001). After further heating for a total of 10 minutes, the corresponding detected temperatures were 42^oC, 27^oC, and 24^oC, respectively. At constant power, once the system had reached steady state the temperature inside the tapered channel should remain constant. However, the temperatures recorded at 3 minutes were higher than those recorded at 10 minutes. This contradicts the expected rise in temperature if the channel was not at steady state at 3 minutes. Therefore, the only solution was that absorption of Rhodamine B into the PDMS increased the overall fluorescent intensity of the image which artificially decreased the apparent temperature (temperature is inversely proportional to intensity). This was further evident thorough images taken at Step 5 where the residual intensity was nearly one half the intensity measured at Step 3 after only 10 minutes of Rhodamine B exposure. This indicated the errors and reliability issues that occur while utilizing Rhodamine B in the bulk liquid for PDMS temperature measurements.

The discrepancy between the measurements obtained using the thin film method and the method reported by Ross et al. (2001) at each point was approximately the same (6-8°C). This meant that the discrepancy was due to the consistent absorption of the Rhodamine B into the PDMS. This error increased continuously during the time in which PDMS was in contact with Rhodamine B. Using the traditional Ross method, it was difficult to reliably obtain and verify temperature measurements with those taken from the thin film PDMS/Rhodamine B. However, it had been shown that qualitatively the measurements were similar.

5.8.3 Angle of Divergence Effects

After verifying the usability of the thin film, it was applied for measuring temperatures in other designs, such as the effects on temperature for different angles of divergence. For these experiments, the inlet width was kept constant while the outlet width was changed. The angle of divergence for an outlet of 2000μm, 4000μm, and 5000μm was 0.92^o, 2.06^o, and 2.63^o, respectively. For decreasing angle of divergence, peak temperature location remained at approximately 2.5mm, while the peak temperature value decreased. In addition, the temperature gradient also decreased. This trend can be explained by analyzing the layout of the different straight tapered channel designs. With an outlet of 2000μm, the change in width throughout the channel was very small, providing less change in the resistance. This allowed for a more gradual decline of the temperature in the axial direction. The temperature was also effectively distributed farther away from the inlet as can be seen in Figure 5.15.

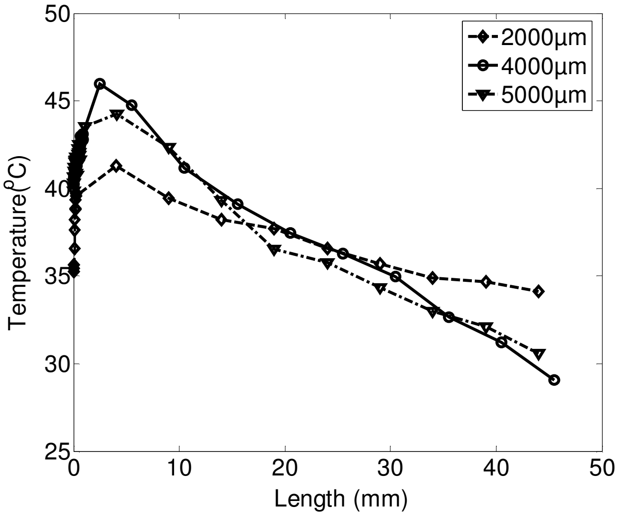

Figure 5.15: Temperature distribution for different outlet widths at 300mW applied power. Smaller outlet widths represents smaller angle of divergence, lowering peak temperatures and reducing the slope of the temperature gradient.

However, the difference in the temperature distribution of the 4000µm and the 5000µm was less distinct. This may possibly be due to the similar profiles of both; the difference in the angle of divergence was only 0.6°. By analyzing the graph, the 5000µm results appeared to follow the trend, with a slope that was slightly steeper than that of the 4000µm. However, the peak temperature for the 4000µm was slightly higher than that of the 5000µm, which was attributed to experimental detection error. This theory is supported upon analyzing the theoretical model previously presented in Figure 5.11, in which the peak temperature was estimated at 43°C for an outlet of 4000µm with an applied power of 300mW. Based upon those results, the peak temperature and slope of the temperature gradient would fit well with experimental results.

5.8.4 Effects of Side Wall Profiles

Experiments were conducted in which the performance of a 400µm inlet, 4000µm outlet, and straight side wall design was compared to that of a 400µm inlet, 4000µm outlet, and parabolic side wall profile. The parabolic side wall profile followed the equation:

$$y = 1.39 \times 10^{6} x^{2} + 200 \qquad (5.11)$$

where x represents the length of the channel in µm, and y the distance to the side wall from the centreline of the channel in µm. By analyzing the layouts, it can be seen that for the parabolic shape, the narrow region at the inlet was extended lengthwise compared to that of the straight wall profile. For both designs, the temperature distribution for an approximate power input of 400mW is shown in Figure 5.16.

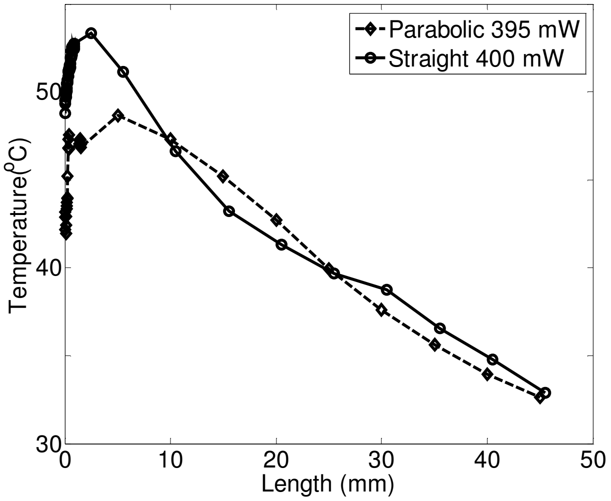

Figure 5.16: Temperature distribution of parabolic and straight side wall profiles for constant applied power.

The peak temperature of the parabolic channel was reduced and consisted of a more gradual temperature gradient. The peak temperature for the parabolic and the straight profile channels were 48°C and 53°C respectively. A reduction in peak intensity may possibly be due to an overall lower total resistance in the channel. The broadening temperature region was due to the comparatively longer region where the channel was close to 400μm in width for the parabolic shape than the straight channel shape. Thus, the high temperature region stretched for a longer length. In addition, at 400mW of applied power, the parabolic profile represented a more linear curve compared to the straight profile, making it the better choice at higher Joule heating values.

In addition side wall profiles may have other advantages in locally controlling and inducing lower or higher temperature regions. For example, a "zig-zag" pattern was developed in PDMS in which several regions of high and low temperature zones were created by repeatedly enlarging and shrinking the channel width along the axial direction. The temperature distribution of such a design is shown in Figure 5.17.

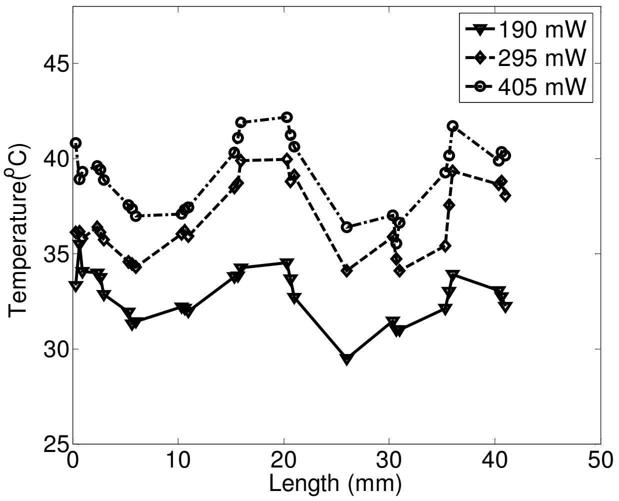

Figure 5.17: Temperature distribution of a zig-zag patterned layout at various applied constant powers.

It can be seen that high temperature regions consistently formed at approximately 1mm, 20mm, and 35mm. Due to the relatively few points taken, it was difficult to provide a smooth curve for experimental results. However, these estimated temperature peaks corresponded to the same locations in which the smallest channel width occured, located at 0mm, 20mm, and 40mm respectively.

The aim of such a design would be to allow pre-processing for Lab-on-a-Chip devices in which multiple processing steps were desired. First, the entire channel would be flushed with the protein mixture samples and upon IEF, regions with the same pH value would isolate the same types of proteins. With multiple locations, each location would then feed the sample into different reactions for performing tests in parallel.

5.8.5 Increasing Applied Powers for Parabolic Profiles

In general, for parabolic profiles there is a consistent gradual broadening of the high temperature regions due to a comparatively longer segment with narrower widths at the inlet. This trend was observed for all three applied constant powers as shown in Figure 5.18.

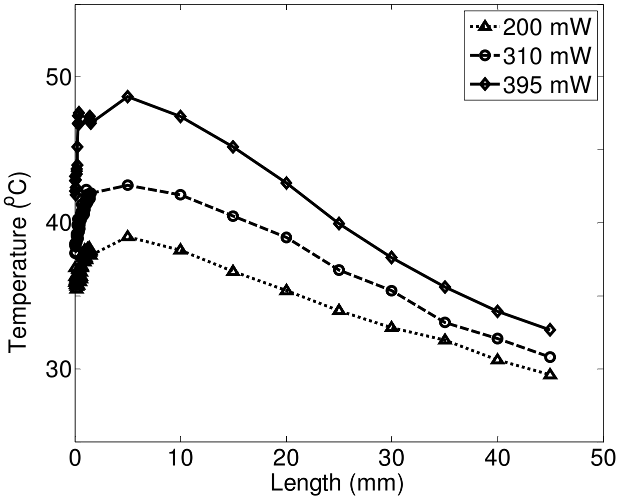

Figure 5.18: Temperature distribution of parabolic tapered design for various applied powers.

The peak temperatures occurred at approximately 5mm, which was slightly shifted compared to the straight tapered designs. In addition, the temperature gradient was linear compared to the straight channel profiles with the same inlet and outlet dimensions, although at higher temperatures of 395mW, the temperature profile was more curved compared to temperatures at 310mW. The peak temperatures at 200mW, 310mW and 395mW were 39°C, 43°C, and 49°C respectively.

5.8.6 Effects of Different Parabolic Profiles

As a comparison, experiments at different power levels were applied to a parabolic tapered channel of 50μm inlet and 4000μm outlet, with the side wall profile satisfying the equation:

$$y = 1.28 \text{ x } 10^6 x^2 + 25 \qquad (5.12)$$

The experimental results of both parabolic profiles are shown in Figure 5.19.

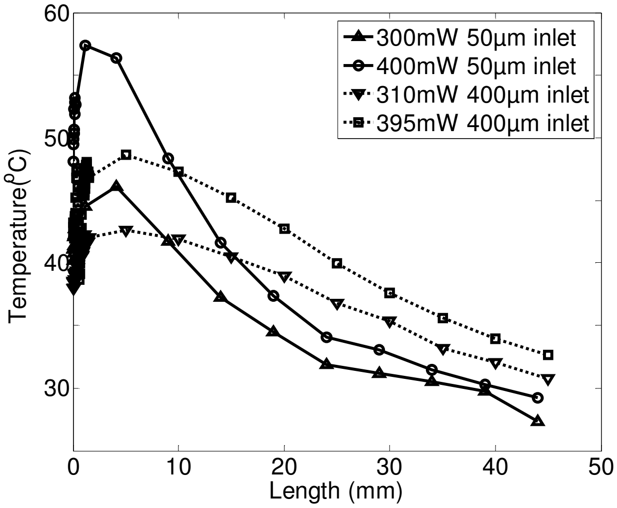

Figure 5.19: Temperature distribution for two different parabolic side wall profiles and different applied powers. Higher peaks and non-linear gradients can be observed for the 50μm inlet.

At applied powers of 300mW and 400mW, the peak temperatures for the 50μm and the 400μm inlet were 46°C, 57°C, 43°C, and 49°C respectively. The effect of having a narrower inlet caused the peak temperature to rise. Comparing the design layouts, the narrower inlet had a more dramatic change in the side wall profiles. This effectively created a steep and non-linear drop in the temperature distribution throughout the separation channel.

5.9 Applicability for Isoelectric Focusing

5.9.1 Resolution and Usability

The resolution of the IEF method was based upon the following equation [Huang (2003)]:

$$\Delta pI = \sqrt[3]{\frac{D(T)(dpH/dx)}{E(x)(-d\mu/dpH)}} \tag{5-10}$$

where ΔpI represents the resolution, D(T) represents the temperature dependent diffusion coefficient, dpH/dx the pH gradient with respect to channel length, E(x) the electric field, and $d\mu/dpH$ the mobility dependence on pH. Analyzing the equation, higher resolutions were possible for lower diffusion coefficients, lower pH gradients, higher electric fields and a higher mobility. The benefit of Tris-HCl for IEF with thermally generated pH gradients was the small pH change within the 20^{o}C to 80^{o}C operation range. Thus, as long as a consistently linear temperature gradient was established along the IEF device, a high resolution can be obtained. The rate of change of mobility with respect to pH was an intrinsic property and cannot be changed. The diffusion coefficient was temperature dependent, however within the operation range, the value was relatively constant and cannot be manipulated. However, a disadvantage in using this IEF method was the constantly changing electric field along the length of the channel, based upon equation 5.3. Thus, the resolution was non-uniform throughout the channel.

Another disadvantage to utilizing the Joule heating based IEF technique was that the usable ranges were between 5mm and 50mm, as only in this range was the temperature gradient relatively linear. This was a disadvantage compared to conventional CIEF techniques where the whole capillary column would be used for separation. A reduced separation length would effectively decrease the pH range available for separation.

The device performance was also limited by the amount of electrolysis occurring inside the channels, which was dependent on the current. At 400mW, the currents generated were routinely in the order of 500μA to 700μA, facilitating bubble generation. Thus, it was impractical to exceed 400mW applied power for all of the experiments due to the large amounts of electrolysis.

5.9.2 pH Distribution Estimates

The temperature distribution derived from experimental results was used to estimate the pH distribution in the axial direction of the channels. The parabolic and the straight tapered design, both with inlets and outlets of 400μm and 4000μm were chosen as prime candidates for practical use, due to their relatively linear temperature gradient extending past the peak temperature. In addition, only the results from the 400mW applied powers were used, as they represented the largest difference between maximum and minimum temperatures, and thereby provided an estimate as to the maximum pH levels attainable for the specific design. The pH level estimates are shown in Figure 5.20.

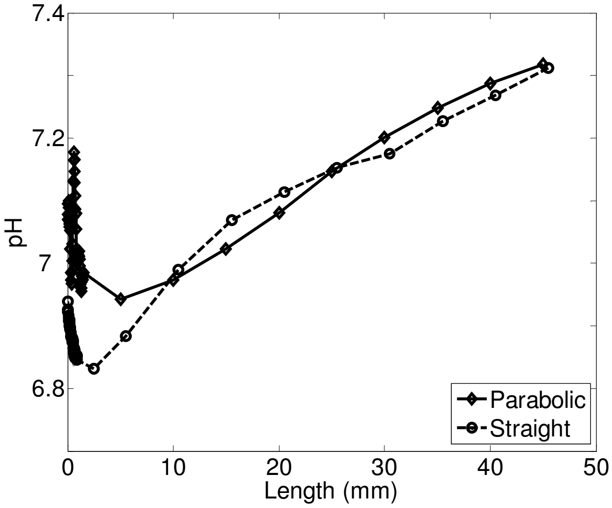

Figure 5.20: pH estimates from straight and parabolic profiles, based upon temperature distributions derived from experimental data. The pH values are based upon Tris-HCl buffer with a pH of 7.5 at room temperature.

The straight profile tapered channel provided a slightly superior performance as the pH range is 6.8 to 7.3, whereas that provided by the parabolic profile can obtain a pH range of 6.9 to 7.3. In addition, the linear gradient portion of the graph occured sooner at 2.5mm for the straight profile compared to 5mm for the parabolic profile. Even though the pH range was small and thus the separation power was higher, it complicated the process as prior knowledge of the pI values of the samples must be known.

5.10 Future Work

Joule heating based IEF is a promising technology which may provide benefits compared to conventional CIEF techniques. However, due to the non-uniform electric field occurring throughout the axial direction of the channel, resolution was non-uniform. In addition, the varying widths along the axial direction of the channel required for Joule heating also detrimentally affected the accuracy and resolution of the process. Thus, the use of Joule heating may not be ideal in such an application. Other techniques for establishing the required temperature gradients such as *via* external heaters should be investigated.

5.11 Summary

A temperature sensitive thin film described in the previous chapter was applied to measure temperature distributions of Joule heating based IEF designs fabricated in PDMS. Straight, parabolic, and zigzag designs of various configurations were fabricated, experimentally tested and compared to simulation.

- Thin film not only provided temperature visualization of the microfluidic channel, but of the surrounding material as well, allowing for the investigation of heat transfer effects throughout microfluidic devices.

- Joule heating based IEF is based on the concept of temperature dependent pH values for Tris-HCl buffer. However, the range of pH values was relatively small (< 1) which was beneficial for samples with very close pI values, but difficult to apply to samples with very different pI values.

- Constant power must be used in this application, as constant voltage or constant current produced thermal runaway problems, preventing the system from reaching steady state and stopping sample focusing.

- Due to the high currents, electrolysis was a common occurrence, which led to bubble formation inside the channels. To reduce the chances of bubble formation, choose a relatively small depth, utilize large reservoirs, and ensure electrodes are far from the channels such that bubbles forming on them will not migrate into the channels.

- At higher applied powers, higher peak temperatures can be obtained, but with tradeoffs such as the generation of higher currents leading to electrolysis.

- Straight tapered channel designs generally produced a straight temperature gradient profile after the peak temperature. With smaller angle of divergences, smaller peak temperatures and a more gradual slope was observed.

- Parabolic tapered channel designs with a gradual change in channel width may at certain powers provide a straighter profile compared to straight tapered channels. Parabolic designs with larger changes in width may result in the production of higher temperature peaks and steep temperature drops throughout the channel.

- Due to cooling effects of the reservoir, segments of the channel directly at the narrow inlet were cooler than the peak temperature. This effectively shrank the usable space of the separation channel by approximately 2.5mm to 5mm depending on the layout chosen.

- Due to the non-linear electric field throughout the axial direction of the IEF separation channel, the resolution was not consistent throughout the device. Other methods that do not require Joule heating should be investigated.

Chapter 6

Chip Format Capillary Isoelectric Focusing

6.1 Introduction

Capillary Isoelectric Focusing (CIEF) has been the most generally accepted method for protein and ampholyte separations. The combination of CIEF and the whole column image detection technology is commercially available [Convergent Bioscience]. In this method, samples are introduced inside a capillary with an established pH gradient using CAs, and separated based upon their individual isoelectric point (pI). At the isoelectric point, the charge of the particle balances with the pH value of the surrounding solution, such that in an electric field, there is no net migration of the sample.

For focusing in CIEF, the pH gradient is established using CAs which are composed of many low molecular weight ampholytes engineered with a predetermined pH range. As each type of ampholyte has a specific pH = pI range, typically a solution of CAs contains hundreds of ampholytes of different pI values that are evenly spaced along the range. The pH gradient is established when a constant voltage is applied and establishes an electric field inside the separation capillary containing the CAs. Due to the size difference of CAs (which are typically of lower molecular weight) compared to sample proteins, CAs have a higher mobility than proteins, allowing the pH gradient to establish quickly, for the subsequent sample separation. After the establishment of a pH gradient, samples migrate according to their respective charge, and will stop upon reaching a charge balance with the surrounding pH.

There are several disadvantages associated with the current commercially used CIEF cartridges and there is strong motivation to develop chip format CIEF technology. This chapter discusses the fabrication of chip format CIEF devices and their performance compared to commercial cartridges.

6.2 Commercial Capillary Isoelectric Focusing Cartridges Design

Current designs used in the industry involved a circular cross section capillary tube for separation, of 100μm inner diameter and 5cm length. At each end of the tube, an injection capillary was attached to the tube *via* a cylindrical hollow fibre membrane section. Large reservoirs filled with electrolyte were positioned over each of the hollow fibre membranes. These membranes were utilized for two reasons. First, they allowed for sample to be introduced through the injection capillary and into the separation capillary. Secondly, it prevented the sample from diffusing into the electrolyte filled reservoirs while at the same time provided electrical conductivity, as ions were freely able to penetrate through the membrane. Due to oxidation and reduction processes at the electrodes which may potentially alter the buffer solution at the CA, the separation capillary was effectively isolated through the use of electrolytes; acid and base was placed in the anode and cathode respectively. A typical CIEF cartridge and machine setup is shown in Figure 6.1 [Wu et al. (2001)].

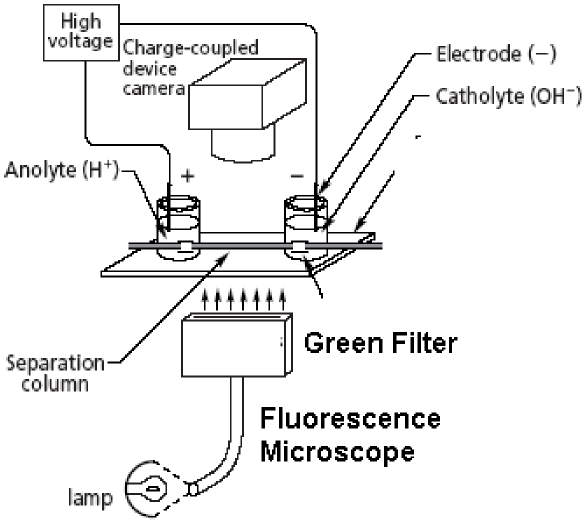

Figure 6.1: Typical CIEF cartridge with machine setup [Wu et al. (2001)].

A very important design issue for the whole column imaging CIEF was the 280nm UV light emitter and detector. The effective width of the detection light path along the channel was approximately 2mm. The location of the light path was built into the machine, and was designed to be centred along the capillary channel cartridge. For alignment purposes, three pegs were built into the machine, such that when the cartridges were pushed flush against the pegs, the detection path was aligned with the capillary. This posed as a problem for cartridge fabrication, as PDMS must be aligned and cut accurately to ensure the separation chamber was located in the light path.

The fabrication of such a device also provided several disadvantages. First, it was labour intensive, requiring difficult tasks which included alignment of the injection and separation capillaries to the hollow fibre membranes, and the alignment of a metallic slit along the separation channel to block out background noise, which when combined may potentially take hours to fabricate. In addition, the use of separation capillaries with circular cross-sections deflected the detection light, providing disadvantages in signal detection. For example, light rays penetrating the fused silica capillary along its curved surface refracted and diffused the light path, thereby reducing peak detection signals. Although the implementation of a slit with a width that was narrower than the width of the capillary is currently employed to reduce the amount of light refraction, the signal intensity had decreased as well, reducing the sensitivity of the measurements. Finally, with circular cross sections, the channel depth in which the light penetrated was limited to the size of the capillaries which can be commercially bought.

6.3 PDMS Cartridge Design and Fabrication Issues

Microchannel fabrication in PDMS *via* soft lithography and replica molding offers several advantages over fused silica capillaries. Channel cross sections are rectangular, providing less amount of refracted light. In addition, any channel width or height can be fabricated; the limitation being the maximum aspect ratio (*h*:*l)* allowed before deformation of the channel structures occur during fabrication of the silicon masters. With the current equipment setup, consistent uniform channels can be reliably fabricated at an aspect ratio of approximately 8:1, with a channel width of 20µm. Due to the small dimensions involved in the fabrication, silicon substrates were utilized. Previous fabrication on glass substrates resulted in poor adhesion, non-uniformity, and lift-off of certain channel segments. Another important benefit using chip format CIEF devices was that it allowed integration with other processes such as pre-column sample treatment and post-column sample labelling. The integration cannot be realized in the current iCE280 analyzer in an easy manner.

As an initial study to the benefits of utilizing rectangular cross sections, a microchannel of 100µm by 100µm cross section and 50mm length was designed and fabricated. However, during the design of the cartridge, several fabrication issues had to be resolved. As previously mentioned, due to the alignment of the separation channel to the detectors in the machine, the mask must be designed to allow for ease of fabrication. As an example of the tolerance allowed, if a 100µm wide channel was fabricated, the sides parallel to the channel had to be cut without exceeding an error of 950µm. Thus, to facilitate its fabrication, an outline of the cartridge was included into the mask and the pattern was transferred to the master.

It was also discovered through preliminary experiments that the microscope glass slides commonly used for chip bonding to microchannels were opaque to the UV 280nm wavelength. Fortunately, PDMS was transparent at that wavelength. Thus, a new approach was utilized in which the PDMS microchannel was bonded to another PDMS with a flat surface. Initially the PDMS “flat” was fabricated by pouring and curing the mixture in an aluminum weighing pan. However, the high surface roughness patterns of the weighing pan was directly transferred to the PDMS. Thus, a blank silicon wafer placed inside an aluminum pan was used to provide a flat surface. To discourage adhesion between the PDMS and silicon wafer, the wafer was pre-treated with tricholoromethylsilane (TCMS) for half an hour.

Creating relatively uniform thickness PDMS molds was also problematic, as contaminants in the vacuum oven had created unevenness along the bottom of the oven. If the aluminum pans were not flat, the PDMS would cure with a slope on the surface, detrimentally affecting the light detection. To resolve this issue, the aluminum pan was placed on an overturned petri-dish such that the walls of the petri-dish were placed against the bottom, reducing the probability that some part of the petri-dish rested on the contaminants. In addition, a leveller was used to ensure levelness before curing.

During cutting and handling, oil and grease from the hands left smear marks onto the PDMS. The PDMS also appeared to absorb dirt and dust from the air and table surface. Dirt and smear marks reduced the ability of the light to accurately detect the separation channel. To ensure its cleanliness, nitrile gloves were worn during handling and a protective cover (Saran wrapping) was placed onto the PDMS surface. Previously, parafilm was used as a protective cover, but it detrimentally affected the PDMS, as high temperatures caused a white film to transfer onto the PDMS surface.

Due to the PDMS-PDMS bonding method used, it was decided that microfluidic access holes be punched into the PDMS flat piece. This allowed for less handling of the microchannel mold, and would be useful for future designs in which a membrane can be bonded in between the access hole on the PDMS flat and the straight channel on the other PDMS mold. However, the microfluidic access hole also required aligning. Thus, a separate mask was created in which a square cavity representing the location for punching the microfluidic access hole was placed. Guidelines and markings corresponding to each other were fabricated in both the top and bottom PDMS molds to facilitate alignment. Due to the resulting increased flexibility of the PDMS-PDMS cartridge, the bonded pieces were placed onto a quartz microscope slide which was transparent to UV 280nm wavelengths.

The master was fabricated according to the steps outlined in Chapter 3, with specific process parameters depending on the channel depths required. After the master was created, approximately 30 grams of PDMS in a 10:1 ratio were poured onto the silicon wafer placed inside an aluminum weighing pan to create an approximate thickness of 1mm of PDMS. The mixture was degassed for 30 minutes and cured at 80°C for 1.5 hours. Once cured, the PDMS was removed and trimmed to the same size as a rectangular microscope slide, corresponding to the exact dimensions of the commercial cartridges.

6.4 Preliminary Results

Hemoglobin samples were prepared by mixing with CA and injecting into a commercial cartridge from Convergent Bioscience and performing CIEF. The sample solution used was composed of 1.0mg/mL hemoglobin, 1% PVP (w/v) and 2% (v/v) CA, within a range of pH 3 to 10. The results are shown in Figure 6.2.

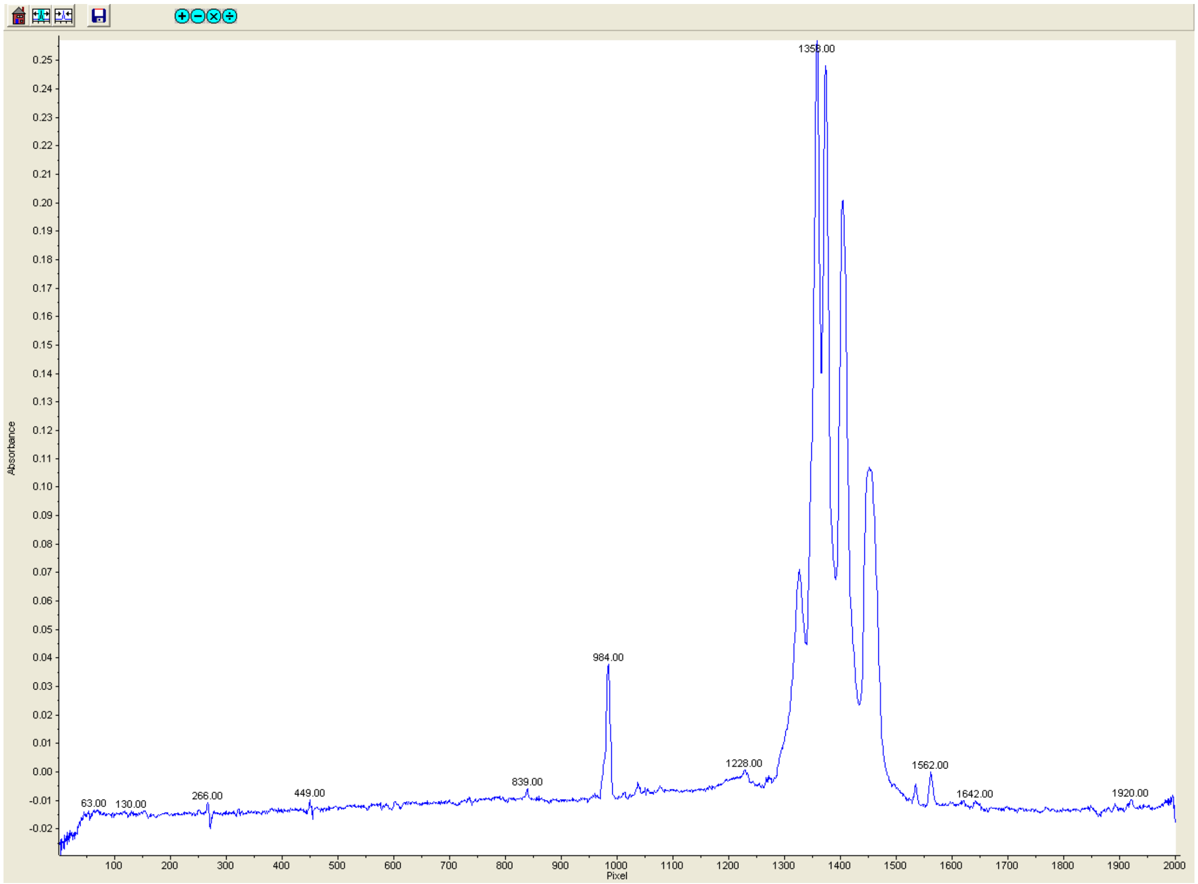

Figure 6.2: CIEF of Hemoglobin on a Convergent Bioscience cartridge.

The same solution was also injected into a PDMS-PDMS cartridge consisting of a single separation channel and microfluidic holes, as shown in Figure 6.3.

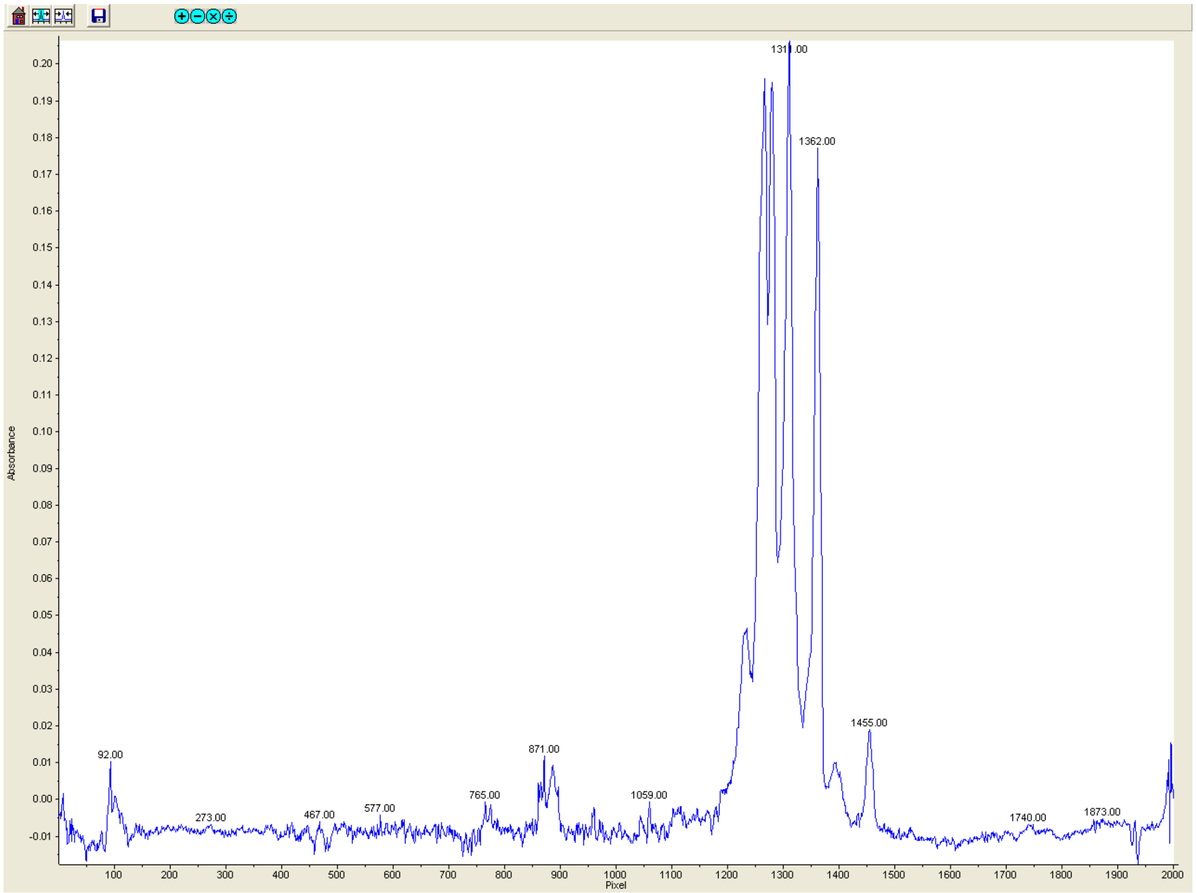

Figure 6.3: CIEF of Hemoglobin on a microfluidic device consisting of a straight separation channel and microfluidic access holes.

Based on the preliminary results, the microfluidic device was able to provide better signal to noise ratio; smaller signals (visible as small peaks throughout) which were barely noticeable in the commercial cartridge, were resolvable with the PDMS cartridge. Upon closer inspection, the PDMS cartridge provided higher background noise. This was possibly due to that fact that no slit was used to cover the sides of the PDMS channel. Thus, when the samples were separated and imaged, imperfections in the PDMS along the 2mm wide light path was also recorded creating the background noise. However, it should be mentioned that small actual peaks were more prominent than the background noise, and similar peaks were also detected in the commercial cartridge, thereby increasing the possibility that the signals were due to the separation process. In addition, increased resolution of the individual peaks was observed (characteristic of narrower band signals), with 7 distinguishable peaks for the PDMS cartridge, compared to 5 separate peaks observed for the commercial cartridge. The reason for this trend is currently not known, as the experiment was repeated with a separate PDMS cartridge. One explanation that was presented was that less Joule heating was created in the PDMS cartridge, reducing sample diffusion and thereby narrowing the bands. However, PDMS was an insulative material, such that any Joule heating formed would be effectively trapped within, producing opposite effects than that which was observed.

6.5 Improvements of Basic PDMS Design

Several components need to be implemented in the basic straight channel design such that its performance and usability matches that of the commercial cartridge. These items include sample injection capillaries, membranes, and UV blocking slits.

6.5.1 Sample Injection Capillary

With the commercial cartridges, an injection capillary at each end of the chip allowed for the sample and CAs introduction. The capillary incorporation into the commercial cartridge was labour intensive, requiring alignment and insertion into a hollow fibre membrane. With the use of PDMS, the microchannel layout was modified, extending the channel to incorporate a tapered region at each end. The same injection capillaries were inserted at both ends of the tapered region allowing for easy insertion and alignment with the separation channel. Liquid PDMS was mixed and applied as an adhesive to the taper opening and capillary interface, preventing sample leakages as shown in Figure 6.4.

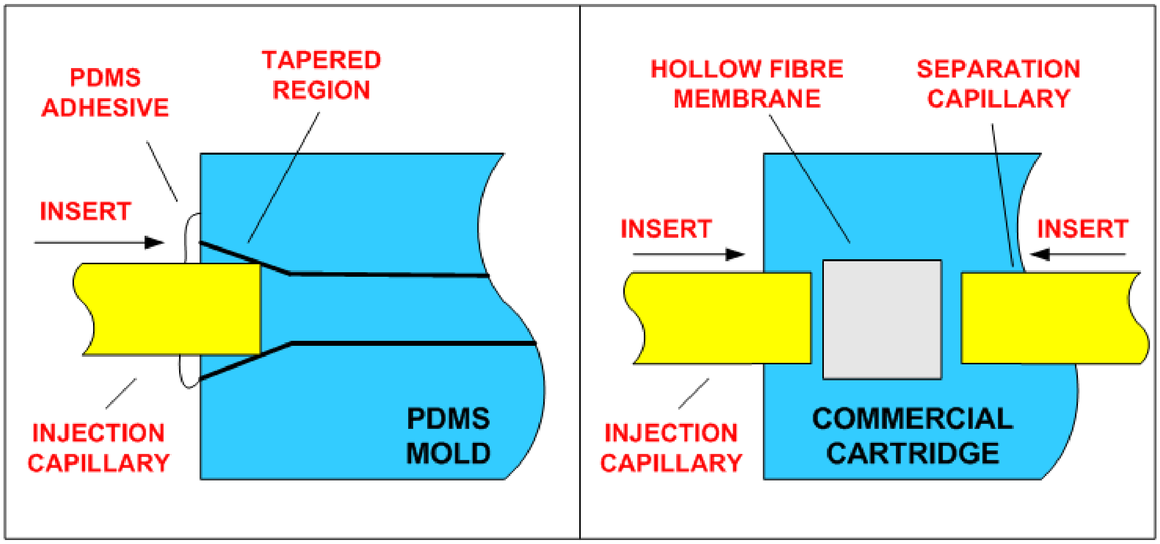

Figure 6.4: Capillary insertion method in PDMS microfluidic device (left) compared to commercial cartridge (right). Difficulty in commercial cartridge method lies in the alignment of the capillary with the hollow fibre membrane.

6.5.2 Membrane

The role of the hollow fibre membrane is to segregate the electrolytes from the separation channel, allowing ions to flow through while preventing samples from flowing out into the electrolyte. For the PDMS cartridge, two different membrane incorporation methods were evaluated. The first involved bonding membranes to the top of the microfluidic access holes. This method was easy to perform, but a dead volume region existed due to the thickness of the top PDMS layer and thereby trapping bubbles, as shown in Figure 6.5.

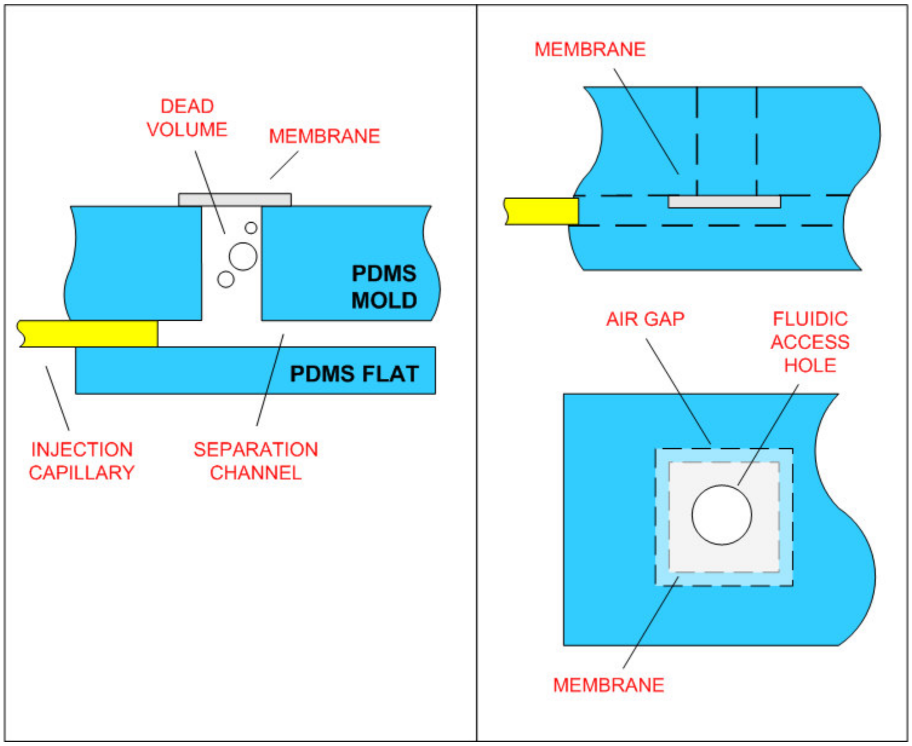

Figure 6.5: Bonding membrane on top of the microfluidic access hole (left) compared to sandwiching membrane between top and bottom PDMS layer (right). The first method will create dead volume, whereas the other method introduces air gaps.

A second method incorporated the membrane by sandwiching the membrane in between the top and bottom PDMS layers. This method eliminated the dead volume problem but was difficult to perform as it required accurate alignment. Since the membrane attached directly onto the channel surface, potential problems include blockage of the channel, and the introduction of air gaps at the membrane boundary due to the poor bonding as a result of the membrane thickness. These air gaps would allow samples to flow and fill the air gaps. For single use, such a PDMS cartridge design would be sufficient. However, commercial cartridges were typically attached to automated machines that perform several CIEF experiments in series on the same cartridge. If used for repeated CIEF with different samples, contamination would occur making the results unreliable. Even though the second option could not resolve all the problems, it still represented the best option, considering all the advantages and disadvantages of both.

6.5.3 UV Blocking

A metallic slit was used to cover unnecessary regions along the separation channel to improve the signal to noise ratio. However, aligning the metal slit was labour intensive, such that other methods were investigated. Research into 1mm thick PDMS doped with high concentrations of Sudan Black and its variants were carried out by Hofmann et al. (2006) and was shown to successfully block out UV, with certain variants blocking out certain UV ranges. Wu et al. (2005) developed a method in which a PDMS microchannel mold was dipped into a thin PDMS film of several microns and used as an adhesive layer for bonding with another PDMS layer to form a continuous material. Combining both research areas, the goal was to develop a thin layer of PDMS which would be able to block UV 280 nm wavelength, thereby acting as metallic slits along the length of the channel.

Experiments were conducted in which PDMS in base to curing agent ratio of 10:1 was mixed with Toluene, with a Toluene concentration of 10%. Sudan Black was added to the mixture at different concentrations, up to a maximum of 100mg per gram of PDMS-Toluene mixture. The mixture was spincoated onto rectangular glass slides at 6000rpm for 60 seconds to create a thin film of 10μm thickness. Next, a PDMS microchannel mold was dipped onto the thin film, lifted off, and subsequently placed onto another PDMS layer and measured for UV blocking. Unfortunately, limited blocking was observed. In addition, the Sudan Black appeared to partially recede, as the coating was non-uniform; small dark circular regions were distributed throughout, preventing consistent uniform UV blocking.

6.5.4 Future Work

Unlike separation capillaries, PDMS separation channels can be fabricated with a wide variety of dimensions. Future work will focus on the effects of channel dimensions on the whole column imaging, in particular the effects of shorter separation lengths. Shorter lengths would allow for faster separation. In addition, fabricating channels with the same cross sectional area but different height to width ratios would allow for optimization of the light path length and the signal to noise ratio. Smaller cross sectional area channel could also be fabricated to reduce the amount of CA required.

6.6 Summary

- The use of soft lithography and replica molding can provide improvements to current commercial cartridges for whole column imagining CIEF. In particular, benefits include:
  - Low fabrication cost and ease of manufacture
  - Possible performance improvements in improved resolution and better signal to noise ratio
- A proof of concept of a straight separation channel in PDMS was fabricated providing slightly better results than current commercial cartridges. An actual chip with the integration of sample injection capillaries, membranes, and UV blocking slit had been built but not tested.

Chapter 7

Micromixers

7.1 Introduction

The benefit of utilizing PDMS material for micromixer fabrication is the ability for optical and UV transparency, allowing for external imaging methods such as optical microscopes and lasers to penetrate and visualize the mixing and formation of reactants. Unfortunately, there are disadvantages as well. For example, due to the low yield strength of the material, irreversible seals can be broken if the internal pressures exceed approximately 207 kPa. In addition, any external forces applied to the device such as bending or sagging, can influence the microchannel and correspondingly change the performance of the flow. However, PDMS microfluidic chips offer a low cost and rapid prototyping alternative to other commercially available micromixers fabricated in glass and silicon. Considering the inaccuracies, the method provides an approximation of the mixing performance and potential of micromixer designs.

In this chapter, a brief discussion on micromixers is presented, with an emphasis on choosing the pumping method and the corresponding fabrication process. The pumping mechanism is very important to the design and operation of micromixers; certain requirements of EOF restrict its applicability to certain chemistries, whereas fabrication issues are important to pressure driven flow. A 2D simulation is created in COMSOL Multiphysics, and an analysis of the results pertaining to micromixer design is presented. In addition, detection methods for experimental validation are briefly discussed.

7.2 Electroosmotic Flow and Pressure Driven Flow

For the mixing of two solutions inside a typical Y-channel micromixer, electroosmotic flow (EOF) or pressure driven flow can be used, with each type having advantages and disadvantages. EOF requires a polar liquid medium and a charged surface. Typically material surfaces of glass and PDMS have a negative surface charge which makes it suitable for EOF. The advantages of EOF include its plug like profile, which makes the analysis of mixing performance easier. It is relatively easy to setup, requiring only a polar medium and electrodes for its control. In addition, as the method is based upon the flow of ions at the solid-liquid interface, by utilizing treatments to alter surface charge and manipulating certain segments of the channel, convection and corresponding pressure gradients can be induced. EOF typically form lower flow rates than pressure driven flow, but is well suited for PDMS applications, as such polymeric materials often break at low pressures. However, there are several disadvantages. Even though EOF is simple to setup, a higher degree of complexity is required to implement in micromixers. Micromixers generally require continuous flow and consistent performance over a long time period. Continuous flow in purely EOF is possible by connecting tubing at the reservoirs but the difficulty lies in embedding electrodes into the PDMS or depositing onto glass slides before bonding to the microchannel during device fabrication. However, pumping is possible, in which pressure driven flow is induced by an electroosmotic pump configuration. With EOF, many different factors affect the flow, such as the concentration of the ions, the pH of the buffer or electrolyte and corresponding ionic surface charge, PDMS zeta potential, temperature (and possible joule heating effects), and the applied electric field.

It is interesting to note that, of all the variables listed, only electric field can be directly controlled in an experiment. Zeta potential, which depends upon the concentration and the pH of the solution, represents a great uncertainty, as all known values are derived from experiments based upon EOF. These measurements represent only an approximation; there is no known method of measuring only the zeta potential. In addition to the unknowns, fluid level heights create pressure gradients, inducing pressure driven components in the flow. Thus, even if EOF is established, it is difficult to utilize and study the variables that may affect micromixing, as changing the solution concentration may affect the characteristics and performance of the EOF. In addition, by applying an electric field, electrolysis occurs at the electrodes, in which bubbles form, which may cause a flow of bubbles into the channels. Electrolysis, over a long duration (depending on the buffer) would change the solution properties, preventing continuous and stable properties from being achieved over time.

Pressure driven flow is another option, in which a syringe pump is connected directly to the inlet of the microfluidic device through tubing. In this option, special microfluidic connectors are required, in which the tubing can be screwed in place to the device, ensuring a leakage free connection. The advantage of pressure driven flow is that it is relatively simple to use and implement for continuous flow. Syringe pumps holding large amounts of liquid can be pumped into a chip with consistent flow rates. In addition, higher flow rates are possible, but are of limited use due to low pressure constraints of the PDMS. Also, pressure driven flow is compatible with organic and inorganic solvents. One significant disadvantage is that, to ensure leakage free connection, the connectors are screwed on, thus requiring a lot of handling. This can put torsion and shear forces on the connectors, making them prone to leakages. This was observed during the fabrication process. In addition, it is slightly harder to induce mixing in PDMS, as mixing with pressure driven flow in microchannels tend to require higher flow rates and three dimensional channel layout and geometries. However, overall pressure driven flow is a reliable and easy method of obtaining continuous flow at relatively higher flow rates.

7.3 General Micromixer Fabrication

Micromixer designs were fabricated using soft lithography and replica molding. In general, microscale flow rates are low and predominantly laminar, and mixing is diffusion dependant. Thus to effectively increase the efficiency of mixing, it is important to obtain large surface areas in which diffusion can occur. This is accomplished by using high aspect ratio channels, consisting of large heights and narrow widths.

The master and mold fabrication is straightforward; once the desired height and width are known, the fabrication process is similar to the steps discussed previously. However, once the mold has been fabricated and is bonded to a glass slide or another PDMS *via* oxygen plasma surface modification, the next steps depend upon the method of fluid flow. For EOF applications, glass reservoirs of 1/4" inner diameter, 3/8" outer diameter, and 1.5cm high are attached to each of the microfluidic access holes. The purpose of the glass reservoirs is to reduce the effects of electrolysis and deter any subsequent bubble formation at the electrode from diffusing into the mixer channel. The reservoir adhesion process involves mixing PDMS in a base to curing agent ratio of 10:1, smearing a thin layer of it onto an aluminum foil, dipping the reservoir onto it and subsequently fixing it onto the access holes. The whole device is then placed inside a vacuum oven for 15 minutes at 80^{o}C. Afterwards, with the glass reservoirs slightly cured in place, more PDMS is applied forming a fillet at the interface. The whole device is heated once again for 1.5 hours at 80^{o}C, solidly curing the reservoirs in place.

When pressure driven flow is used, due to the requirement of integrating a syringe pump, nanoport connectors are utilized with a slight modification of the fabrication step. After creating the mold, an approximately 1mm diameter hole is punched for the access hole. The size of the hole is different than when glass reservoirs were used requiring a hole diameter of 2mm. A smaller hole is necessary due to the smaller inner diameter of the nanoport connector. These nanoport connectors are fitted with ferrules that eliminate the amount of dead volume inside the connectors, such that switching of the fluid occurs faster. The outlet was fitted with a connector (Mcmaster Carr, New Jersey) which employed a simple low cost design. For reusability of the connectors, the nanoport connectors were cleaned with isopropanol and adhered to a 1cm by 1cm acrylic piece of approximately ¼" thickness. A large paperclip was used to apply pressure to the connector and the acrylic to ensure good bonding. It was found that, due to the unevenness of the paperclip surface and the low melting point of the acrylic, the acrylic should rest on a flat surface when heated to minimize deformations. Deformations caused leakages at the connector/device interface. After curing the connector-acrylic assembly in an oven at 130°C for 1.5 hours, the connector holes were aligned to that of the PDMS chips. Initially, PDMS was used as an adhesive with a process similar to that for attaching glass reservoirs. However, it was discovered that, attaching the syringe pump to the connectors required several twists and turns to screw the connector in place. This action, coupled with high pressures when the syringe pump was activated, created leakages at the connectors. After an application of 10μL/min, the connectors leaked fluid. Thus, silicone adhesive was purchased and applied to the surfaces and bonded in a vacuum oven for 30 minutes at 80°C, providing a good seal.

7.4 Potential Micromixer Designs and Fabrication

To investigate mixing in the microscale and to find candidate designs for fabrication and testing, two designs utilizing pressure driven flow were chosen and simulated in COMSOL Multiphysics (Figure 7.1).

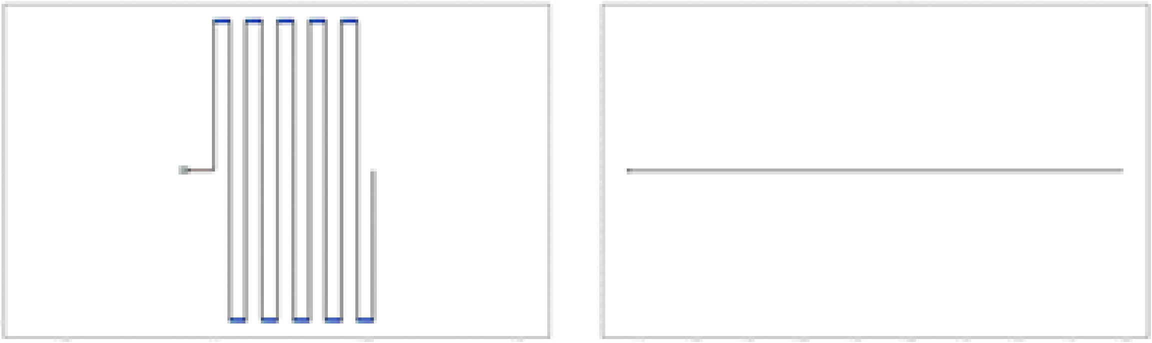

Figure 7.1: Channel layout of the serpentine (left) and the straight (right) channels from simulations. The width of both channels is 25µm.

In both simulations, COMSOL Multiphysics allows for the coupling of the Incompressible Navier-Stokes, continuity, and convection-diffusion equations:

$$\rho \frac{\partial v}{\partial t} - \mu \nabla^2 \mathrm{v} + \rho(\mathrm{v} \cdot \nabla)\mathrm{v} + \nabla \mathrm{P} = 0 \qquad (7.1)$$

$$\nabla \cdot \mathrm{v} = 0 \qquad (7.2)$$

$$\delta_{ts} \frac{\partial c}{\partial t} + \nabla \cdot (-D\nabla c + c\mathrm{v}) = 0 \qquad (7.3)$$

where ρ is the density (set at 1000 kg/m^3), v is the velocity field, μ is the dynamic viscosity (10^{-3} Pa·s), P is the pressure field, δ_{ts} is the time scale coefficient, D is the diffusion coefficient (10^{-9} m^2/s), and c is the concentration.

As a standard method for comparison, a straight channel design was chosen consisting of a rectangular cross section of 25µm by 200µm, with no slip boundary conditions. The two inlet channels, each consisting of a cross sectional area of 25µm by 200µm, merged into the main straight channel. The side walls were set to a no slip boundary condition (v = 0), the outlet was set to a neutral (no constraints) condition. The constraints for the convection-diffusion equation involved an insulation boundary side wall, convective flux outlet, one inlet with a concentration of 1.0 mol/m^3, and the other inlet with a concentration of 0 mol/m^3. To solve the model, a mesh of 32000 elements was utilized.

The serpentine design was chosen due to its ease of fabrication involving soft lithography techniques. In addition, such a design allowed for compactness of the mixer and makes detecting easier as the design is localized in a small surface area. The main channel dimension consisted of a rectangular cross sectional area of 25μm by 200μm with short segments at each bend consisting of 100μm by 200μm rectangular cross sections. Similar to the straight channel conditions, no slip side wall boundary condition and neutral outlet were employed for the Navier-Stokes equation. Insulation side wall boundary condition, convective flux outlet, two inlet concentrations of 1.0 mol/m^3 and 0 mol/m^3, respectively were utilized for the convection-diffusion equation. To solve the model, a mesh of 36000 elements was utilized.

Both models were operated for fluid velocities of 0.05m/s and 0.5m/s, representing a volumetric flow rate of 9x10^{-4}L/hr and 9x10^{-3}L/hr respectively. A concentration of 0.5mol/m^3 represented perfectly mixed dye. For simplicity, a mixing efficiency was estimated by using the following equation:

$$E = \left(\frac{C_0 - C_{avg}}{C_{avg}} \right) x100\% \qquad (7.4)$$

where E is the mixing efficiency, C_0 is the concentration at the side wall, and C_{avg} is the concentration at the centre of the channel. A mixing efficiency of 95% is taken as complete mixing. Both models were solved using a direct (UMFPack) linear system solver. Afterwards, cross-channel concentration profiles were taken at various locations along the length of the channel and compared (Figure 7.2 to Figure 7.5).

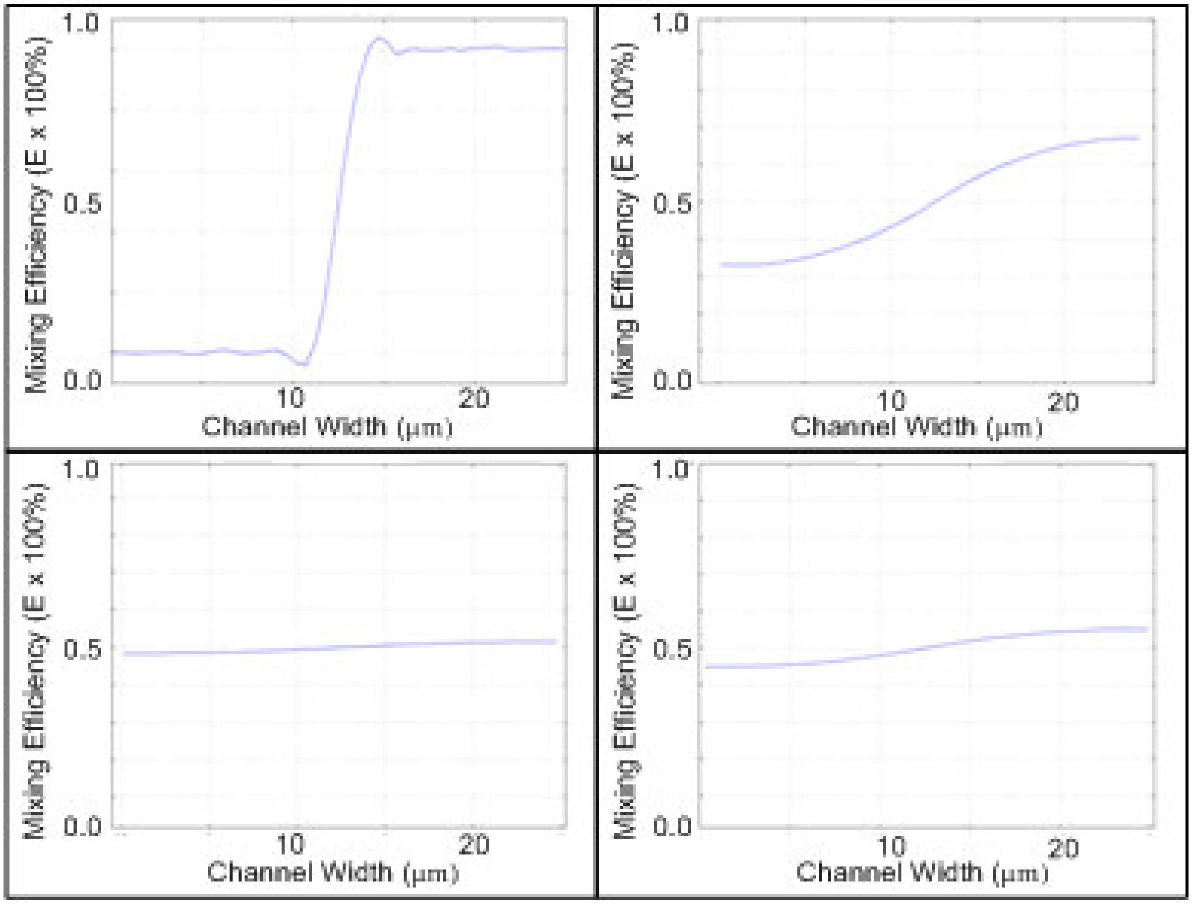

Figure 7.2: Cross-channel concentration profiles are taken for a straight channel at (clockwise from top left) inlet, 5mm, 10mm, and 15mm from the inlet for a fluid velocity of 0.5m/s.

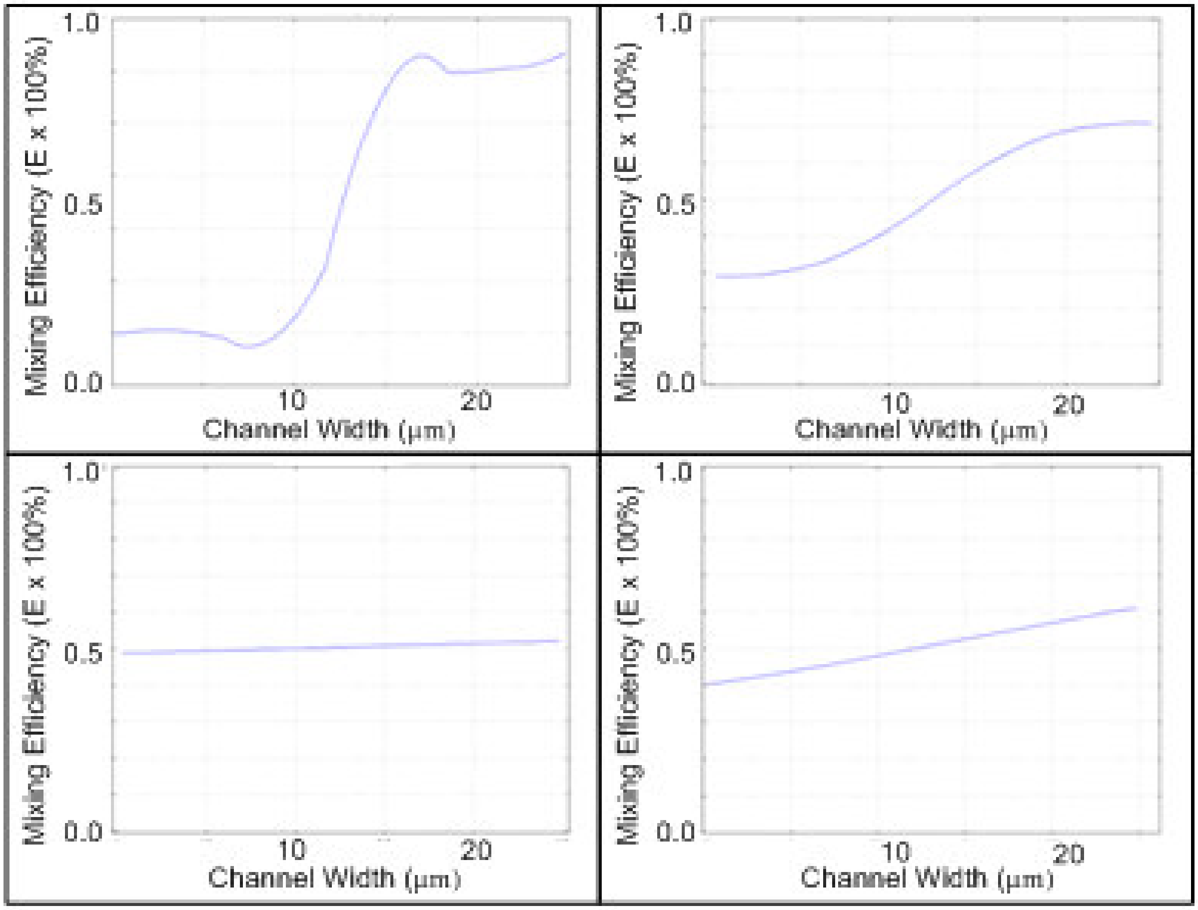

Figure 7.3: Cross-channel concentration profiles are taken for a serpentine channel at (clockwise from top left) inlet, 5mm, 10mm, and 15mm from the inlet for a fluid velocity of 0.5m/s.

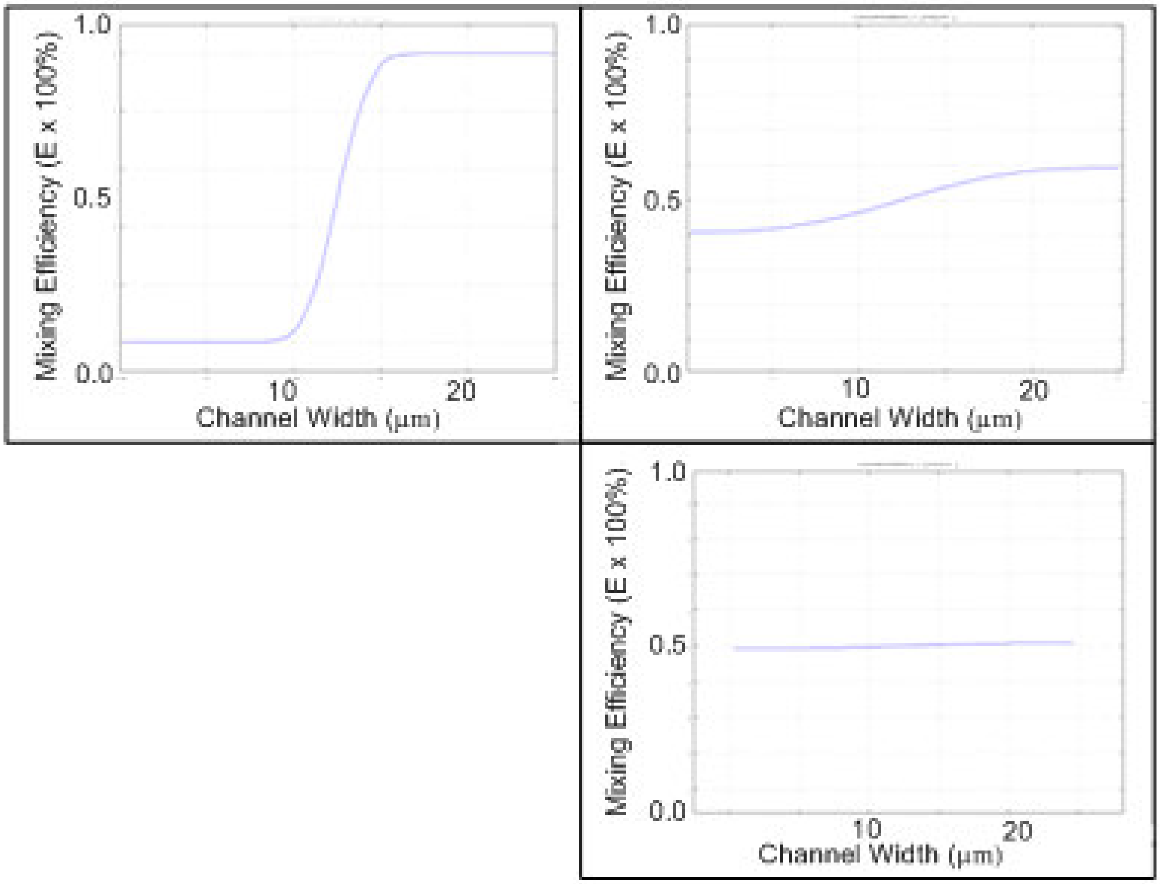

Figure 7.4: Cross-channel concentration profiles are taken for a straight channel at (clockwise from top left) inlet, 1mm, and 1.8mm from the inlet for a fluid velocity of 0.05m/s.

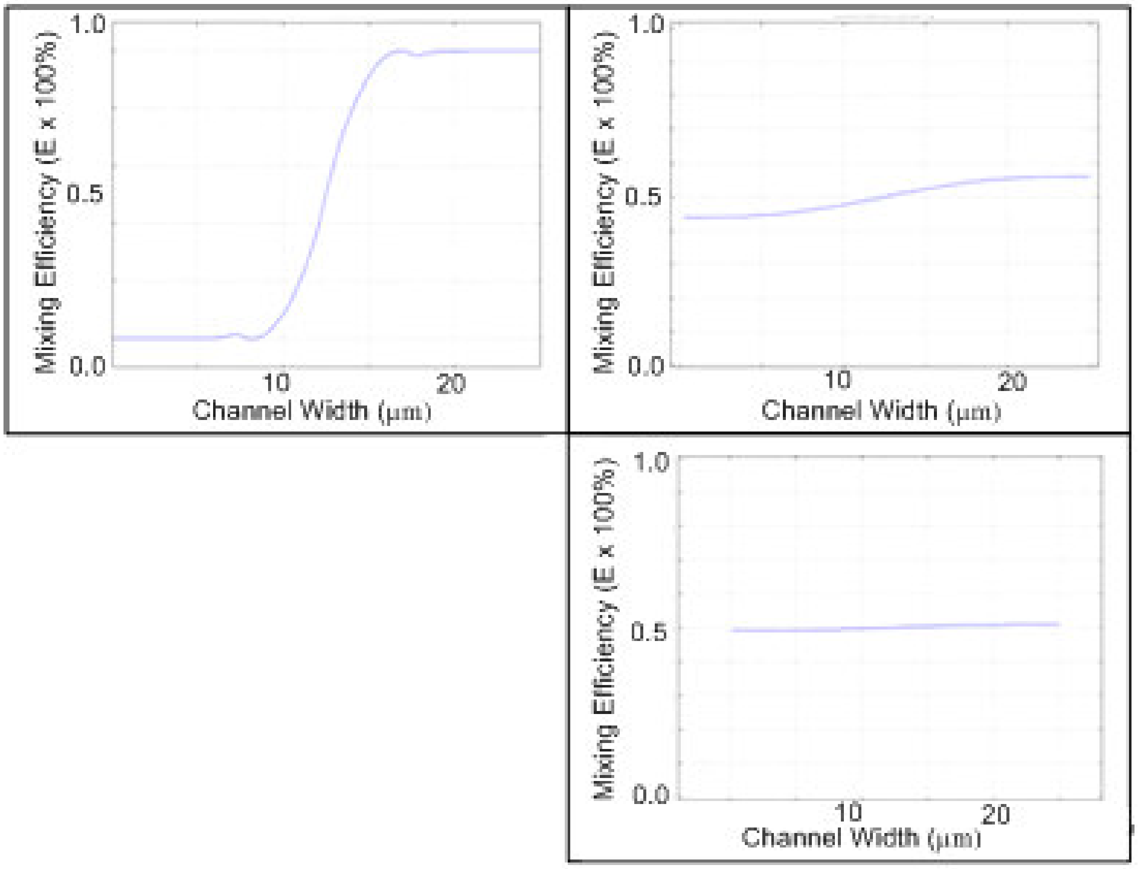

Figure 7.5: Cross-channel concentration profiles are taken for a serpentine channel at (clockwise from top left) inlet, 1mm, and 1.8mm from the inlet for a fluid velocity of 0.05m/s.

At an applied velocity of 0.5m/s for both the serpentine and straight geometries, there is negligible difference in the mixing efficiencies. Both designs reach the 95% mixing efficiency at approximately 15mm from the location where the two streams converge. However, at an applied velocity of 0.05m/s for both geometries, 95% mixing efficiency is reached at only 1.8mm from the inlet. In this scenario, geometry also played a negligible effect on the overall mixing efficiency. These two simulations highlight several issues that must be considered in the design of micromixers.

Generally, geometry has negligible effect on the overall mixing efficiency due to the laminar flow experienced in the channels; streamlines remain relatively separated and consistent along the length of the channel. As an example, an analysis of the first bend for the serpentine mixer shows streamlines and its effect on mixing (Figure 7.6).

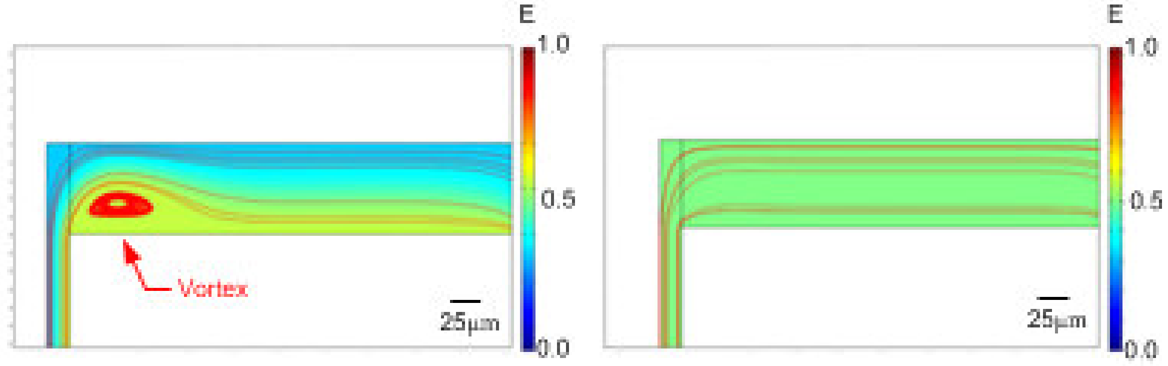

Figure 7.6: Simulation of serpentine mixer with fluid flow of 0.5m/s (left) and 0.05m/s (right) respectively. Vortices can be seen at the higher flow rate (enclosed red circle).

Vortices, although non-existent at low flow rates, can be observed at higher flow rates due to the 90° bend in the channel. However, the vortex only circulates a small region of the channel, which limits its effect on the overall mixing. Ideally, the vortex would circulate along the whole width of the channel if possible to simulate cross-channel mixing.

In addition, for different flow rates, different lengths are required to obtain good mixing. Faster flow rates require longer lengths but the reactants are obtained quickly, making them ideal for continuous operation. Slower flow rates only require short paths and the designs are relatively compact, but may require longer times to obtain the products. Having multiple micromixers operating in parallel can resolve this issue but increases the costs. Due to these factors, for each flow rate an optimum length is required to allow for efficient mixing.

It is interesting to note that higher flow rates increases the pressure inside the micromixer system. Unfortunately, PDMS micromixers are fabricated with a soft polymeric material which breaks easily at relatively high pressures.

7.5 Detection Methods for Experimental Verification

For the purpose of experimentally quantifying mixing, two possible methods can be considered. Fluorescent dye particles such as fluorescin can be injected into the fluid stream of one inlet, whereas the other inlet contains only the buffer or electrolyte. Upon activation of the flow mechanism, both inlets converge in the mixing stream. Using a microscope with a CCD camera, segments of the mixing channel can be analyzed for fluorescent intensity. The mixing ratio is used to quantify the degree of mixing and can be expressed by the equation [Chang and Yang (2004)]:

$$\sigma = \left(1 - \frac{\int_0^W \left| c - c_\infty \right| dy}{\int_0^W \left| c_0 - c_\infty \right| dy} \right) x100\% \tag{7.5}$$

where C is the fluorescent intensity concentration across the width (W) of the channel, C_0 and C_∞ represents the fully unmixed fluorescent concentration (0 or 1) and fully mixed fluorescent concentration 0.5, respectively.

Another method for flow visualization is the use of an iodine chemistry, whose reactants are used to measure the efficiency of mixing [Guichardon and Falk (2000) and Guichardon et al. (2000)]. The chemistry involves two competing reactions:

$$H_2BO_3^- + H^+ \leftrightarrow H_3BO_3 \tag{7.6}$$

$$5I^- + IO_3^- + 6H^+ \leftrightarrow 3I_2 + 3H_2O \tag{7.7}$$

where Equation 7.3 is a quasi-instantaneous process, and Equation 7.4 is a relatively fast process. Both reactions compete for H^+ ions. If efficient mixing occurs in a system, most of the reaction occurs along the path in equation 7.3. However, if inefficient mixing occurs, some of the reactants follow the path as illustrated in equation 7.4, creating iodine in the system. Upon absorbance detection via UV 353nm wavelength, the iodine concentration can be detected and estimated, giving a percentage of iodine formed.

During initial tests using this method, it was discovered that as the fluid passes through a micromixer and is collected at the outlet, due to incomplete mixing and the length of time required collecting the sample, mixing continues while in the collection vial. This secondary mixing effectively increases the concentration of iodine, and correspondingly affecting the UV absorbance detected. However, fluorescent chemistries such as Rhodamine B and fluorescin, while frequently used to characterize mixing, was seen to absorb into the channel walls for microfluidic devices fabricated with PDMS. Thus, it is important to consider the tradeoffs, and choose an ideal method that provides good detectable results with minimal interference.

7.6 Future Work

The fabrication process for creating PDMS micromixers has been investigated in the hopes that future channel design layout can be quickly fabricated and integrated with the necessary connectors for rapid prototyping purposes. At this point, actual experimental verification with one of the above mentioned methods should be chosen and tested on a micromixer.

7.7 Summary

A brief discussion relating to the design and implementation of micromixers has been presented, with emphasis on the fabrication process in creating these devices. A discussion of the fluid flow type and the corresponding integration issues has been provided. Typical channel designs have also been simulated.

- Electroosmosis and pressure driven are two possible flow methods. Although PDMS is suitable for EOF due to a readily formed zeta potential, limitations include the requirement of a polar medium, and difficulty in implementing continuous flow. In addition, it is difficult to quantify due to the stability and repeatability of the zeta potential that depends on such things as pH, and PDMS surface charge. Pressure driven flow can be easily established using syringe pumps, however high flow rates are not possible due to a buildup of pressure that can produce leaks in the PDMS device.

- Channel geometry has limited effects on micromixers in general. However, flow rates directly govern the required length for mixing such that an optimization of flow rates and channel lengths should be performed to obtain high mixing efficiencies while ensuring a high output of products.

.

Chapter 8

Conclusions and Recommendations

8.1 Contributions of this Thesis

The purpose of this work was to demonstrate and discuss several microfluidic applications and the use of soft lithography for their fabrication. Soft lithography allows for the rapid fabrication of devices allowing for testing of many designs in a short period of time. The whole process, including common defects observed and corresponding solutions are provided to aid readers that are learning and attempting the fabrication. A novel microfluidic thermometry method utilizing PDMS thin film soaked in Rhodamine B was demonstrated (Chapter 4). Its performance was verified with an IEF application, in which tapered channel designs with axially changing cross sectional areas create uneven Joule heating along the device (Chapter 5). It has also been demonstrated that the conventional method of mixing Rhodamine B dye with bulk fluid and injecting into the microchannels for temperature measurements provide inconclusive and unreliable results; absorption and adsorption of the dye artificially lowers the detected temperature. An important component to the thin film fabrication is the spincoating of PDMS to achieve the desired thickness. Thus, a calibration curve of spin speed versus thickness of native PDMS and with additives was presented (Chapter 4). Attempts at reducing the thin film thickness further were unsuccessful; however the results are provided, in the hopes that it may aid others.

The concept of IEF with thermally generated pH gradients was also demonstrated by measuring the temperature distributions in several different tapered channel designs (Chapter 5). In general, these devices offer a relatively narrow pH range, thus allowing for high resolution. However, disadvantages to this method include a varying electric field along the axial length of the device, which reduces the reliability of the method. In addition, a small "dead-zone" occurs at the first several millimetres of the inlet, effectively shortening the focusing length. Electrolysis is always a major concern, which can be minimized by reducing channel height, using large reservoirs, and ensuring electrodes are away from the channel openings. However, depending on the width of the channels, reducing the height may promote collapses in the channel as small amounts of PDMS sagging deformation may seal the channels.

IEF utilizing CA was also demonstrated by comparing focusing results of a PDMS IEF device with commercial cartridges of similar design (Chapter 6). In general, the results match well; indicating soft lithography and the corresponding PDMS devices warrants further study as to their applicability in IEF applications. This technique provides a faster process in fabricating microfluidic devices.

The design of micromixers, flow mechanism selection, and its overall integration was discussed (Chapter 7). The selection of fluid flow is important; pressure driven flow can be easily integrated to produce continuous flow but are prone to leaks due to pressure build up, whereas EOF provides good plug-like characteristics, are readily implementable in PDMS, but suffer from low flow rates, electrolysis and reliability issues. In addition, PDMS is at a disadvantage due to the difficulties in obtaining good mixing; for a given length, low flow rates provide low throughput and high efficiency, whereas higher flow rates increase throughput but reduces the mixing efficiency. Channel layout plays a limited role in the mixing mechanism, as at such low flow rates at the micro-scale, mixing is diffusion dominant.

8.2 Recommendations for Future Work

There are several areas in which further research and development is required to improve the overall designs. These projects and the recommendations for future development are outlined according to their application.

Microfluidic Thermometry

Due to the relatively large thermal resistance of the PDMS and glass combined, reducing the thin film thickness is a major improvement. The proximity of the thin film would increase the accuracy of the detected temperatures. However, attempts were made by using Toluene additives which, even though successfully reduced the thin film, it inadvertently also reduced the Rhodamine B intensity. SU-8 was also used to create Rhodamine B thin films; however the photoresist eliminates the temperature dependence. Thus, other materials should be explored in which to embed the fluorescent chemicals while providing a small thermal resistance.

IEF with Thermally Generated pH Gradients

With the aid of the thin film temperature measurement technique, actual in-channel temperatures were measured allowing for heat transfer studies of whole chip designs. These designs should be tested under the same conditions with pH markers mixed in with the Tris-HCl to detect actual pH distribution. In addition, several samples should be utilized to observe the devices' ability for focusing.

IEF with CA

Further testing of these devices is required, especially after the implementation of reservoirs, membranes, and capillary injection channels. It is theorized that these effectively create resistances in the electrical connection, thereby reducing the performance and narrowing the pH range of these devices. In addition, the effects of Joule heating on the in-channel heat distribution and subsequent focusing performance of samples should be studied further, as current results of the PDMS device seem to indicate that, even though PDMS is a highly insulative material, it has negligible effect on the overall separation process, compared to commercial cartridges of silica microchannels.

Micromixers

Numerical simulation, design, fabrication and subsequent testing of different device layouts to promote mixing should be explored. Three-dimensional channel schemes may offer additional advantages compared to current two-dimensional layouts. Of course, these three dimensional schemes will require creative modifications to the current soft lithography fabrication process. Also, a successful on-chip detection system is required to experimentally characterize the mixing.

Bibliography

Allen, P.B.; Rodriguez, I.; Kuyper, C.L.; Lorenz, M.; Spicar-Mihalic, P.; Kuo, J.S.; Chiu, D.T. (2003) "Selective Electroless and Electroytic Deposition of Metal for Application in Microfluidics: Fabrication of a Microthermocouple" Analytical Chemistry, 75, 1578-1583

Baker, D.R. (1995) Capillary Electrophoresis, John Wiley & Sons, New York, NY

Benninger, R.K.P.; Koc, Y.; Hofmann, O.; Requejo-Isidro, J.; Neil, M.A.A.; French, P.M.W.; deMello, A.J. (2006) "Quantitative 3D Mapping of Fluidic Temperatures within Microchannel Networks Using Fluorescence Lifetime Imaging" Analytical Chemistry, 78, 2272-2278

Bird, R.B., Stewart, W.E., Lightfoot, E.N. (1960) Transport Phenomena, John Wiley & Sons, New York, NY

Cad Art Services Inc., "CAD/Art Services: Photoplotting" August 2007. [Online] Available www.outputcity.com

Chang, C.C., Yang, R.J. (2004) "Computational analysis of electrokinetically driven flow mixing in microchannels with patterned blocks" Journal of Micromechanics and Microengineering, 14, 550-558

Chaudhari, A.M.; Woudenberg, T.M.; Albin, M.; Goodson, K.E. (1998) "Transient Liquid Crystal Thermometry of Microfabricated PCR Vessel Arrays" Journal of Microelectromechanical Systems, 7, 345-355

Convergent Bioscience, "Convergent Bioscience" November 2007. [Online] Available http://www.convergentbiosci.com

Davis, K.L.; Liu, K-L.K.; Lanan, M.; Morris, M.D. (1993) "Spatially Resolved Temperature Measurements in Electrophoresis Capillaries by Raman Thermometry" Analytical Chemistry, 65, 293-298

Davis, R.; Das, S. (2005) "Fluorescent Aggregates of 1-(*p*-Butyloxyphenyl)-4-(*p*-cyanophenyl)Buta-1*E,3E*-Diene: Temperature Sensing and Photoimaging Applications" Journal of Fluorescence, 15, 749-753

Dow Corning Corp. (2005) “Material Safety Data Sheet – Sylgard 184 Silicone Elastomer Base”

Dow Corning Corp. (2005) “Material Safety Data Sheet – Sylgard 184 Silicone Elastomer Curing Agent”

Efimenko, K; Wallace, W.E.; Genzer, J. (2002) “Surface Modification of Sylgard-184 Poly(dimethylsiloxane) Networks by Ultraviolet and Ultraviolet/Ozone Treatment” Journal of Colloid and Interface Science, 254, 306-315

Erickson, D.; Sinton, D.; Li, D. (2003) “Joule Heating and Heat Transfer in Poly(dimethylsiloxane) Microfluidic Systems” Lab on a Chip, 3, 141-149

Fung, Y.S.; Tung, H.S. (2000) “Application of Capillary Electrophoresis for Trace Ion Analysis in Rain Water” Journal of Microcolumn Separations, 12, 337-344

Gebauer, P; Bocek, P. (2002) “Recent Progress in Capillary Isotachophoresis” Electrophoresis, 23, 3858-3864

Guichardon,P., Falk, F. (2000) “Characterisation of Micromixing Efficiency by the Iodide-Iodate Reaction System. Part I: Experimental Procedure” Chemical Engineering Science, 55, 4233- 4243

Guichardon, P., Falk, L., Villermaux, J. (2000) “Characterisation of Micromixing Efficiency by the Iodide-Iodate Reaction System. Part II: Kinetic Study” Chemical Engineering Science, 55, 4245-4253

Hellmich, W.; Regtmeier, J.; Duong, T.T.; Ros, R.; Anselmetti, D.; Ros, A. (2005) “Poly(oxyethylene) Based Surface Coatings for Poly(dimethylsiloxane) Microchannels” Langmuir, 21, 7551-7557

Hirokawa, T.; Okamoto, H.; Ikuta, N. (2001) “Operational Modes for Transient Isotachophoretic Preconcentation-Capillary Zone Electrophoresis and Dectable Concentration of Rare Earth Ions” Electrophoresis, 22, 3483-3489

Wu, H.; Huang, B.; Zare, R.N. (2005) “Construction of microfluidic chips using polydimethylsiloxane for adhesive bonding” Lab on a Chip, 5, 1393-1398

Huang, T.; Pawliszyn, J. (2002) “Microfabrication of a Tapered Channel for Isoelectric Focusing with Thermally Generated pH Gradient” Electrophoresis, 23, 3504-3510

Huang, X.; Gordon, M.J.; Zare, R.N. (1988) "Current-Monitoring Method for Measuring the Electroomotic Flow-Rate in Capillary Zone Electrophoresis" Analytical Chemistry, 60, 1837-1838

Huang, T. (2003) "New Carrier-Ampholyte-Free Isoelectric Focusing Approachs for Protein Separation" Ph.D. dissertation, University of Waterloo, Waterloo, ON

Hunter, R.J. (1981) Zeta Potential in Colloid Science: Principles and Applications, Academic Press, New York, NY

Incropera, F.P.; DeWitt, D.P. (2002) Fundamentals of Heat and Mass Transfer, 5th Edition, John Wiley & Sons, Hoboken, NJ

Jorgenson, J.W.; Luckacs, K.D. (1983) "Capillary Zone Electrophoresis" Science, 222, 266-272

Kates, B.; Ren, C.L. (2006) "Study of Joule Heating Effects on Temperature Gradient in Diverging Microchannels for Isoelectric Focusing Applications" Electrophoresis, 27, 1967-1976

Kirby, B.J.; Hasselbrink, E.F. (2004) "Zeta Potential of Microfluidic substrates: 2. Data for Polymers" Electrophoresis, 25, 203-213

Kuhn, R.; Hoffstetter-Kuhn, S. (1993) Capillary Electrophoresis: Principles and Practice, Springer, Verlag, Germany

Lacey, M.E.; Webb, A.G.; Sweedler, J.V. (2000) "Monitoring Temperature Changes in Capillary Electrophoresis with Nanoliter-Volume NMR Thermometry" Analytical Chemistry, 78, 2272-2278

Li, D. (2004) Electrokinetics in Microfluidics, Elsevier Academic, San Diego, CA

Lide, D.R. ed. (1998) CRC Handbook of Chemistry and Physics: 79th edition, CRC-Press

Liu, K-L.K.; Davis, L.; Morris, M.D. (1994) "Raman-Spectroscopic Measurement of Spatial and Temporal Temperature Gradients in Operating Electrophoresis Capillaries" Analytical Chemistry, 66, 3744-3750

McDonald, J.C.; Duffy, D.C.; Anderson, J.R.; Chiu, D.T.; Wu, H.; Schueller, O.J.A.; Whitesides, G.M. (2000) "Fabrication of Microfluidic Systems in Poly(dimethylsiloxane)" Electrophoresis, 21, 27-40

Mcdonald, J.C.; Whitesides, G.M. (2002) “Poly(dimethylsiloxane) as a Material for Fabricating Microfluidic Devices” Accounts of Chemical Research, 35, 491-499

MEMS and Nanotechnology Exchange, “Photoresist develop (SU-8): View”, October 2005. [Online] Available http://www.mems-exchange.org/catalog/P2109/

MicroChem Corp., “SU-8 2000 Permanent Epoxy Negative Photoresist Processing Guidelines for: SU-8 2000.5, SU-8 2002, SU-8 2005, SU-8 2007, SU-8 2010 and SU-8 2015”, December 2005. [Online] Available http://www.microchem.com/products/pdf/SU-82000DataSheet2000_5thru2015Ver4.pdf

MicroChem Corp., “Photoresists, Resists, Developers, Removers, & Optical Dyes”, October, 2005. [Online] Available http://www.microchem.com/

MicroChem Corp. (2001) “Material Safety Data Sheet – SU-8 Series Resist”

MicroChem Corp. (2002) “Material Safety Data Sheet – SU-8 2000 Series Resist”

MicroChem Corp. (2002) “NANO SU-8 2000 – Negative Tone Photoresist Formulations 2002-2025”

MicroChem Corp. (2002) “NANO SU-8 2000 – Negative Tone Photoresist Formulations 2035-2100”

Mikkers, F.E.P.; Everaerts, F.M.; Verheggen, Th P.E.M. (1979) “High Performance Zone Electrophoresis” Journal of Chromatography, 169, 11-20

Mosier, B.P.; Molho, J.I.; Santiago, J.G. (2002) “Photobleached-Fluorescence Imaging of Microflows” Experiments in Fluids, 33, 545-554

Ng, J.M.K.; Gitlin, I.; Stroock, A.D.; Whitesides, G.M. (2002) “Components for Integrated Poly(dimethylsiloxane) Microfluidic Systems” Electrophoresis, 23, 3461-3473

Nguyen, N; Wu, Z. (2005) “Micromixers – A Review” Journal of Micromechanics and Microengineering, 15, R1-R16

Nguyen N.T.; Wereley, S.T. (2006) Fundamentals and Applications of Microfluidics, 2nd Edition, Artech House Inc., Boston

Nishikawa, T.; Kambara, H. (1996) “Temperature Profile of Buffer-Filled Electrophoresis Capillaries Using Air Convection Cooling” Electrophoresis, 17, 1115-1120

Noh, J.; Sung, S.W.; Jeon, M.K.; Kim, S.H.; Lee, L.P.; Woo, S.I. (2005) "In Situ Thermal Diagnostics of the Micro-PCR System Using Liquid Crystals" Sensors and Actuators A, 122, 196-202.

Hofmann, O.; Wang, X.; Cornwell, A.; Beecher, S.; Raja, A.; Bradley, D.D.C.; deMello, A.J.; deMello, J.C. (2006) "Monolithically Integrated Dye-Doped PDMS Long-Pass Filters for Disposable On-Chip Fluorescence Detection" Lab on a Chip, 6, 981-987

Otal, E.H.; Inon, F.A.; Andrade, F.J. (2003) "Monitoring the Temperature of Diluted Aqueous Solutions Using Near-Infrared Water Absorption" Applied Spectroscopy, 57, 661-666

Photronics Inc., "Photronics, Inc: Photomasks & Reticle Lithography Solutions", December 2005. [Online] Available http://www.photronics.com/about/basics.jsp

Pittman, J.L.; Henry, C.S.; Gilman, S.D. (2003) "Experimental Studies of Electroosmotic Flow Dynamics in Microfabricated Devices during Current Monitoring Experiments" Analytical Chemistry, 75, 361-370

Plummer, J.; Deal, M.; Griffin, P. (2000) Silicon VLSI Technology, Prentice Hall, New Jersey

Ren, L.; Escobedo-Canseco, C.; Li, D. (2002) "A New Method of Evaluating the Average Electro-osmotic Velocity in Microchannels" Journal of Colloid and Interface Science, 250, 238-242

Righetti, P.G. (2005) "Electrophoresis: The March of Pennies, the March of Dimes" Journal of Chromatography A, 1079, 24-40

Righetti, P.G. (1983) Isoelectric Focusing: Theory, Methodology, and Applications, Elsevier Science Publishers B.V., Amsterdam

Rilbe, H. (1996) PH and Buffer Theory – A New Approach, Wiley and Sons Ltd., Chichester, England

Roman, G. T.; Hlaus, T.; Bass, K.J.; Seelhammer, T.G.; Culbertson, C.T. (2005) "Sol-Gel Modified Poly(dimethylsiloxane) Microfluidic Devices with High Electroosmotic Mobilities and Hydrophilic Channel Wall Characteristics." Analytical Chemistry, 77, 1414-1422

Roman, G.T.; McDaniel, K.; Culbertson, C.T. (2006) “High Efficiency Micellar Electrokinetic Chromatography of Hydrophobic Analytes on Poly(dimethylsiloxane) Microchips.” Analyst, 131, 194–201

Ross, D.; Gaitan, M.; Locascio, L.E. (2001) “Temperature Measurement in Microfluidic Systems Using a Temperature-Dependent Fluorescent Dye” Analytical Chemistry, 73, 4117-4123

Ross, D.; Locascio, L.E. (2003) “Effects of Caged Fluorescent Dye on the Electroosmotic Mobility in Microchannels” Analytical Chemistry, 75, 1218-1220

Sakakibara, J.; Adrian, R.J. (1999) “Whole Field Measurement of Temperature in Water Using Two-Color Laser Induced Fluorescence” Experiments in Fluids, 26, 7-15

Samy, R.; Glawdel, T.; Ren, C. (accepted 2007) “A Novel Method for Microfluidic Whole-Chip Temperature Measurement Using Thin-Film PDMS/Rhodamine B” Analytical Chemistry

Schrum, K.F.; Lancaster III, J.M.; Johnston, S.E.; Gilman, S.D. (2000) “Monitoring Electroosmotic Flow by Periodic Photobleaching of a Dilute, Neutral Fluorophore” Analytical Chemistry, 72, 4317-4321

Serra, C.; Sary N.; Schlatter, G.; Hadziioannou, G.; Hessel V. “Numerical simulation of polymerization in interdigital multilamination micromixers” Lab on a Chip, 5, 966-973

Sinton, D. (2004) “Microscale Flow Visualization” Microfluid Nanofluid, 1, 2-21

Tan, J.; Liu, Wendy.; Nelson, C.M.; Raghavan, S.; Chen, C.S. (2004) “Simple Approach to Micropattern Cells on Common Culture Substrates by Tuning Substrate Wettability” Tissue Engineering, 10, 865-872

Tabeling, P. (2005) Introduction to Microfluidics, Oxford University Press, New York, NY

Taylor, J.K. (2007) “The Design and Evaluation of a Microfluidic Cell Sorting Chip” MASc thesis, University of Waterloo, Waterloo, ON

Teh, W.H.; Durig, U.; Drechsler, U.; Smith, C.G.; Guntherodt, H.J. (2005) “Effect of Low Numerical-Aperture Femtosecond Two-Photon Absorption on (SU-8) Resist for

Ultrahigh-Aspect-Ratio Microstereolithography" Journal of Applied Physics, 97, 054907

The SU-8 Photo-resist for MEMS, "SU-8: A Thick Photoresist for MEMS", August 2005. [Online] Available http://mems.mirc.gatech.edu/msmawebsite/members/processes/processes_files/SU8/SU-8.htm

Thompson, S.A.; Andrade, F.J.; Inon, F.A. (2004) "Light Emission Diode Water Thermometer: A Low-Cost and Noninvasive Stategy for Monitoring Temperature in Aqueous Solutions" Applied Spectroscopy, 58, 344-348

Vickers, J. A.; Caulum, M. M.; Henry, C. S. (2006) "Generation of Hydrophilic Poly(dimethylsiloxane) for High-Performance Microchip Electrophoresis" Analytical Chemistry, 78, 7446-7452

Wang, B.; Chen, L.; Abdulali-Kanji, Z.; Horton, H.; Oleschuk, R. (2003) "Aging Effects on Oxidized and Amine-Modified Poly(dimethylsiloxane) Surfaces Studied with Chemical Force Titrations: Effects on Electroosmotic Flow Rate in Microfluidic Channels" Langmuir, 19, 9792-9798

Westermeier, R. (2001) Electrophoresis in Practice: A Guide to Methods and Applications of DNA and Protein Separations, 3rd Edition, Wiley-VCH, Weinheim, Germany

White, F.M. (1999) Fluid Mechanics, 4th Edition, McGraw-Hill, New York, NY

Wu, X.Z.; Wu, J.; Pawliszyn, J. (2001) "Whole-Column-Imaging Detection for Capillary Isoelectric Focusing and Capillary Electrophoresis" LCGC, 19, 526-545

Xia, Y; Whitesides, G.M. (1998) "Soft Lithography" Annual Review of Material Science, 28, 153-184

Xuan, X.; Xu, B.; Sinton, D.; Li, D. (2004) "Electroosmotic Flow with Joule Heating Effects" Lab on a Chip, 4, 230-236